ELECTRIC QUADRUPOLE RADIATION STRENGTH IN NEUTRON CAPTURE

By

© M. AMINUL ISLAM, B.Sc.(Hons.), M.Sc.

A Thesis

Submitted to the School of Graduate Studies

in Partial Fulfilment of the Requirements

for the Degree

Doctor of Philosophy

McMaster University

November 1982

QUADRUPOLE RADIATION STRENGTH

DOCTOR OF PHILOSOPHY (1982) McMASTER UNIVERSITY
(Physics) Hamilton, Ontario.

TITLE: Electric Quadrupole Radiation Strength in Neutron Capture

AUTHOR: M. AMINUL ISLAM,

B.Sc.(Hons.) (Rajshahi University)
M.Sc. (Rajshahi University)
M.Sc. (McMaster University)

SUPERVISOR: Professor W.V. Prestwich

NUMBER OF PAGES: xiii, 184

ABSTRACT

A high resolution NaI(Tl)-Ge pair spectrometer has been used to detect the primary E2 transitions following thermal neutron capture in ^{143}Nd, ^{162}Dy, ^{164}Dy, ^{165}Ho, ^{167}Er, ^{173}Yb and ^{179}Hf. These data, as well as other thermal, resonance and average-resonance data have been analyzed to study the radiative quadrupole strength. Some calculations have been done to retrieve the E2 intensities from the average-resonance work. A quantitative theoretical expression for the quadrupole strength function $\langle\Gamma_{\gamma i}/D\rangle$ on the basis of the giant quadrupole resonance model is deduced. A comparison between the experimental and theoretical values for nuclei spanning the mass region between A=12 to A=239 shows the presence of the influence of the GQR on the radiation strength. A depression in the quadrupole strength has been observed in the mass range $144<A<180$. The gross dependence of the E2 radiation width on the photon energy and the nuclear mass number is deduced. The reduced E2 transition probabilities for several mass numbers have been determined.

The energy and intensity of all the observed high energy transitions in most of the nuclei under study are presented. A set of neutron separation energies of 15

isotopes of Nd, Gd, Dy, Ho, Er, Yb and Hf has been estimated. The thermal radiative capture cross section of ^{14}N, a standard used in this work, is determined with improved precision.

ACKNOWLEDGEMENTS

I wish to express my sincere thanks to my supervisor Professor W.V. Prestwich whose guidance and generous assistance were invaluable in the completion of this work. His inspiring talks and stimulating discussions have contributed greatly to my understanding of the field. I am grateful to Professor T.J. Kennett for his help and advice during the course of this research. I would like to thank the members of my supervisory committee Professor A.A. Harms and Professor J.C. Waddington for keeping me oriented in the right direction.

I must thank Mr. Kenrick Chin for developing an excellent and hassle-free network of computers. I acknowledge the kind help and assistance of Dr. Jen-Sen Tsai and Dr. Mahboob Ashraf. Thanks are due to Ms. Diane Lowe for drawing some of the figures.

I thank my fellow students and other friends in the Nuclear Research Building and the Nuclear Reactor Building for making my stay interesting and enjoyable. I appreciate their help and co-operation in different ways.

The financial assistance to me provided by the Canadian Commonwealth Scholarship and Fellowship Administration is gratefully acknowledged.

I am thankful to Mrs. Dreena Burrows for taking the laborious and difficult task of typing this manuscript. I appreciate her artistry and perfection in typing, and her cheerful disposition.

I wish to express my regards to my parents and relatives for their patience and encouragement during the course of this work.

Finally, I wish to thank my wife Nasima for her moral support and understanding and I am grateful for her continued patience and encouragement. I appreciate her helping me in different ways, particularly in some computations. I dedicate this work to her.

TABLE OF CONTENTS

LIST OF FIGURES

LIST OF TABLES

CHAPTER I

INTRODUCTION

Neutron capture gamma-ray spectroscopy is an important tool for studying nuclear structure, properties of nuclear levels and characteristics of transitions between levels in general and that of highly excited states in particular. This versatile field of nuclear physics has aided in the knowledge of different nuclear models and in the understanding of various nuclear reaction mechanisms. The electric and magnetic dipole transitions originating from the neutron capture state (known as primary E1 and M1 transitions) have been extensively studied in the past to investigate the spreading of single-particle transition strength in highly excited states and to examine the nature of the so-called giant dipole resonance in the region of its lower energy tail. But electric quadrupole transitions (E2) have rarely been observed in the past because of their extreme weakness, and as a result very few works have been done on such transitions.

In this work experiments have been performed to

detect several unmixed primary E2 transitions following thermal neutron capture. Results from this work have been combined with those from other thermal, resonance, and average-resonance reaction to perform several analyses in order to extract information related to the quadrupole strength. To retrieve primary E2 intensities from the resonance-averaged data some special calculations have been done. The possibility of the influence of the giant quadrupole resonance on the E2 strength has been investigated. Some quantities related to the E2 transition probability have been estimated. Furthermore, precise values of neutron separation energies of all the nuclides involved and the precise thermal neutron capture cross section of ^{14}N, a common standard used in this work, have been determined.

1.1 General Background

1.1.1 Basic Process

A neutron, being electrically neutral, readily enters a nucleus without encountering any Coulomb repulsion. The capture of a neutron in a nucleus generally leads to the formation of a compound nucleus which, with a mean life of the order of 10^{-15} sec, emits a gamma-ray photon,

$$n + {}^{A}X \rightarrow A + {}^{1}C^{*} \rightarrow A + {}^{1}X + \gamma \qquad 1.1$$

In fact the complete de-excitation of a compound nucleus mostly takes place through the emission of more than one photon. This reaction is customarily known as the radiative capture of neutrons and the emitted photons are called prompt gamma-rays. The branch of science dealing with prompt gamma-rays from the (n,γ) reaction is broadly known as neutron capture gamma-ray spectroscopy.

The capture state decays to the ground state either directly or through a cascade of gamma-rays (see figure 1.1). A gamma-ray originating from the capture state is known as a primary. The primary radiation populates a lower nuclear level which de-excites further emitting another gamma-ray known as a secondary. Thus in this reaction, following the neutron capture a primary radiation and one or more secondaries are emitted till the final nucleus reaches the ground state or an isomeric state.

Thermal capture is due to thermal neutrons (neutrons having a Maxwellian distribution with the maximum at 0.025 eV). As the energy of the incident neutrons is varied different resonances of neutron capture are found. These resonances occur when the excitation of

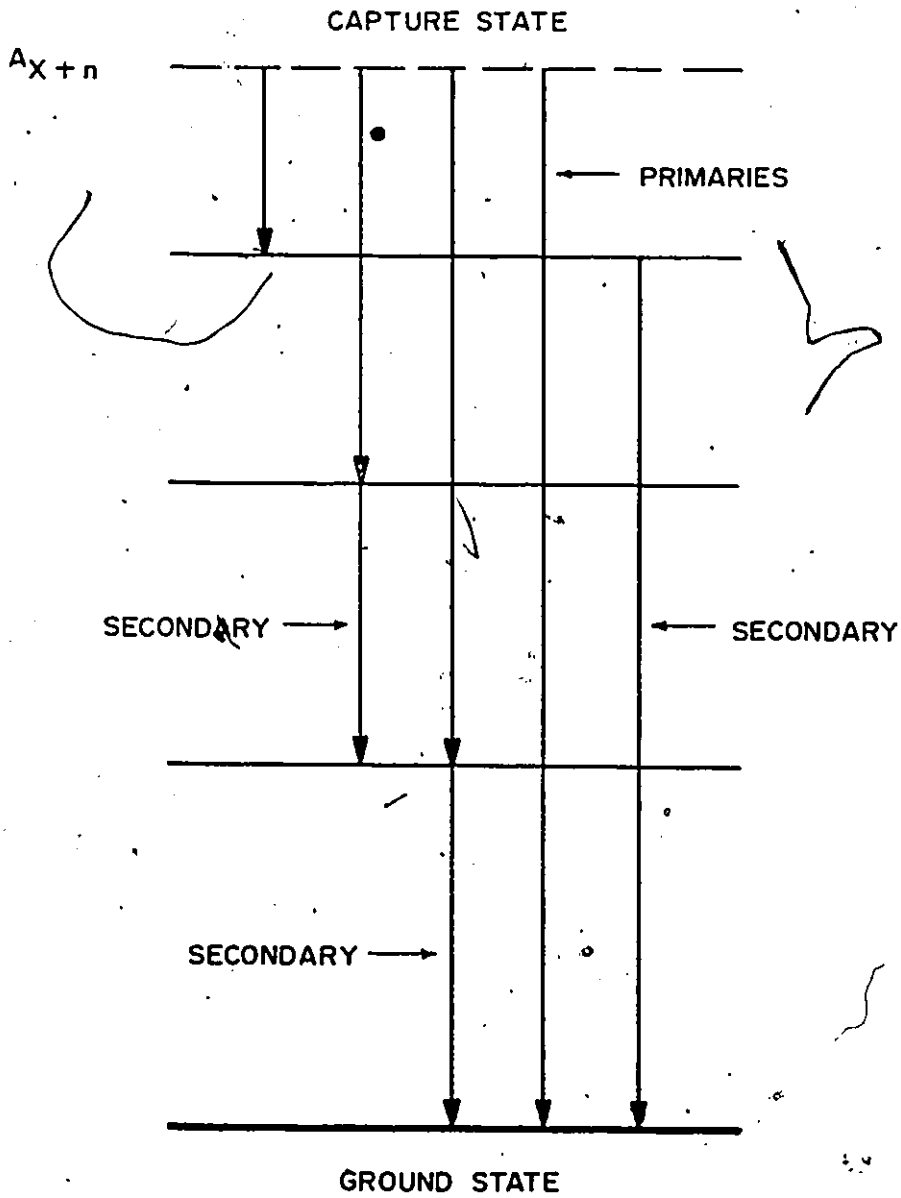

Figure 1.1. Neutron capture gamma-ray transitions in a hypothetical simple nucleus.

the compound nucleus matches the energy of one of its eigenstates. For a particular nuclide these resonances may have different spins and parities. As the level densities of medium and heavy nuclei are very high in this energy region, resonances are frequently encountered. In some cases the spacing between resonances may be only a few electron volts. Resonances rarely occur at thermal neutron capture. However, thermal capture cross section is contributed by the sum (including interference terms) of the tails of neighbouring resonances, both positive (unbound) and negative (bound) and also by direct capture component (Bo70a). Average-resonance capture occurs when neutron filters are used to select a band of energy that is broad enough to excite many resonances. Each of these reactions, resonance, thermal or average-resonance has its own success and limitation.

1.1.2 Neutron Separation Energy

The energy of excitation of a compound nucleus, formed by the capture of a neutron, is contributed to by the kinetic energy of the incoming neutron and the neutron separation energy. Thus the excitation energy is given by

$$E_x = E_n + S_n, \qquad 1.2$$

where E_n is the kinetic energy of the incident neutron in

the c-m system and S_n is the neutron separation energy of the final nucleus. The neutron separation energy may be defined by

$$S_n = (m_X + m_n - m_Y)c^2, \qquad 1.3$$

where m is the mass of a nucleus or a nucleon; X and Y refer to the target and final nucleus in the (n,γ) reaction. Since the kinetic energy of a thermal neutron is only 0.025 eV and the S_n values are in the MeV range, the former in equation 1.2 may be neglected and thus,

$$E_x = S_n \qquad 1.4$$

The excited compound nucleus, in the case of radiative capture, decays to the ground state either directly or through a cascade of several gamma rays. For the direct ground state transition,

$$S_n = E_{\gamma 0} + E_R, \qquad 1.5$$

where $E_{\gamma 0}$ is the energy of the photon; and E_R, the recoil of the nucleus. The recoil energy can be deduced from the conservation of momentum and is found to be

$$E_R = 5.3677 \times 10^{-7} E^2 M^{-1} \text{ keV} \qquad 1.6$$

the energy of the emitted gamma-ray E being in keV and the mass of the nucleus M in a.m.u.

When a primary photon of energy $E_{\gamma j}$ populates a low-lying level of the nucleus the energy balance may be

expressed as

$$S_n = E_{\gamma j} + E_j + E_R, \qquad 1.7$$

where E_j is the energy of the populated level and is often a precisely reported quantity.

Alternatively the total energy released may be expressed as the sum of the energies of primary and secondary photons plus the recoil energies of the nucleus in each step. Thus,

$$S_n = \sum_i (E_{\gamma i} + E_{Ri}), \qquad 1.8$$

where i refers to the photon in the cascade involved.

1.1.3 Transition Intensity

The total radiative transition probability of a resonance is the reciprocal of the mean life of the capture state for the emission of a photon and thus is proportional to the radiative level width Γ_γ. The transition probability is, therefore, given by

$$T = \frac{1}{\tau_\gamma} = \frac{\Gamma_\gamma}{\hbar} \qquad 1.9$$

The intensity I_γ (%) of a primary transition is the number of photons emitted in that transition per 100 neutron captures. Now, as the total radiative width is given by

$$\Gamma_\gamma = \Sigma \Gamma_{\gamma j}, \qquad 1.10$$

the sum of the partial widths of all the γ-ray transitions

from the capture state, the partial width $\Gamma_{\gamma j}$ is given by

$$\frac{\Gamma_{\gamma j}}{\Gamma_{\gamma}} = \frac{I_{\gamma j}}{\Sigma I_{\gamma j}} .$$

But since the sum of the primary intensities, from the definition, is 100,

$$\Gamma_{\gamma j} = \frac{I_{\gamma j}}{100} \Gamma_{\gamma} \qquad 1.11$$

Thus knowing the absolute intensity and total Γ_{γ} of a resonance, the partial width of a γ-ray for that resonance can be determined.

In the case of thermal neutrons, the capture is rarely dominated by a single resonance. Thus to convert the absolute intensity into the partial width, the former is generally multiplied by the average of the total γ-widths of several resonances. This procedure is justified by the observed constancy in this quantity for a given nucleus.

1.2 Related Theories

1.2.1 Properties of Transition Probability

The transition probability for emission of a photon of energy $\hbar\omega$, angular momentum ℓ,m, and of electric or magnetic type, with the nucleus going from a state i to a state f, is (Pr75)

$$T_{if}(\sigma\ell m) = \frac{8\pi(\ell+1)}{\ell[(2\ell+1)!!]^2}\left(\frac{k}{\hbar}\right)^{2\ell+1}|\langle f|O_{\ell m}|i\rangle|^2 \qquad 1.12$$

where $O_{\ell m}$ stands for $Q_{\ell m}$ or $M_{\ell m}$ i.e. electric or magnetic dipole operator. The type of radiation is indicated by σ. These operators have the forms

$$Q_{\ell m} = \sum_i e_i r_i^{\ell} Y_{\ell}^{m*}(\Omega i) \qquad 1.13$$

and

$$M_{\ell m} = \mu_o \sum_i (g_{si}\vec{S}i + \frac{2}{\ell+1} g_{\ell i}\vec{\ell}i).\text{grad}(r^{\ell}Y_{\ell}^{m*}), \qquad 1.14$$

μ_o is the nuclear magneton, and g's are gyromagnetic ratios.

In general there is little interest in the orientation of either initial or the final nucleus. Since the components M_i and M_f of J_i and J_f are not usually measured, it is customary to take an average over all possible transitions with given ℓ in order to get the transition probability that can be directly compared with experiment. The reduced transition rate, or reduced matrix element, is defined as

$$B(\sigma\ell, J_i \to J_f) = (2J_i+1)^{-1} \sum_{M_i, M_f} |\langle f|O_{\ell m}|i\rangle|^2 \qquad 1.15$$

which represents the sum over final states and average over initial states. Here only one value of m, that is

$m = M_f - M_i$, contributes to each term. Thus the transition probability between states J_i and J_f is

$$T(\sigma\ell) = \frac{8\pi(\ell+1)}{\ell[(2\ell+1)!!]^2}\left(\frac{k}{\hbar}\right)^{2\ell+1} B(\sigma\ell). \qquad 1.16$$

There are some selection rules for the electromagnetic transitions between two nuclear states. Since a photon in the mode ℓm carries an angular momentum $\sqrt{\ell(\ell+1)}\hbar$, radiation of multipolarity ℓm must remove from the nucleus a total angular momentum exactly equal to $\sqrt{\ell(\ell+1)}\hbar$, that is, the vector difference between the angular momenta J_i and J_f must be $\sqrt{\ell(\ell+1)}$. Reversing the argument, the possible multipolarities of transitions between states J_i and J_f are given by

$$|J_i - J_f| \leq \ell \leq J_i + J_f \qquad 1.17$$

There is the additional constraint of parity depending on the type of radiation. In order to get a non-zero value of the matrix element in equation 1.12, applying symmetry arguments to the functions in the $Q_{\ell m}$ operator, one gets the following rule for the combination of parities of the initial and final state in an electric multipole transition:

$$\pi_i \pi_f = (-1)^{\ell}. \qquad 1.18$$

For the magnetic multipole transition the relationship is

$$\pi_i \pi_f = (-1)^{\ell+1} \qquad 1.19$$

The above rules can be appreciated by considering the following example. If a transition takes place between states $J_i = 2^+$ and $J_f = 3^-$, according to the selection rule (1.17) alone there can be E1, E2, E3, E4, E5 and M1, M2, M3, M4, M5 transitions. But since there is a change of parity between the two states relations (1.18) and (1.19) demand that the radiation possesses only odd electric multipolarity or even magnetic multipolarity. Thus in this example only E1, M2, E3, M4 and E5 transitions may be involved.

Certain properties of the transition probabilities follow from their formulas (Bl52). For the same multipolarity, the electric transition is in general much stronger than the magnetic transition. Secondly, for the same type of radiation, the transition probability decreases with increasing multipolarity. Thus the electric dipole (E1) transition, for example, is expected to be much stronger than the electric quadrupole (E2).

The above properties of intensities are evidenced by the fact that throughout the periodic table, several thousand E1 and a few hundred M1 primary transitions have been found (Ra81), while there are few reports of primary E2 transitions in thermal neutron capture (see section 1.3).

1.2.2 Porter-Thomas Distribution

The highly excited states formed by the capture of a neutron by a medium weight or heavy nucleus have complex configurations and often have random overlaps with the wave functions of the lower states. As a result the partial radiative widths are broadly distributed, fluctuating widely from one resonance to another. For the transitions from different resonances with the same spin and parity to a particular final state the partial widths follow a chi-square distribution of one degree of freedom, which is known as the Porter-Thomas distribution (Po56). The Chi-square probability density function of ν degrees of freedom is

$$P(x) = [\Gamma(\nu/2)]^{-1}[(\nu/2)x]^{(\nu/2)-1}e^{-\nu x/2} \qquad 1.20$$

where $x = \Gamma_j/\bar{\Gamma}_j$, Γ_j being a partial width and $\bar{\Gamma}_j$, the average of the widths. Thus the Porter-Thomas distribution is

$$P(x) = \frac{1}{\sqrt{2\pi x}}\, e^{-x/2} \qquad 1.21$$

The chi-squared distribution for ν = 1, 2, 4, 16, and ∞ degrees of freedom is plotted in figure 1.2. The partial radiative widths from a resonance capture state follow the P-T distribution. The widths in the case of thermal capture dominated by a single resonance will

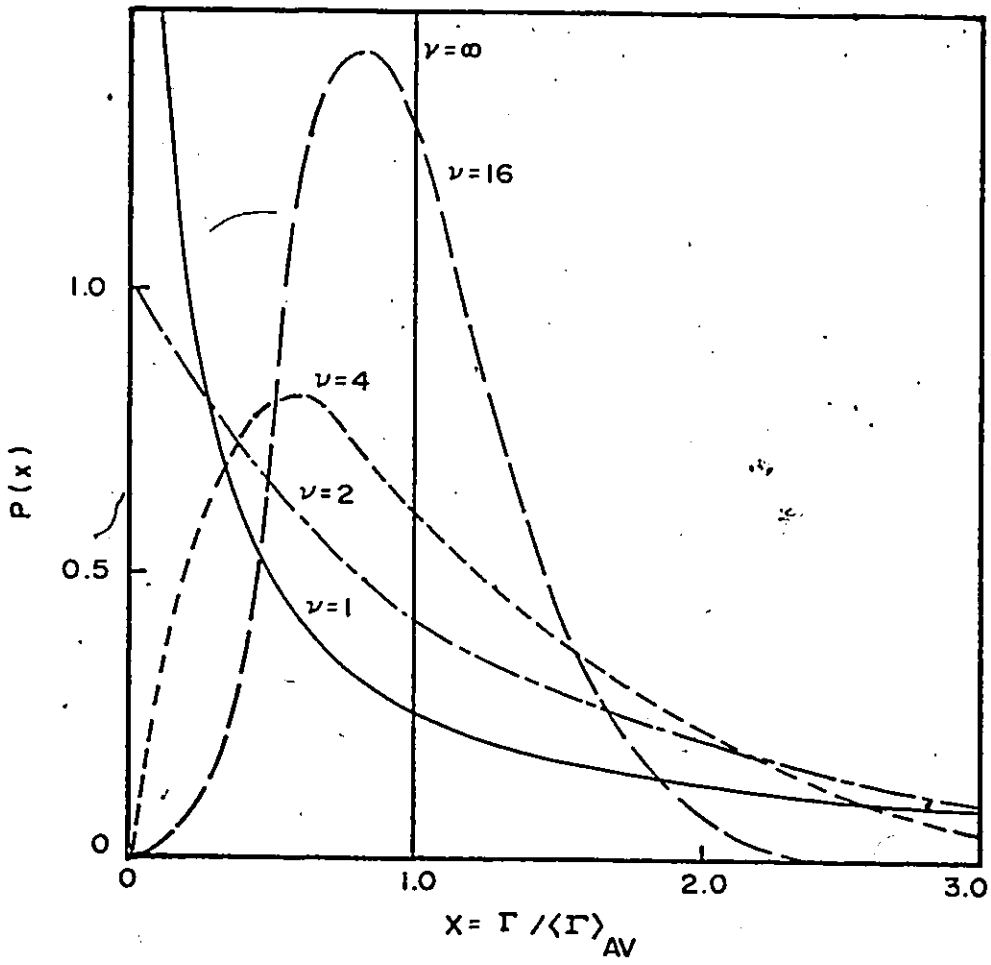

Figure 1.2. The chi-squared distribution is plotted for ν=1, 2, 4, 16, and ∞ degrees of freedom. The abscissa x is the ratio of the width Γ to its average $\langle\Gamma\rangle_{AV}$.

follow the same distribution. But when in thermal capture one resonance does not dominate, there are two cases to be considered:

CASE I - when the resonances contributing to thermal capture are of the same spin. In this case there is full interference between resonance amplitudes, and the sum of amplitudes represents the independent variable whose square determines the partial width. In this case the sum follows a Gaussian distribution, if each variable is presumed to follow a Gaussian. Hence the square of the sum, or the width, follows the Porter-Thomas.

CASE II - when the mixed resonances are of different spins. In this case the distribution depends on the final state spin. If the final state spin is $I \pm 3/2$, only one capture spin state contributes (in the case of a dipole transition) and the distribution is Porter-Thomas as above. For final states of spin $I \pm 1/2$, both possible initial state spins may contribute incoherently and the distribution will correspond to ν between 1 and 2.

The primary E2 transitions, considered in the present study, populate a state with spin $I \pm 5/2$, and thus

only one capture spin state contributes, resulting in a P-T distribution as in case I.

1.2.3 Quadrupole Gamma-Ray Strength Function

The gamma-ray strength function is the distribution, as a function of γ-ray energy, of the average reduced width for transitions of particular multipole type. This function is defined in analogy with the well-established neutron strength functions (Ly68). The gamma-ray strength function for decay of levels of a particular spin and parity by emission of radiation of multipole σL

$$f_{\sigma L}(E) = \frac{\bar{\Gamma}^{\sigma L}_{\lambda\gamma f}(eV)}{D_\lambda(eV)E^{2L+1}(MeV)}, \qquad 1.22$$

where $\bar{\Gamma}^{\sigma L}_{\lambda\gamma f}$ is the gamma-ray partial width averaged over states λ of a given spin and parity at the capture state, D_λ is the average level spacing for such states and E is the transition energy. The factor E^{2L+1} is analogous to the penetration factor which is removed from nucleon widths to obtain nucleon strength functions. Thus the function $f_{\sigma L}(E)$ is proportional to the reduced transition probability for the particular transition.

According to equation 1.22 the electric quadrupole gamma-ray strength function

$$f_{E2}(E) = \left\langle \frac{\Gamma^{E2}_{\lambda\gamma f}(eV)}{D_\lambda(eV)\,E^5(MeV)} \right\rangle \qquad 1.23$$

The function $f_{E2}(E)$ is directly related to the well-known reduced transition probability $B(\sigma L)\downarrow$ (the symbol $\downarrow$ indicates the γ-decay in contrast with the symbol $\uparrow$ which implies photo-absorption) in the following way (Lo79):

$$\bar{B}E2 \text{ (per MeV)} = \frac{1}{\Delta_\Delta}\Sigma B(E2)\downarrow = 1.25\times10^{12} f_{E2}(E) \qquad 1.24$$

$$[e^2 fm^4 MeV^{-1}]$$

For a general understanding of the transition strength irrespective of the type of reaction it is customary (Lo79) to compare the strength of electromagnetic transitions between bound states with the Weisskopf single particle units. For the quadrupole transition, the unit is

$$B_w(E2)\downarrow = 5.94\times10^{-2} \times A^{4/3}\ e^2 fm^4 \qquad 1.25$$

From the observed $f_{E2}(E)$ it is possible to compute $\bar{B}E2$ per MeV and compare it with the single-particle Weisskopf unit in order to get an estimate of the spreading of the transition strength.

Unfortunately there is no single universally accepted definition of the radiative strength function (Lo79). Besides equation 1.22, there are other

expressions for the strength function defined for the sake of convenience and to test specific theoretical models. For E1 transitions, for example, expressions such as $\bar{\Gamma}_{\lambda\gamma f} D_\lambda^{-1}$, $\bar{k}(E1) = \bar{\Gamma}_{\lambda\gamma f} D_\lambda^{-1} E^{-3} A^{-2/3}$ and $\bar{S}(E1) = \bar{\Gamma}_{\lambda\gamma f} D_\lambda^{-1} E^{-5} A^{-8/3}$ are also used.

On the assumption of uniform distribution of the single-particle configuration among the highly excited states, Blatt and Weisskopf (Bl52) gave the following estimates for the widths of E1, M1 and E2 transitions.

$$\Gamma_{\lambda\gamma f}(E1) = 6.8 \times 10^{-8} E^3 A^{2/3} D_\lambda D_o^{-1}$$

$$\Gamma_{\lambda\gamma f}(M1) = 2.1 \times 10^{-8} E^3 D_\lambda D_o^{-1} \qquad 1.26$$

$$\Gamma_{\lambda\gamma f}(E2) = 4.9 \times 10^{-14} E^5 A^{4/3} D_\lambda D_o^{-1}$$

where Γ, E and D_λ are in eV, MeV and eV respectively, and D_0, the single particle level spacing, is in MeV. For the E1 and M1 data the empirically fitted typical value of D_0 has been found to be 15 MeV (Lo79).

The single-particle predictions led Bartholomew (Ba61) to define a dipole radiative strength

$$k(E1) = \Gamma_{\lambda\gamma f} D_\lambda^{-1} E^{-3} A^{-2/3} \qquad 1.27$$

and

$$k(M1) = \Gamma_{\lambda\gamma f} D_\lambda^{-1} E^{-3}$$

These expressions have been used to test the single-particle model predictions. Since in this model K(E1) and K(M1) are independent of the γ-ray energy, often a value of K averaged over all transitions in a particular nucleus is reported.

Following the same approach, one can define the "quadrupole strength" as

$$k(E2) = \Gamma_{\lambda\gamma f} D_\lambda^{-1} E^{-5} A^{-4/3} \qquad 1.28$$

The quantity K(E2), averaged over several transitions in a nucleus or nuclei with adjacent mass numbers is absent in the literature. We shall call $\bar{K}(E2)$ "average quadrupole strength" instead of quadrupole strength function.

Many previous studies have demonstrated that the single-particle (SP) model is certainly over-simplified for high excitations (except for some extreme cases of nonstatistical origin) and collective effects must be considered, resulting in the influence of the giant resonance. The influence of the giant dipole resonance (GDR) on the electric dipole strength in (n,γ) transitions is an established fact (Lo79). Generally, the giant dipole resonance is described by a classical Lorentzian line shape. An expression was

developed (Br55, Ax62, Ba73) for the average radiative partial width of E1 transitions using the tail of a GDR. Some plausible assumptions gave an approximate relationship (Ax62) which in turn led to another definition of the E1 strength function

$$\bar{S}(E1) = \bar{\Gamma}_{\lambda\gamma f} D_\lambda^{-1} E^{-5} A^{-8/3} \qquad 1.29$$

No equivalent expression for $\bar{S}(E2)$ is available in the literature. However, it is possible to express $\langle\Gamma_{\gamma i}/D\rangle$ for the quadrupole transition on the basis of its relation to the photo-absorption cross section which in turn is due to the tail of a giant quadrupole resonance. We shall call $\langle\Gamma_{\gamma i}/D\rangle$ the quadrupole strength function following a similar convention for the E1 case (Bo70).

It may be necessary to mention a point before closing this general discussion on quadrupole strengths. In the case of thermal capture, there are contributions at best from a few resonances and the distribution of the widths of unmixed quadrupole transitions follow a chi-square distribution with 1 degree of freedom (see section 1.2.2). To overcome this dispersion, wherever necessary, instead of averaging over the initial states, the average over the final states may be taken. In

general there is no correlation between the transitions to different final states (Bo70) and the average over m final states will have a chi-square distribution of m degrees of freedom with a variance reducing to 2/m.

1.2.4 Giant Resonances

The influence of the Giant Dipole Resonance (GDR) on the electric dipole strength in (n,γ) transitions is an established fact (Lo79). Although the existence and properties of another type of collective nuclear motion which leads to the Giant Quadrupole Resonance (GQR), have been studied widely in the last decade by inelastic hadron scatterings (Be76), its role in the low energy (n,γ) reaction has rarely been investigated (Ra78, Ko81).

The collective motion of the nucleons in a nucleus gives rise to so-called "giant vibrations". There are mainly three modes of electric vibrations in which a large fraction of the nucleons participate: monopole (E0), dipole (E1) and quadrupole (E2). The giant resonances may be of two types: isoscalar and isovector. Collective motion in which neutrons and protons move in phase are isoscalar ($T = 0$); if out of phase, they are isovector ($T = 1$). The GDR is an

example of isovector oscillation, while the GQR may be either isoscalar or isovector. Of the two types of the GQR, the isoscalar one is well-studied and its existence is widely accepted.

In both the monopole and quadrupole modes, all the nucleons move coherently in a direction which depends on their position in the nucleus. In T = 1 dipole motion the neutrons and protons within a nucleus move collectively against one another, providing a separation between the centres of mass and charge, thus creating a dipole moment. A pictorial representation of the various collective nuclear oscillations associated with each multipole resonance is given in figure 1.3. It is to be mentioned here that the El_{IS} mode corresponds to Nuclear Thomson Scattering from the dipole oscillation of the nuclear centre of mass (Ha64).

As discussed in several review articles (Be76, Sa74), the above collective motions result from coherent superpositions of single-particle transitions between shell-model states. Such transitions in a hypothetical nucleus are depicted in figure 1.4. The major shells are denoted as N, N+1, etc., and within each of them there are several subshells. The major shells are separated by ~1 $\hbar\omega$ or ~41 $A^{-1/3}$ MeV. The interaction

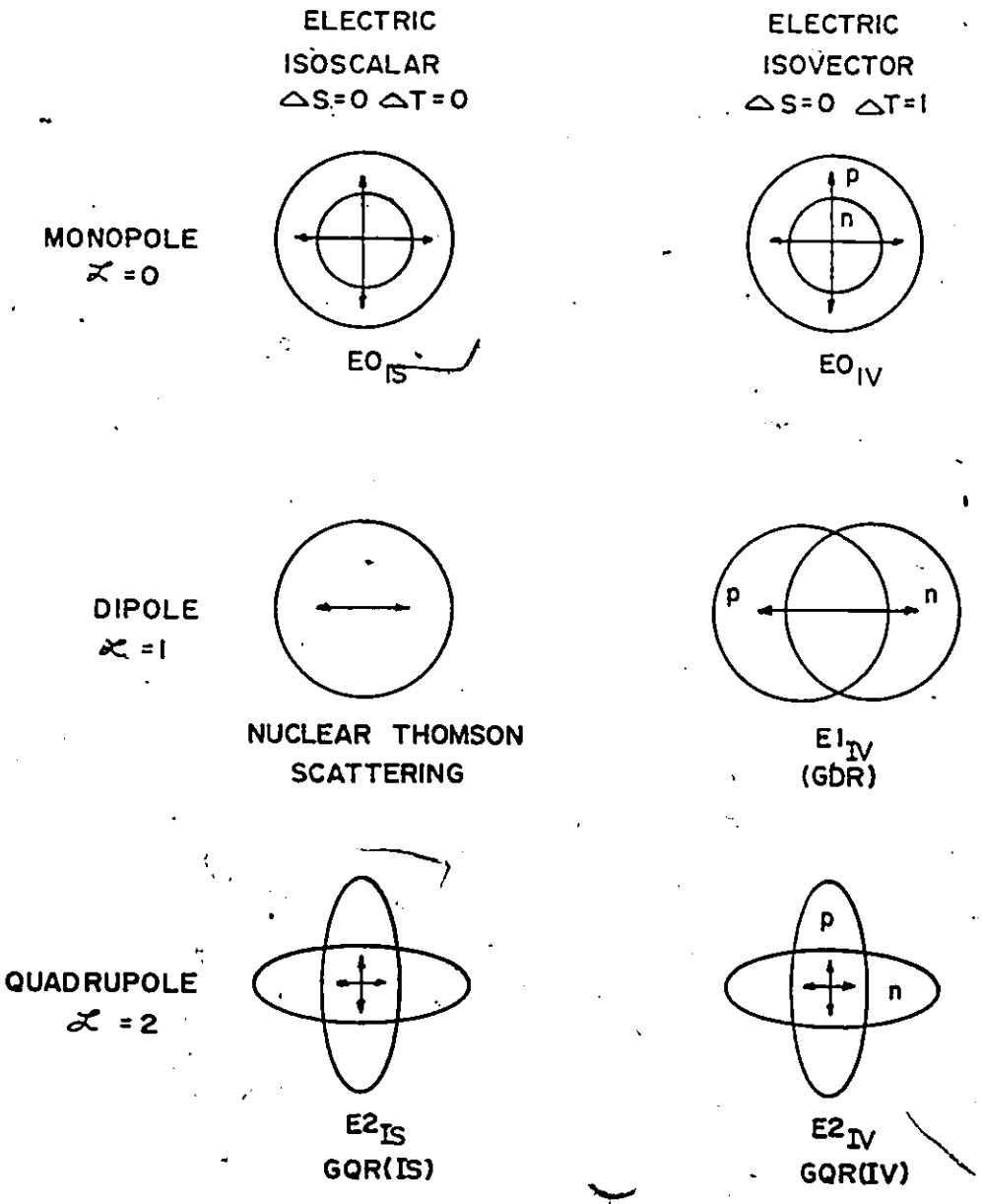

Figure 1.3. Collective Multipole Oscillations of the Nucleus.

operator can excite a nucleon by at most Lħw (L is the multiplicity), or in other words, the nucleon can be promoted by at most L major shells. The number of shells is either odd or even in order to conserve parity. In figure 1.4 the transitions giving rise to GDR and GQR are indicated.

In the diagram, two different sets of E2 transitions are evident: one set within a major shell and the other between shells N and N+2 ($\Delta N = 2$). The former set comprises the so-called Oħw ($\Delta N = 0$) (the familiar low-lying 2+ levels is an example). The GQR is built on the second set of transitions and its energy might be expected to be located at 2ħw or ~82A-1/3. But the resonance energy is pushed up or down depending on whether it is isoscalar or isovector. This is because the particle-hole residual interaction is attractive for the isoscalar mode and repulsive for the isovector (Be76). The isoscalar GQR is located at an excitation energy of $\sim 63A^{-1/3}$ MeV and the isovector GQR at $\sim 120A^{-1/3}$ MeV.

The experimental evidence for the GQR resonances has been provided by inelastic scattering of medium-energy electrons and nuclear projectiles, rather than the photonuclear reactions traditionally

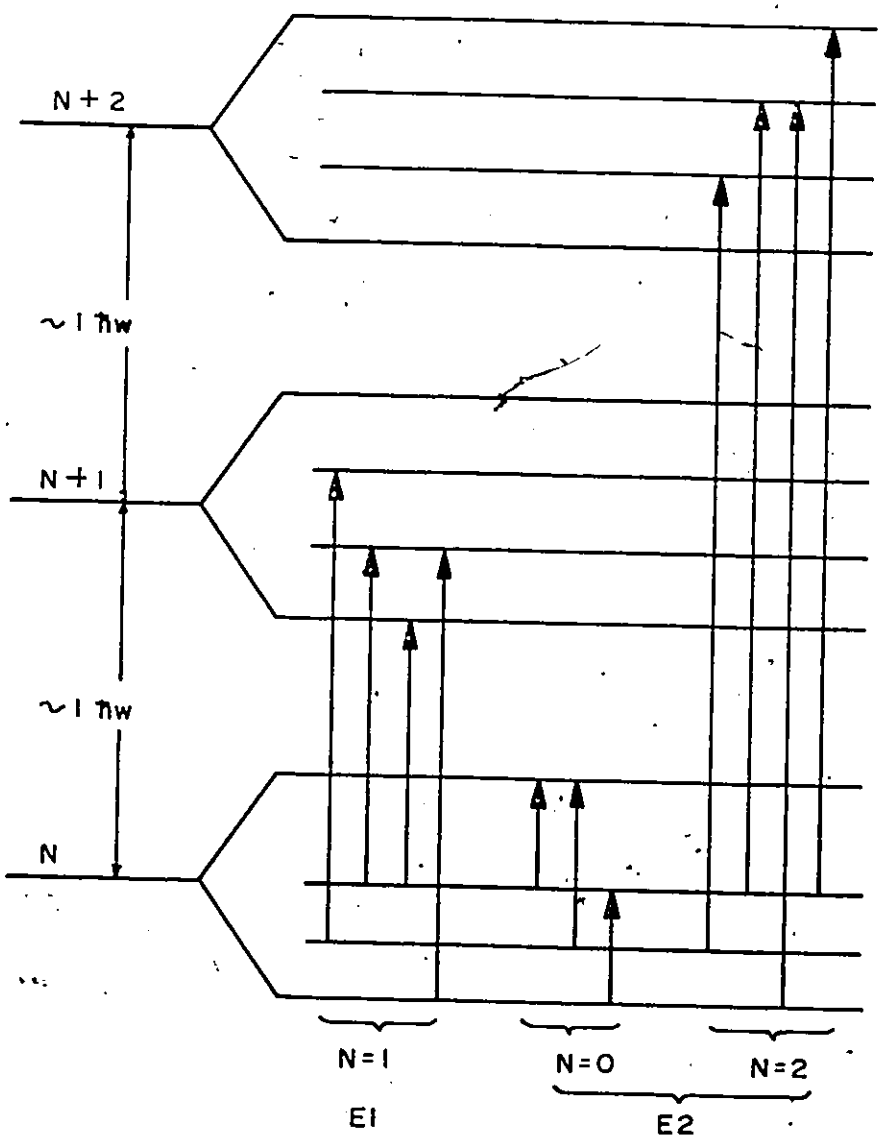

Figure 1.4. Schematic representation of E1 and E2 single-particle transitions between shell-model states of a hypothetical nucleus. Major shells are denoted as N, N+1, and N+2 and lie ~1ħw or ~41$A^{-1/3}$ MeV apart.

used to study the GDR. The isoscalar GQR has been found for many nuclei spanning the mass range 12 to 238 (Be76). On the other hand, the isovector GQR has been detected for fewer number of nuclides because of some inherent experimental difficulties.

1.3 Research Motivation

The primary transitions in the (n,γ) reaction are predominantly electric dipole (E1) or magnetic dipole (M1) in nature. The primary electric quadrupole (E2) transitions are very weak and are rarely detected. This is understandable because the strength of the electromagnetic transition decreases with the increase in multipolarity (Bl52). Even with the influence of the giant quadrupole resonance on the (n,γ) reaction, the E2 transition is weak for low energy capture. In such cases the capture state which is essentially at the S_n value of the nucleus is far down from the GQR energy, which follows approximately $\sim 63A^{-1/3}$ MeV (Be76) and thus the influence is only from the tail of this resonance.

Some unambiguous primary E2 transitions following the thermal and resonance neutron capture have been previously reported. These were first compiled by S. Raman (Ra79) and the compilation has recently been

extended by J. Kopecky (Ko81) and S. Raman (Ra81) bringing the number of primary E2 transitions to 28 in total. These transitions are listed in Appendix A. [Originally S. Raman (Ra78) compiled ^{91}Zr and ^{93}Zr as nuclides emitting primary E2 transitions. These two transitions (Gr72) were identified as E2 transitions on the basis of incorrect neutron separation energies and they cannot be established as E2 transitions if the correct S_n-values are considered]. Almost all of these transitions were incidentally found in different works. Only for the target ^{207}Pb, Raman et al. (Ra78) detected primary E2 transitions to the ground state for many individual resonances.

A further survey in the literature in the present study has revealed 2 more primary E2 transitions (Mi70, Ke81b) in thermal spectra. Quadrupole transitions have also been reported for average-resonance capture. These have been excluded from the compilation of S. Raman and J. Kopecky presumably because most of these E2 transitions are mixed with the p-wave capture E1 transition (see section 3.5). This average-resonance data is used in the present study after making a correction for the p-wave contribution. A literature survey in the present study gives a total of 9 primary

E2 transitions and the upper limits of intensities of two more transitions following average-resonance capture.

When this project was undertaken there was virtually no work in the literature on the quadrupole strength other than that on the localized strength in ^{208}Pb (Ra78). J. Kopecky analyzed (Ko81) the thermal and resonance data of the E2 transitions from the literature. These data lack any information on the mass region between A = 137 to 207. However, his analysis of the E2 transitions is not exhaustive. One can carry on the analysis further which will be facilitated by the availability of the data on their missing mass region.

In the past, there was a theoretical paper by Fubini et al. (Fu72) on the radiative quadrupole strength. The data used in that work was inadequate. Also a portion of that data seems to be taken by mistake. For example, ^{156}Gd, ^{158}Gd and ^{167}Er were taken as primary E2 emitters following the statement of the original average-resonance work (Bo70). This seems to be simply a mistake because it is obvious that the transitions $2^- \rightarrow 4^+$; $2^- \rightarrow 4^+$ and $1/2^+ \rightarrow 7/2^+$ in those three nuclei are not E2 transitions. Besides, it seems that they used the average data without taking into account the contamination of p-wave capture E1 transitions. The contamina-

tion is about 95% in the case of ^{106}Pd (see section 3.5.4).

It appears from the literature that until this work there has been no specific plan for detecting thermal neutron capture E2 transitions. We decided to carry out experiments to detect primary E2 transitions in several nuclides. Such a plan was expected to increase data on the quadrupole transition. Furthermore, a premeditated search has a special significance. Because of the P-T fluctuation some of primary E2 radiations will not be observed at all; but it is possible to estimate an upper limit for the intensity of such unobserved transitions.

As the primary E2 transition is very weak high sensitivity experiments are needed to identify them. In identifying the E2 strengths, investigation of the angular distributions from the (n,γ) reactions at high energies as suggested by Saporetti and Guidotti (Sa78) may be useful. With our irradiation system, the latter alternative is not feasible, while the high sensitivity of our system can be employed to identify the E2 lines directly from the (n,γ) spectrum. The identification of the E2 transitions is made on the basis of energy which in turn is decided upon on the basis of the spins

and parities of the capture and final states.

The targets selected for the thermal neutron irradiation were within the mass region $142<A<180$. This is the region where the s-wave neutron strength function is high and the p-wave strength function is low and the probability of p-wave contribution which might contaminate the E2 transition is expected to be negligibly small. As the energy of the giant quadrupole resonance varies as $\sim A^{-1/3}$, for the high mass number nuclei the GQR is located relatively close to the neutron capture state and the influence of the GQR may be observed. A survey of the literature revealed the absence of any reported primary E2 transitions in this mass region. (Later, however, we found such a transition in ^{168}Er previously reported in the literature).

Now we shall discuss the way in which expected E2 transition energies were determined. If the spin and parity of a target nucleus is J_t and π_t, the spin and parity of the final nucleus will be

$$J_c = J_t \pm 1/2 \quad (J_c = 1/2 \text{ if } J_t = 0) \qquad 1.30$$

$$\pi_c = \pi_t ,$$

if only s-wave capture is assumed. The E2 transition

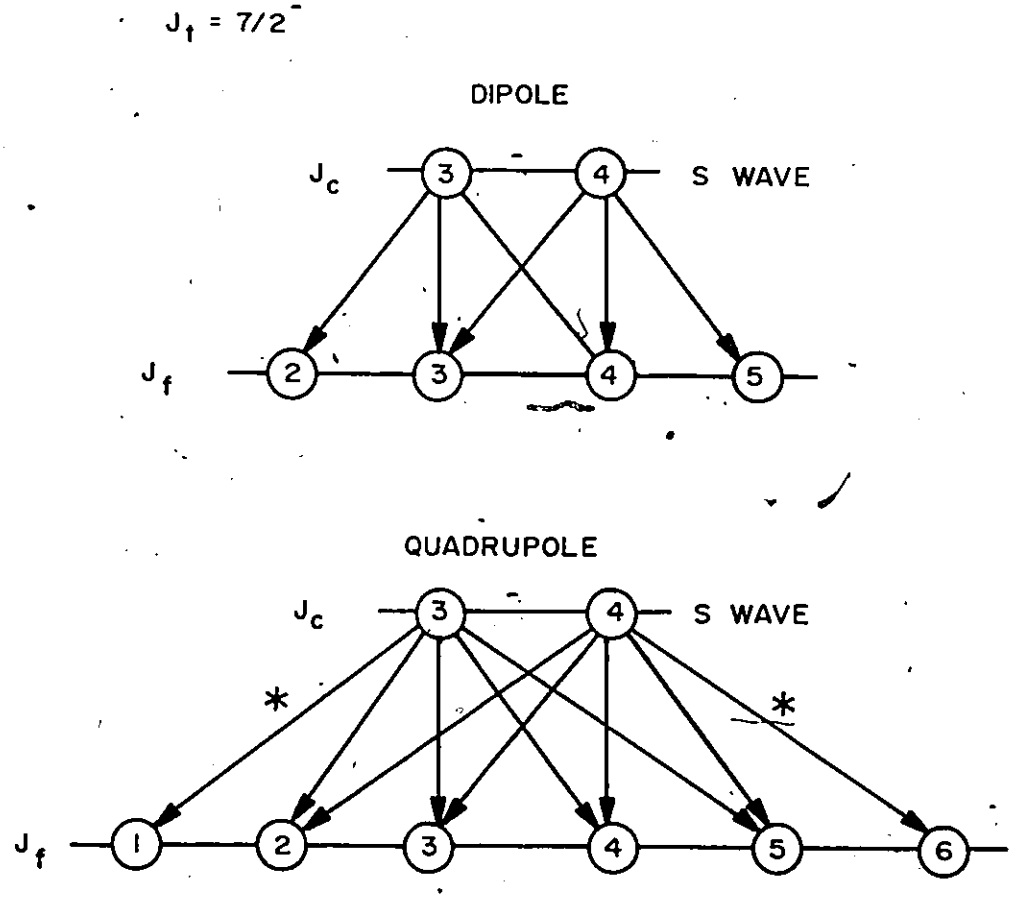

Figure 1.5. Schematic representations of the different modes of feeding final states with primary γ transitions following s-wave neutron capture by a nucleus with spin $7/2^-$. Symbol * indicates E2 transition unmixed with the dipole.

from the capture state will populate the nuclear levels with $J_f = J_c \pm 2, J_c \pm 1, J_c$ (the constraint that $J_f > 0$ should be remembered) and $\pi_f = \pi_c$ (see figure 1.5). Among these $J_c \rightarrow J_c \pm 1$ or J_c transitions will be accompanied by M1 radiation. This leaves out the possibility $J_c \rightarrow J_c \pm 2$ i.e. $J_c \rightarrow J_t \pm 1/2 \pm 2$. But the quadrupole transition $J_c \rightarrow J_t + 1/2-2$ is mixed with the dipole transition $J_c \rightarrow J_t - 1/2 - 1$ and similarly $J_c \rightarrow J_t - 1/2 + 2$ is mixed with $J_c \rightarrow J_t + 1/2 + 1$. Therefore finally we get the condition for the unambiguous primary E2 transition as

$$J_f = J_t \pm 5/2 \text{ (preserving the positivity of J)}$$

$$\pi_f = \pi_t \qquad 1.31$$

The region 142<A<180 was examined for appropriate cases. Target nuclei giving final nuclei with the required J_f and π_f values were compiled. Among these, some nuclei belong to an element having adjacent isotopes with capture cross-section several orders of magnitude greater. In some cases the expected E2 transition is interfered with by a line of an accompanying isotope. Cost of the separated isotope was another factor limiting selection in the choice. Considering all these factors the final list of the target isotopes with the expected

TABLE 1.1

Selection of Targets to Detect Primary E2 Transitions

Target nucleus	Spin	Capture state spin	Populated state spin	Populated level[a] (keV)	S_n[b] (keV)	E (keV)
^{143}Nd	$7/2^-$	3^-, 4^-	1	3244.2	7817.11	4572.8
^{165}Ho	$7/2^-$	4^-, 3^-	1^-	82.5	6243.69	6161.1
^{162}Dy	0^+	$1/2^+$	$5/2^+$	781.1	6270.98	5489.8
			$5/2^+$	949.3		5321.6
			$5/2^+$	250.9		6020.0
^{164}Dy	0^+	$1/2^+$	$5/2^+$	584.0	5715.96	5131.9
^{173}Yb	$5/2^-$	3^-, 2^-	(5^-)	2378.7	7464.63	5085.8
^{179}Hf	$9/2^+$	5^+, 4^+	(2^+)	1724.8	7388.64	5663.7
			(2^+)	1637.3		5751.2
			(2^+)	1300.6		6087.9
			2^+	93.1		7295.4
^{167}Er	$7/2^+$	4^+, 3^+	6^+	548.5	7771.47	7222.9

[a] Ref. Le78.
[b] This work.

E2 transitions is presented in table 1.1. The S_n values given in the table are from this work (see section 4.1). The energies of expected primary E2 radiations were determined by subtracting the final level energies from the neutron separation energies. The expected photon energies are less than the transition energies by a small nuclear recoil energy.

To investigate the influence of the GQR on the quadrupole transition strength, it was decided in this study to rigorously deduce a quantitative expression for $\langle\Gamma_{\gamma i}/D\rangle$ on the basis of its relation to the photo-absorption cross section. This cross section can be estimated from the tails of the isoscalar and isovector giant quadrupole resonances. The experimental values of $\Gamma_{\gamma i}/D$ for the primary quadrupole transitions both from this work and the literature are compared with the corresponding theoretical values to investigate the possible influence of the resonances. In the theoretical work of Fubini et al. (Fu72), the final expression for $\langle\Gamma_{\gamma i}/D\rangle$ was given, but not deduced explicitly. It is to be mentioned here that their value is higher by a factor of 2 than what we have obtained.

The reduced transition probability $\bar{B}E2$ per MeV expressed in Weisskopf unit will be a useful quantity

(Lo79). With the accumulation of more data and with the inclusion of corrected resonance-averaged results from the literature, it is possible to estimate this quantity for some masses or mass regions. Similarly the average quadrupole strengths $\bar{K}(E2)$ (see equation 1.28) for a nucleus, or nuclei with adjacent mass numbers are reported. Such values are the first of their type to appear in the literature.

As discussed above the energy of the expected E2 transition is determined using the level energy from the literature and the neutron separation energy S_n. The S_n values of heavy nuclides are often imprecisely known (Wap77). Since precise S_n values are needed in the present study, it was decided to determine these quantities for all the nuclides involved. The consistency in the S_n values of a nucleus determined by taking different cascades is a check on the reliability of the energy scale. Precise S_n-values of the (n,γ) reactions are used to calculate the odd-even energy shift and for developing more sensitive models of binding energy systematics.

The precision in the intensity of a transition is dependent on the precision of the cross sections of the sample and the standard (see section 4.2.1). The common

standard that has been used in this work for energy, efficiency, and intensity calibration is nitrogen. Unfortunately the best previously reported value of the radiative capture cross section of ^{15}N was 75 ± 7.5 mb (Ju63) and using that value would not enable one to determine the intensity of a transition with better than 10% precision. Thus it was necessary to determine precisely the thermal radiative capture cross section of ^{14}N. Moreover a precise value of σ_γ for ^{14}N is a useful quantity because this element is frequently used as a calibration standard.

In order to detect the primary E2 transitions, the samples were run for long periods of time. This produced excellent statistics for the spectra and many previously unknown peaks were detected. The high resolution of the thermal spectra coupled with good statistics made the identification of new lines possible. The energies and absolute intensities of the high energy transitions of most of the nuclides involved are tabulated in the present study.

CHAPTER 2

EXPERIMENTAL DETAILS

Various samples, enriched and natural, were irradiated with neutrons near the core of the McMaster reactor and the prompt gamma-rays produced were detected by a pair spectrometer. In this chapter, descriptions of the samples, the irradiation system and the gamma-ray detection system are presented.

2.1 Samples

The main samples (supplied by Union Carbide Corporation Nuclear Division) used in this work are presented in table 2.1. Their masses and the total length of time during which their (n,γ) spectra were collected are given. Each of the samples was in oxide form. As the main objective of this work is the detection of very weak E2 primary transitions any possible contribution from the impurities was carefully considered. A list of the important impurities with their atomic percent is displayed in Appendix B. Natural erbium was used to exploit the ^{167}Er target whose effective cross-section is 90% of the total. Natural

TABLE 2.1

Irradiation of Samples

Target Isotope	Atomic Percent	Mass of Samples (mg)	Time of run (hr)
^{143}Nd	91.68	148	190
^{162}Dy	96.26	310	60
^{164}Dy	98.43	20	290
^{165}Ho	99.9	400	210
^{167}Er[a]	22.9	400	30
^{173}Yb	92.08	456	340
^{179}Hf	81.85	280	190

[a]Natural erbium is used.

TABLE 2.2

Experiments for σ_γ of ^{14}N

Sample Number	Component of sample	Mass (mg)	Ratio N-atom / Cl or Al atom	Time of run (hr)
1	$C_3N_6H_6$	1450.3	127.7	18
	NH_4Cl	38.4		
2	$AlNH_4(SO_4)_2.12H_2O$	2001.6	1	90

samples of all the separated isotopes of table 2.1 were run separately in order to check for any interference from the accompanying isotopes. For energy, efficiency and absolute intensity calibration, experiments in addition to those mentioned in table 2.1 were also performed in which each of the targets of known mass was homogeneously mixed with a known amount of melamine ($C_3H_6N_6$). Mixtures with NH_4Cl have also been used on several occasions.

For the determination of σ_γ of ^{14}N, chlorine and aluminum were used as standards. Precise values of both intensity (Ke81) and cross section (Mu81) are available for chlorine. Also available are those of aluminum (Pr81, Mu73). For calibration with chlorine, ammonium chloride was mixed homogeneously with melamine. The ratio of nitrogen to chlorine was chosen properly to ensure a balanced spectrum. The compound $AlNH_4(SO_4)_2 \cdot 12H_2O$ was used to provide an accurate aluminum/nitrogen mixture. The data for these samples are presented in table 2.2.

In addition a spectrum of the empty tangential tube and that of a typical carbon capsule was observed to check for any possible interference from these sources.

2.2 Experimental Facility

The McMaster University nuclear reactor is a swimming pool type reactor which uses light water for the triple purpose of moderation, cooling and reflection. The reactor has a loading capacity of about 5 kg of uranium containing 94% enriched ^{235}U and it normally runs at 2 MW thermal power although it has a maximum capacity of 5 MW. At 2 MW the average thermal neutron flux in the core is 2×10^{13} cm^{-2} sec^{-1}.

2.2.1 Irradiation System

For neutron capture gamma-ray spectroscopy, high neutron flux and the absence of γ-ray background from nuclear fission and reactor construction material are desired. To achieve this condition, a tangential tube (Ni70) passes near the core of the reactor. The tube, made of Al, is 2 m long and 7.6 cm in diameter (figure 2.1). The thermal neutron flux at the sample site is 6×10^{12} cm^{-2} sec^{-1} at normal reactor operation. The gamma-rays from the sample and its container are extracted through the stepped lead collimators in the reactor wall that produce 1 cm collimation, and impinge on a detector placed at a total distance of 4 m from the sample site. A 50 cm lucite rod in the collimator and a

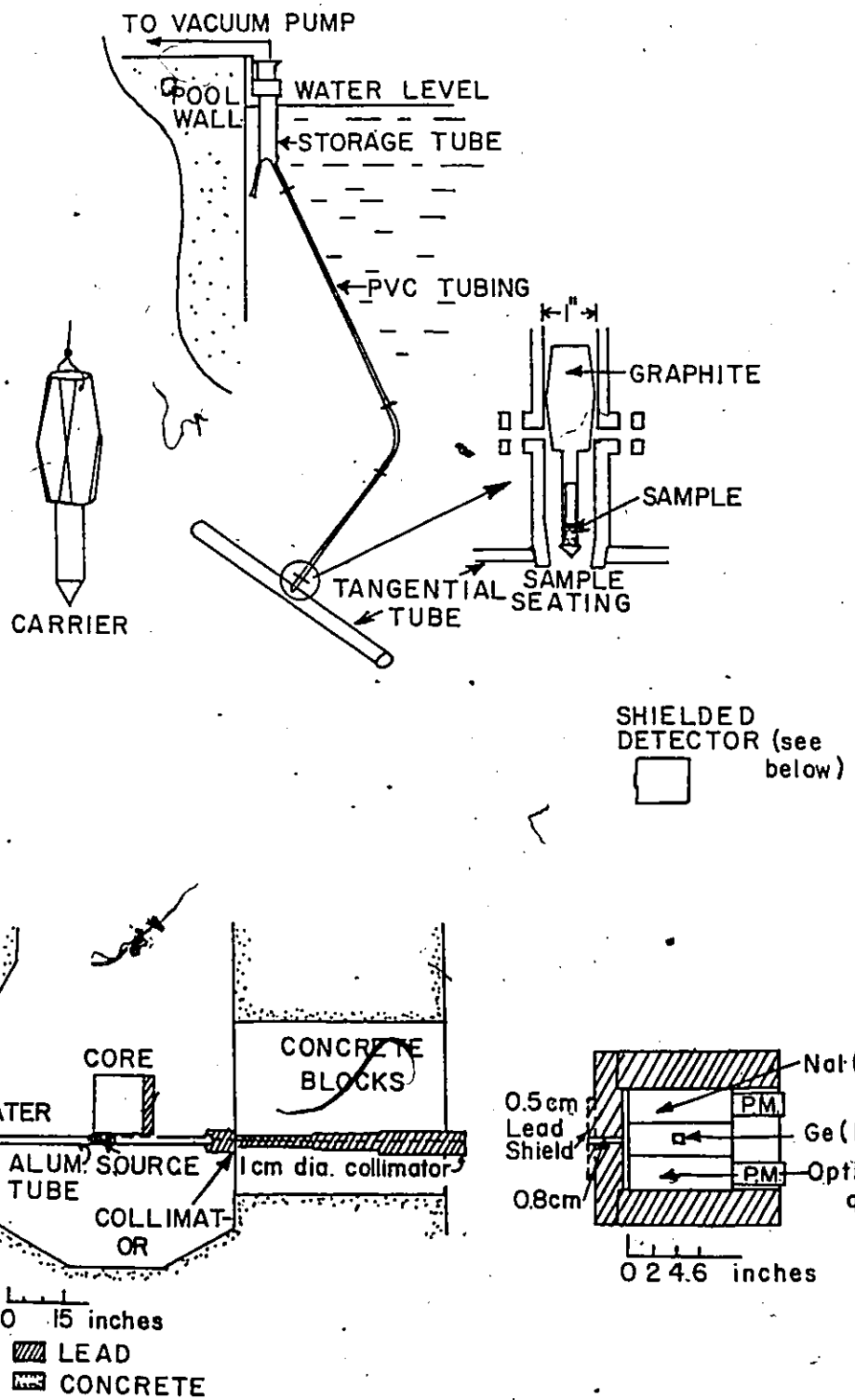

Figure 2.1. The irradiation facility

paraffin slab of 30 cm thickness between the reactor wall and the detector absorbs much of the low energy photons and scatters the fast neutrons which would otherwise damage the Ge detector.

The tangential tube is at 8 m below the water surface of the reactor. A 10 m long and 2.5 cm inner diameter flexible polyvinyl chloride tube runs from the water surface to the sample site through this tube. When a sample is removed from the system following irradiation, a high level of radioactivity is expected for several hours from the short lived radionuclides formed in the sample and the container. To decrease the turn-around time there is a storage located near the water surface and the sample can be brought out of the core and immediately stored without causing radiation hazard to the experimenter. The entire system is evacuated using an on-line dual-seal pump. This is done to prevent the formation of radioactive Ar from the air and eliminate $^{14}N(n,\gamma)^{15}N$ background from nitrogen in the air.

2.2.2 Sample Holder

The choice of material for the sample holder was such that it provides a minimum (n,γ) background and a low level of radioactivity when the irradiation ends. Reactor

grade graphite is particularly suitable as its cross-section is low (Pr81) and it has only three (n, γ) lines of significant intensity all below 5.0 MeV, the main region of interest in this work. Graphite can be machined to the desired shape of the container capsule. For the irradiation of all the samples in the present study, 1 or 2 cm^3 inner volume graphite capsules were used.

2.3 Detection System

In this work, the gamma-rays were detected by a pair spectrometer capable of producing high energy resolution and low continuum to peak ratio in the pulse-height spectrum. The spectrometer consists of an intrinsic Ge detector surrounded by a quadrisected NaI(Tl) annulus. Before describing different features of the pair spectrometer and the improvement of the response function, a brief description of a Ge detector and photon interactions in germanium may be meaningful.

2.3.1 Ge Detector

The essential features of the semiconductor detectors, of which the Ge detector is the most widely used, are the production of large numbers of electron-

hole pairs by the interaction of gamma-rays and the rapid collection of these charges by electrodes so that an electrical signal is produced in an external circuit. The requirement of very low energy to produce an electron-hole pair, the high carrier mobility, and low trapping cross section make the resolution of the Ge detector very high. The usefulness of this detector is also due to the linearity of the electron-hole production to the initial energy of the ionizing photon. The efficiency of detection is dependent on the probability of deposition of all energy by the incoming photon in the detector, which is in turn dependent on the cross section of various interactions of the photon in the detector and the detector size.

The Ge detector is essentially a junction type semiconductor detector with p- and n-type semiconducting electrodes separated by an intrinsic region. Ionizing particles enter the intrinsic region producing electron-hole pairs and these charges are collected at the electrodes.

In order to secure the advantages of high resolving power and low noise background, it is necessary to maintain the detector at a very low temperature.

Liquid nitrogen at a temperature of -190°C is generally used for this purpose.

2.3.2. Photon Interactions in Germanium

There are three major interaction mechanisms which play an important role in radiation measurements. At low energies photoelectric absorption predominates. The photoelectron creates charge carriers in the germanium intrinsic region and the photon is completely absorbed. The x-rays from the photoelectron emitting atom are more likely to be absorbed by a second photoelectric interaction. This contributes further charge carriers to the germanium. The probability of photoelectric absorption is roughly approximated as (Ev55)

$$\tau \approx \text{const} \times \frac{Z^n}{E_\gamma^3} \qquad 2.1$$

where n varies from 4 to 5. The photoelectric absorption coefficient of germanium (Z = 32) is shown in figure 2.2.

At energies above 0.1 MeV, the Compton effect becomes important. The Compton scattering cross-section is (K129)

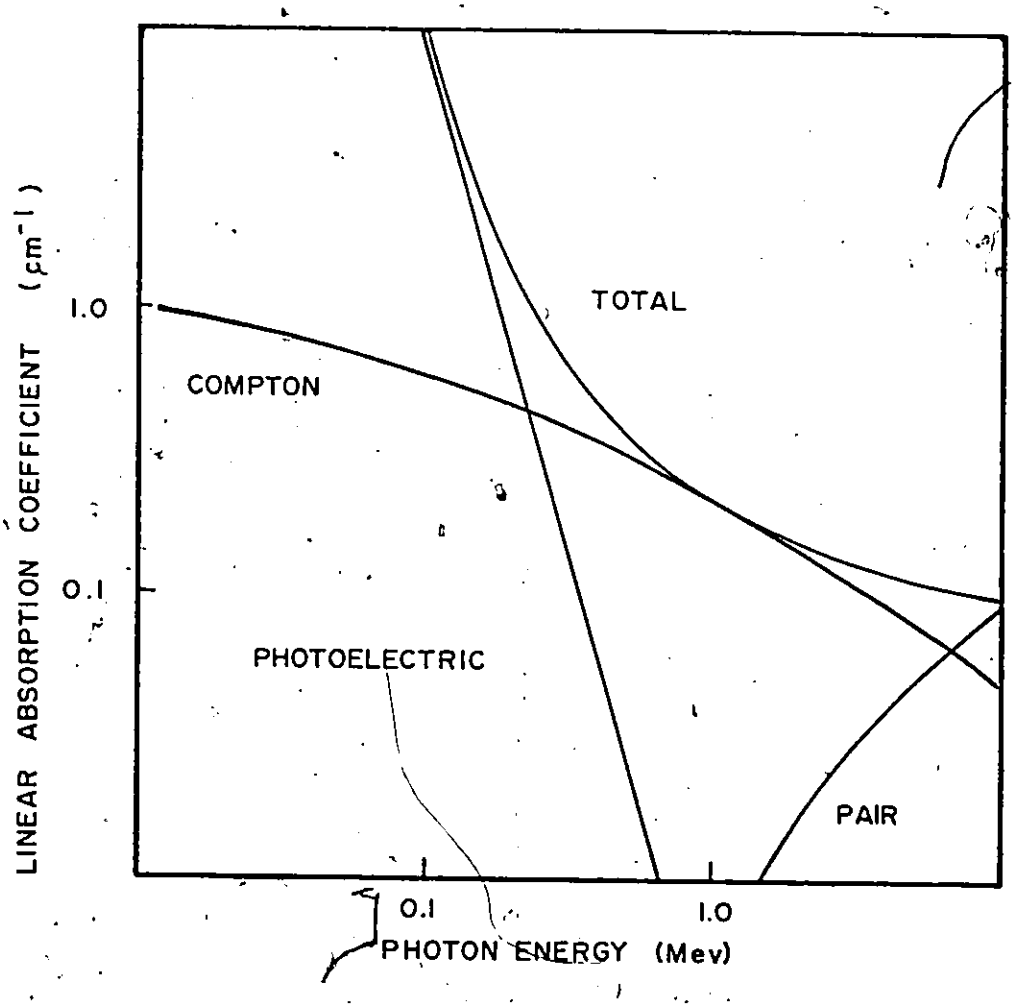

Figure 2.2. Linear absorption coefficents for gamma rays in Ge. After de Soete et al. (60)

$$\sigma = \pi\left(\frac{e^2}{4\pi E_0 m_0 c^2}\right)^2 \left\{ \left[1 - \frac{(2\gamma+1)}{\gamma^2}\right] \ell n(2\gamma+1) + \frac{1}{2} + \frac{4}{\gamma} - \frac{1}{2(2\gamma+1)^2} \right\} \qquad 2.2$$

$$\text{for } \gamma = \frac{E_0}{m_0 c^2}$$

where E_0 is the incident photon energy.

The Compton electron contributes directly to the charge carriers. The scattered photon can then either undergo further Compton scattering, escape from the detector or be absorbed in a photoelectric process. The probability of escape is fairly high in a small detector, giving rise to the large Compton step below each full gamma energy peak that is typical of gamma-ray spectra.

The third process of interaction, and one that is the most important for our work, is that of pair production. In the presence of the large Coulomb field near a nucleus a high energy photon can be completely absorbed and produce an electron-positron pair. For an intermediate energy region, defined by $2m_0c^2 << h\nu << 137m_0c^2Z^{-1/3}$, the cross section for pair production in the field of the nucleus is (En66)

$$\sigma_{pair} = \frac{Z^2}{137}\left(\frac{e^2}{4\pi\varepsilon_0 m_0 c^2}\right)^2\left(\frac{28}{9}\ell n\frac{2h\nu}{m_0c^2} - \frac{218}{27}\right). \qquad 2.3$$

The kinetic energy $E - 2m_0c^2$ is shared by the

electron and positron is transferred to the detector through ionizing collisions. The positron will eventually be annihilated, producing two oppositely directed 0.511 MeV photons. If both of these photons are reabsorbed the detector output pulse represents the full energy peak. If one or both photons escape from the detector the spectrum will show first and second escape peaks that are displaced 0.511 and 1.022 MeV below the full energy peak. Complications arise if the electron and positron do not transfer their full energy to the detector but instead slow down by emitting bremsstrahlung radiation which subsequently escapes from the detector. This results in a continuum of degraded events that are added to the spectrum below each peak. Also the 0.511 MeV photons could lose part of their energy to the detector producing a toe or high energy step on the first and second escape peaks.

Figure 2.2 shows the total absorption coefficient for photons as a function of energy for germanium. The relative contribution of the three processes is also shown and from this it can be seen that the photoelectric effect makes little contribution above 1 MeV.

2.3.3 Pair Spectrometer

If the Ge detector is run in the singles mode, the corresponding spectrum contains all three types of peaks corresponding to the escape of both annihilation quanta, single quanta or none. In addition, there is the Compton continuum produced by inelastic scattering of the incident γ-ray. The elimination of the single escape and full energy peaks and the Compton continuum is made possible by selection of double escape events. To achieve this the Ge detector was surrounded by a quadrisected NaI(Tl) annulus (Ni70). Each of the four NaI(Tl) detectors had separate photomultiplier tubes and was connected to a SCA which was set with proper window to accept 511 keV quanta. The auxiliary circuit was designed to accept only those Ge events for which there was sensed 511 keV quanta by two opposite NaI(Tl) quadrants. This suppresses the single escape and full energy peaks and also the continuum background. Thus a great simplification of the spectra and highly increased peak to background ratio was achieved. The choice of window of the NaI(Tl) detectors was a compromise between the count-rate and the background rejection. After proper investigation the window was set between $511 - 2\sigma$ and $511 + 2\sigma$, σ being 0.425 times the FWHM of the

NaI(Tl) detector. At high energies, the double escape peaks are dominant and thus by eliminating the other peaks, little information was lost. However, not all the double escape events were detected, as many annihilation quanta lost their energy and fell short of the window level. In fact only 20% of the double escape events were ultimately detected. This loss of efficiency was over-compensated by the simplification and improved peak to background ratio of the spectrum.

The pair mode discussed above could not eliminate the following aspects of the response function:

1. Bremsstrahlung Effect: The electrons and positrons following pair creation may emit bremsstrahlung radiation while deccelerating. This gives a bremsstrahlung continuum with a dip just before a peak. The dip results from modulation of the bremsstrahlung cross section with the absorption cross section for low energy photons in the Ge detector.

2. Range Effect: The pair products may themselves escape the detector and this gives rise to a long flat continuum from 0 to E_γ - 1.022 MeV.

3. High Energy Toe: The annihilation quanta may lose some energy by small angle Compton scattering and produce an output in the SCA. This event which deposits

more energy than E_γ - 1.022 MeV in the Ge detector is then detected, causing a characteristic high energy toe in the peak.

The last effect is due to inherent poor resolution of the NaI(Tl) detector and nothing can be done about it. The first two effects can be minimized by proper auxiliary circuitry. To eliminate the first effect, while two annihilation quanta were sensed by opposite NaI(Tl) quadrants, if any radiation above 50 keV was detected in either of the remaining quadrants, the event was rejected. The threshold of 50 keV was chosen because below this there may be cross-talk between the adjacent NaI detectors and moreover, below this energy the escape probability for the bremsstrahlung photons is very small. It may be noticed that instead of going to the third quadrant if the bremsstrahlung radiation would go to either quadrant accepting an annihilation quantum, the event would also be rejected because that would offset the energy outside the window of the SCA, providing the energy was sufficient.

The range effect can be minimized by the method of pulse shape discrimination (Ro75). However, during the present study no circuit was included to eliminate

this effect which was not significant for the present Ge detector.

2.3.4 Electronic Circuitry

The spectrometer and the auxiliary circuits are shown in figure 2.3. Located at the centre of the spectrometer there is a high purity Ge detector (fabricated by Princeton Gamma Tech. Inc.) with efficiency 4% of a 3" by 3" NaI detector. The quadrisected NaI(Tl) annulus (manufactured by the Harshaw Chemical Company) surrounding the Ge detector is 15.2 cm long and has inner and outer diameters of 8.6 and 23.0 cm. The function of the electronic circuit is evident from the discussion in section 2.3.3. The logic provides a final output when there is an event in the Ge detector in time coincidence with the presence of 511 keV photons in two opposite quadrants and in anti-coincidence with the sensing of radiation above 50 keV in any other quadrant.

Encodement of acceptable pair events was achieved through use of a 13 bit NS-621 ADC (manufactured by Northern Scientific Inc.). A dual point NS-454 stabilizer (manufactured by Northern Scientific Inc.) tracked a ^{22}Na source for the zero correction and

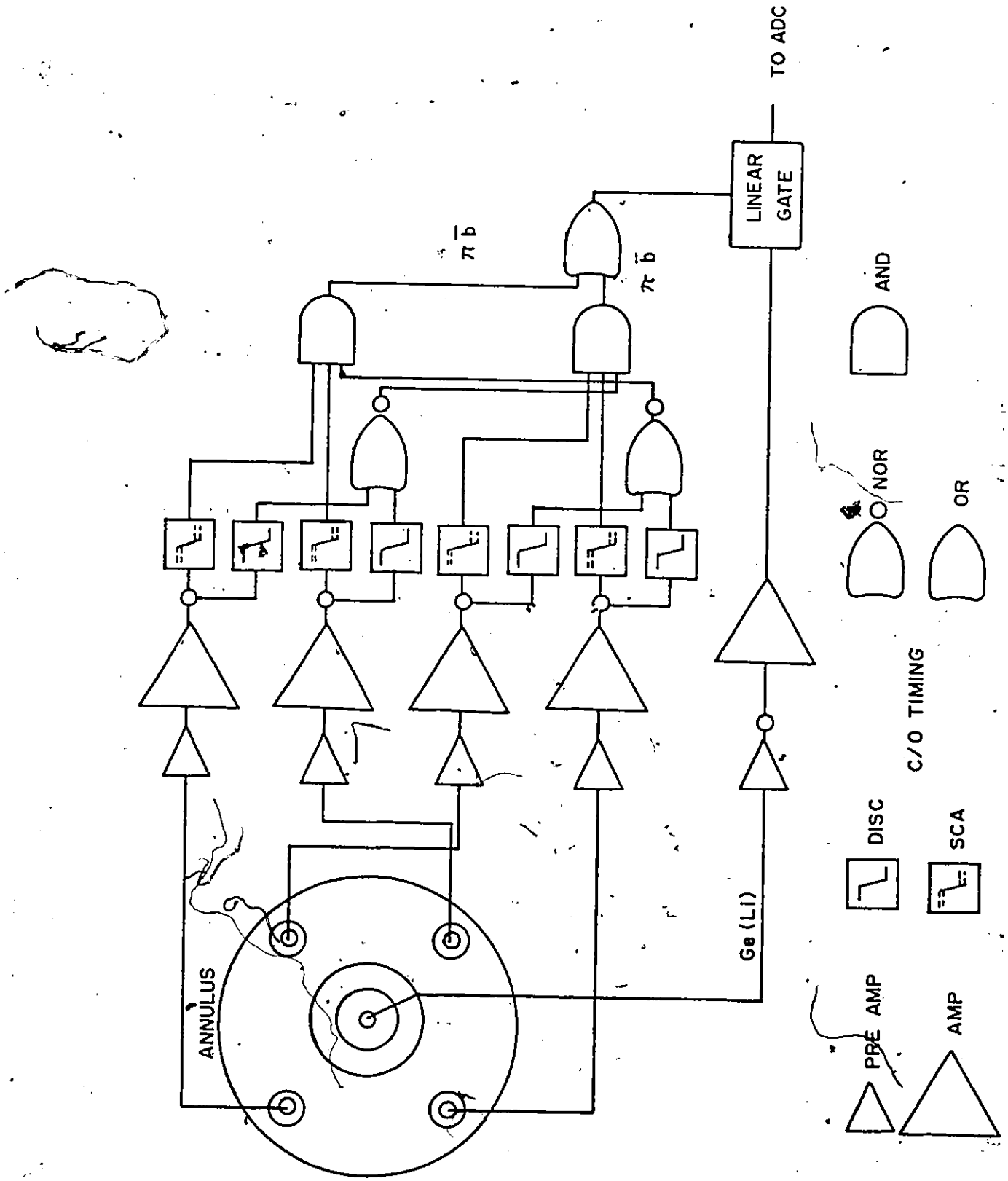

Figure 2.3 Circuit diagram.

a strong isolated high energy transition in each (n,γ) spectrum for gain sensing. This ensured the acquisition of a high resolution spectrum over a long period of time. After encodement the digital information was transmitted over 100 m to a Nova computer dedicated to data logging (Co75). Throughout the present study a gain of approximately 0.74 keV/channel was used for each experiment. The detector resolution in general ranged from 3.0 keV at 4000 keV to 4.1 keV at 7000 keV.

CHAPTER 3

DATA ANALYSIS

3.1 Determination of Peak Area

The area of a photopeak in a complex spectrum can be determined by applying the deconvolution technique. The bulk of intensity values for the dipole transitions tabulated in the present study were determined using this method. For the quadrupole transitions, all of which are extremely weak, the deconvolution method for area measurement was not satisfactory and each of the peaks was analyzed manually using straightforward methods. With respect to the background these peaks fall into three categories:

(a) peaks in the vicinity of a very strong peak,

(b) peaks partially overlapped by another peak with comparable area,

and (c) peaks with a well-defined background.

The areas of the peaks of the first category could not be determined and the peaks were ignored. The region of a peak of the second type was fitted with the method of least squares using a Gaussian model and then the continuum and the overlapping peaks were subtracted

resulting in a residual peak which is the peak of interest. In other words, the fitting can be performed for the region by the function

$$\bar{y}(i) = \sum_{j=1}^{\text{all peaks}} A_j \exp\left\{-\frac{(i-P_j)^2}{2\sigma_j^2}\right\} + \Sigma B_n i^n \qquad 3.1$$

where P_j is the centroid of a peak and the last sum is from n = 0 to 1 or 2 depending on the nature of the continuum. Then the area of the peak of interest j is

$$A = (\text{Data points in the region}) - \sum_{j \neq j} A_j \exp\left\{-\frac{(i-P_j)^2}{2\sigma_j^2}\right\} - \Sigma B_n i^n \qquad 3.2$$

Details of the method and error analysis are discussed in Ref Is79. The third type of peak could be analysed with relative simplicity as is discussed below.

The area of some of the peaks with a well-defined background was determined by simple numerical integration and were corrected for the contribution from the continuum. The latter was estimated from the counts in the regions adjoining the integration limits using the assumption of a linear variation over the region analyzed. Symbolically, the area

$$A = \sum_{i=\ell}^{r} a_i - \left(\frac{r-\ell+1}{2k_1}\right) \sum_{i=\ell-k_1}^{\ell-1} a_i - \left(\frac{r-\ell+1}{2k_2}\right) \sum_{i=r+1}^{r+k_2} a_i, \qquad 3.3$$

where ℓ and r are the channel numbers at the left hand and right hand limit of the peak, k_1 is the number of points on the left side of the peak chosen for background estimation and k_2 is that on the right side. The variance of the peak area is

$$S^2(A) = \sum_{i=\ell}^{r} a_i + \left(\frac{r-\ell+1}{2k_1}\right)^2 \sum_{i=\ell-k_1}^{\ell-1} a_i + \left(\frac{r-\ell+1}{2k_2}\right)^2 \sum_{i=r+1}^{r+k_2} a_i . \quad 3.4$$

For some E2 peaks, only one point adjacent to each side of the peak was used for the background estimation. The relation used for these cases is, by substituting $k_1 = k_2 = 1$ in equation 3.1,

$$A = \sum_{i=\ell}^{r} a_i - (a_{\ell-1}+a_{r+1})\left(\frac{r-\ell+1}{2}\right). \quad 3.5$$

The variation corresponding to equation 3.3 is

$$S^2(A) = \sum_{i=\ell}^{r} a_i + (a_{\ell-1}+a_{r+1})\left(\frac{r-\ell+1}{2}\right)^2 . \quad 3.6$$

The areas of some other E2 peaks and also a limited number of peaks used for efficiency and absolute intensity calibration or for radiative capture cross section determination were determined by taking as many channels in the background as in the peak. This approach where $k_1 = k_2 = \frac{r-\ell+1}{2}$ gives the least relative error and it is applicable if there is no interference in the

background within the integration limit. Here, equation 3.1 takes the form

$$A = \sum_{i=\ell}^{r} a_i - \sum_{i=\ell-\frac{r-\ell+1}{2}}^{\ell-1} a_i - \sum_{i=r+1}^{r+\frac{r-\ell+1}{2}} a_i \qquad 3.7$$

which can be abbreviated as,

$$A = G - B_1 - B_2, \qquad 3.8$$

where G and B are gross counts and background respectively. The standard deviation of the peak area is simply,

$$S(A) = G+B_1+B_2 \qquad 3.9$$

Because of the weakness of the E2 transitions and the sensitivity of the peak areas to minor interference in the background, equation 3.5 instead of equation 3.7 was used more often to determine the areas:

3.2 Automatic Centroid and Area Determination

The effectiveness of data reduction is indicated by the amount of information that can be reliably extracted from the acquired data with a minimum of interaction in the procedure by the experimentalist. A high degree of automation is specially needed for the complete analysis of (n,γ) spectra which often spans thousands of channels and hundreds of components.

3.2.1 Zero Area Filter

The zero area filter (Ro72) method is highly automated and noninterventive in determining centroids and areas of peaks. In this method, the convolution with a zero area filter yields a resultant spectrum which is virtually free from background. Although it is fast, simple and precise and does not require previous subtraction of the continuum residing beneath the structure of interest, it is primarily applicable only in the case where the spectrum is composed of isolated components or when only prominent structure is sought. It cannot be applied successfully to a complex spectrum with closely spaced components.

3.2.2. Deconvolution

The pair-spectrometer used in this study exhibits a resolving power at the limit of currently achievable values. The only way to remove to some extent the constraints of the existing resolution is to be sought in the data reduction method. A deconvolution algorithm constrained to positivity of solution has been reported (Ke78a, 78b, 78c) and is ideally suited for general spectral analysis, particularly for complex structure. This algorithm, which is iterative in nature,

retains both area and centroid. The operation entails low magnification in noise. The deconvolved spectrum shows single components which occupy only two channels and a simple search routine can readily determine the centroid and area.

In Ref. Ke78a, the iterative algorithm based upon Bayes' postulate is developed, following the initial work of Richardson (Ri72). Using matrix notation, iterations can be expressed as

$$T_i^{(n+1)} = T_i^{(n)} \sum_k \frac{R_{k,i} M_k}{\sum_j R_{kj} T_j^{(n)}} \qquad 3.10$$

where $T_i^{(n)}$ is the estimate of the sought signal T after n iterations, R is the response matrix and M the measured spectrum.

In the present study, the response function can be represented well by a Gaussian function modified by the finite channel width. The speed of the algorithm, which is iterative, is increased if the response function is stationary. An examination of the energy dependence of the resolution indicated that 512 channel intervals could be considered as quasistationary while, beyond this range, the width changed sufficiently so as to reduce the effectiveness of the procedure. Generally the number of iterations was adjusted in such a way that when no

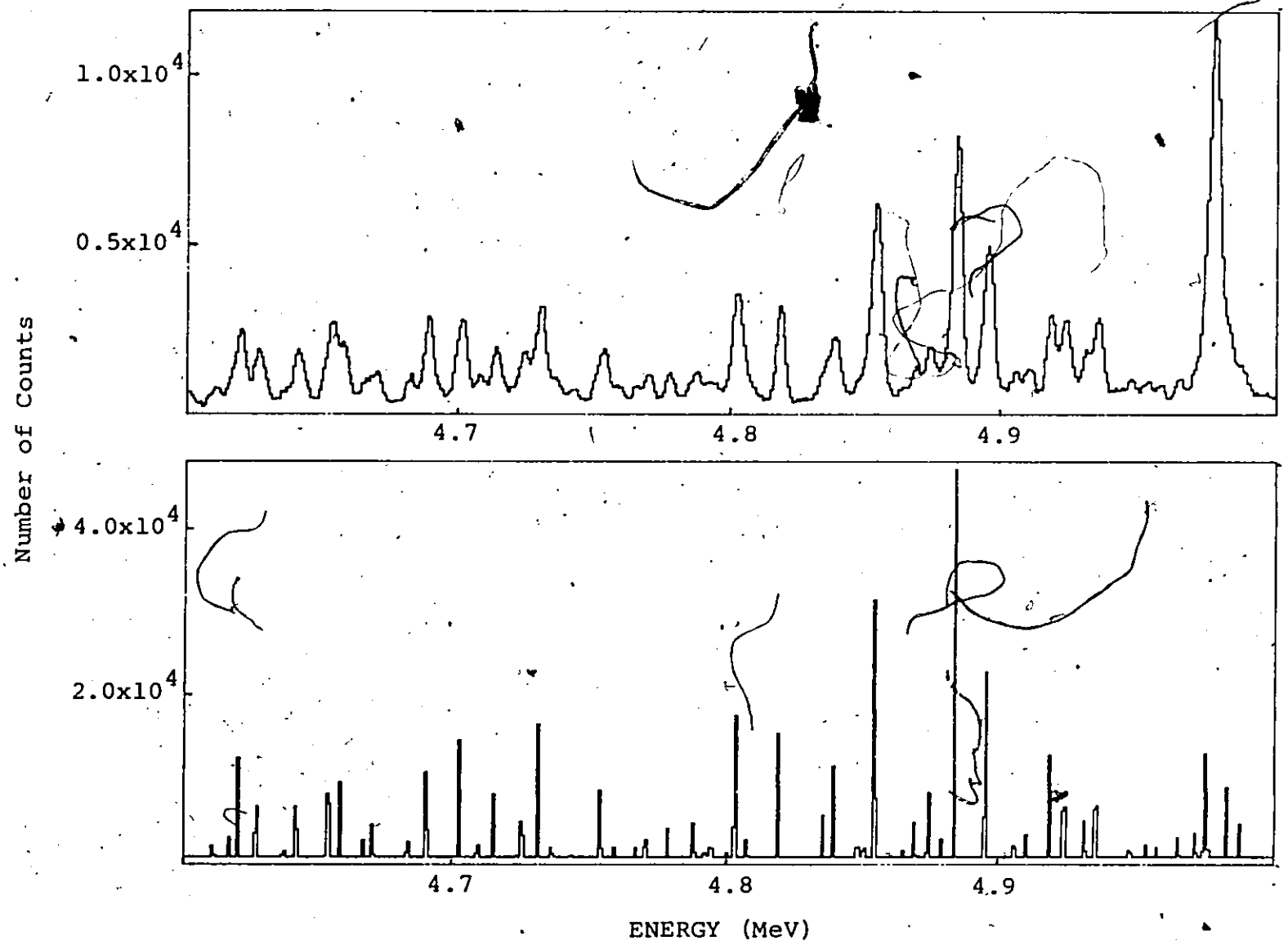

Figure 3.1. The $^{165}Ho(n,\gamma)$ spectrum is shown. The upper portion illustrates the experimental data while the lower, the deconvolved spectrum.

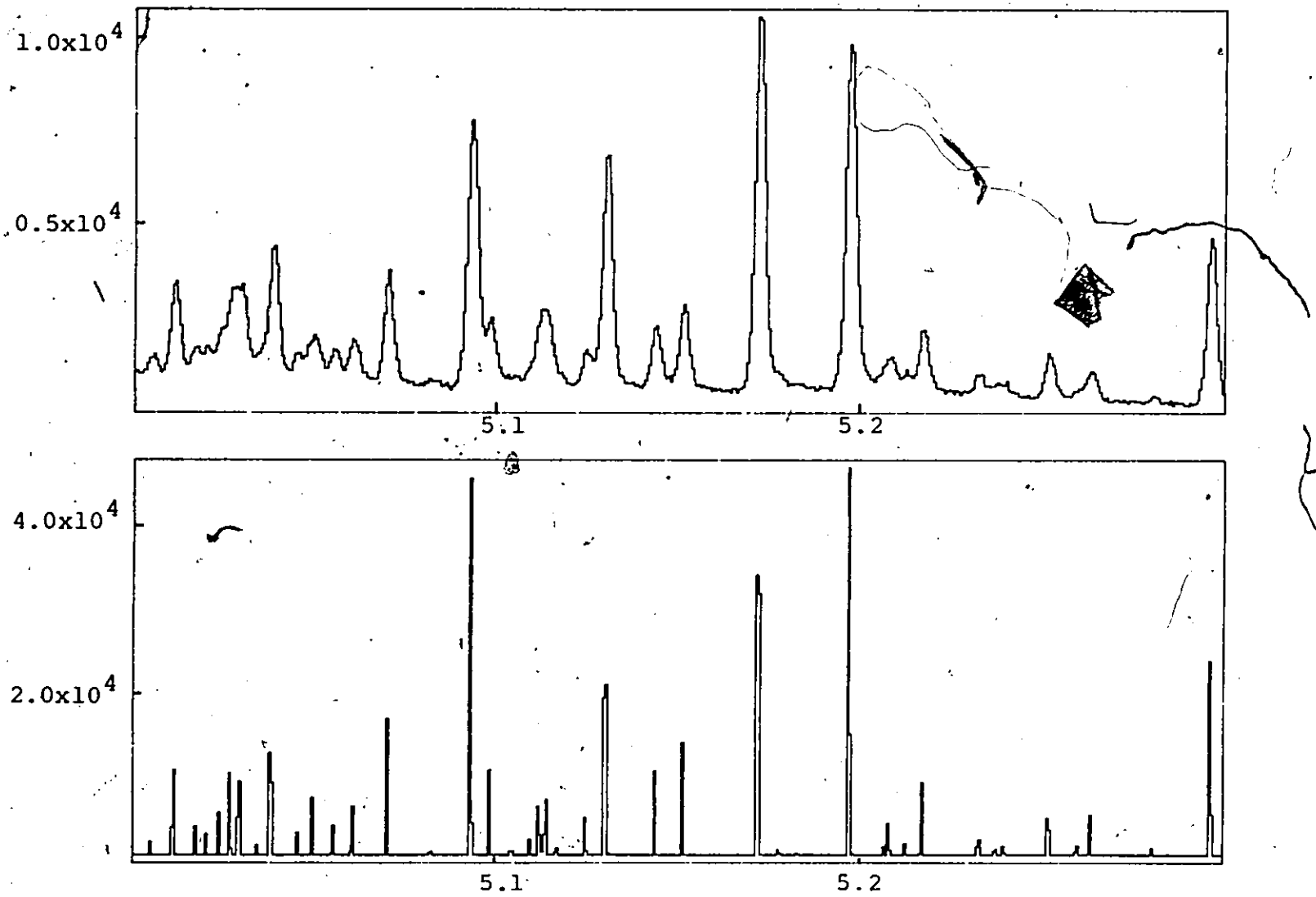

Figure 3.1 (cont'd.)

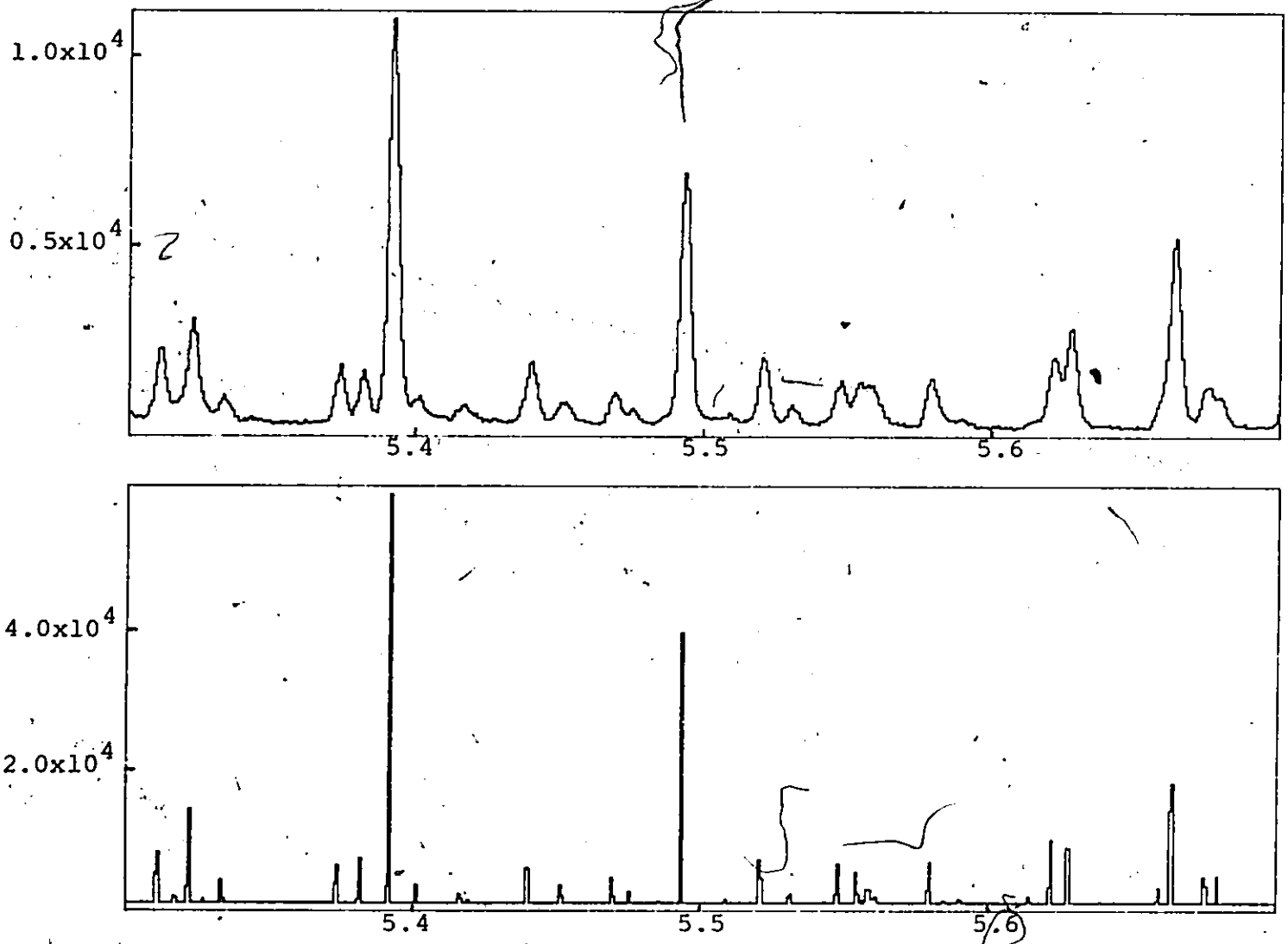

Figure 3.1 (cont'd.)

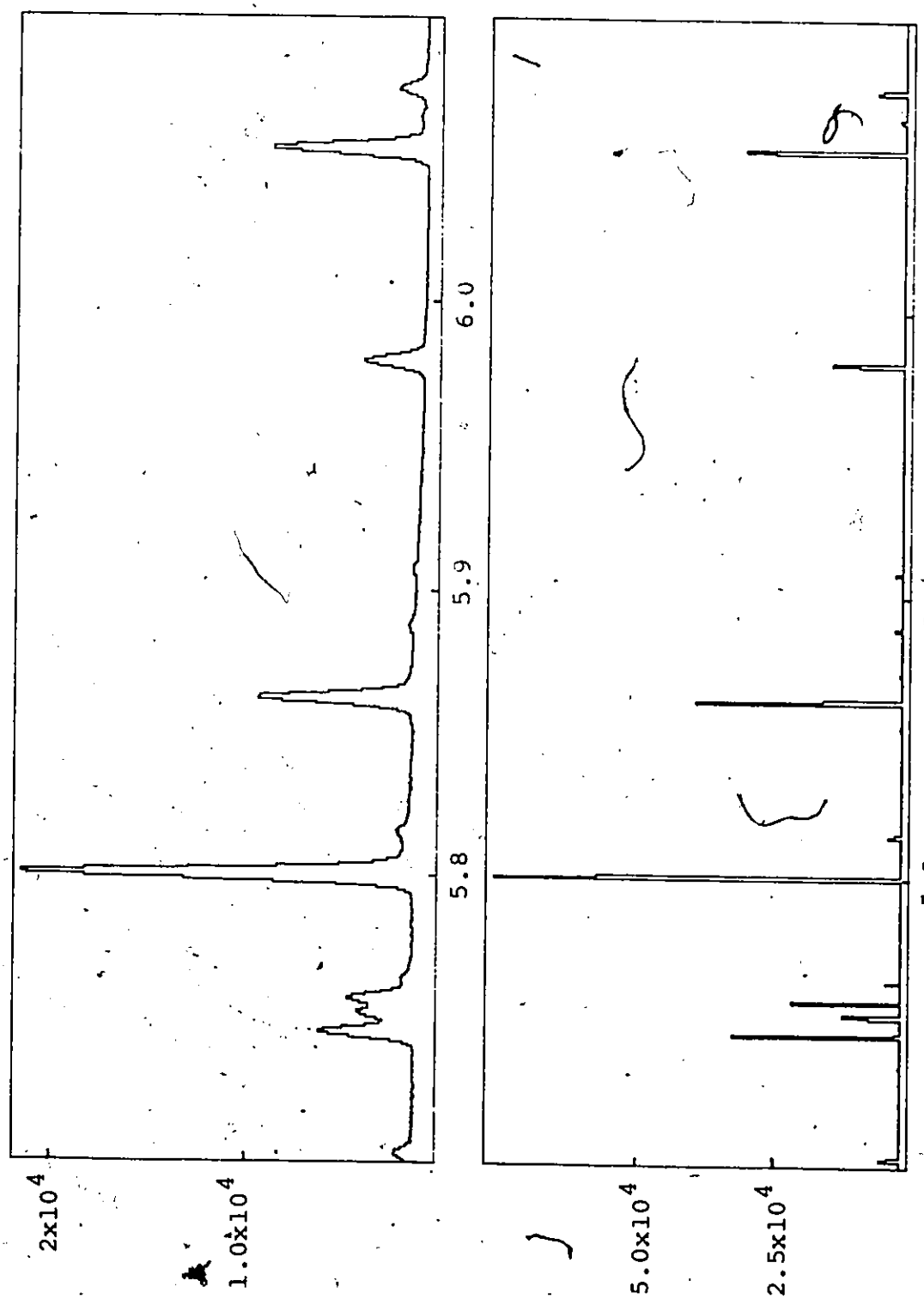

Figure 3.1 (cont'd.)

significant change occurred between iterations, the procedure was stopped. Usually this resulted in at least 5000 iterations being necessary for closely spaced multiplets. For the Nova 2 computer used, 0.7 s were required for each iteration when a 512 channel record was processed. It is always necessary to remove the background or underlying continuum in the original spectrum before the deconvolution is carried out. In this study, the prominent toes of the peaks arising from small angle scattering of the annihilation radiation and the remaining background were both removed by using the automated background extraction technique mentioned in Ref. Ke81c. For illustration, in figure 3.1, the original and deconvolved spectrum of an arbitrary nucleus ^{166}Ho between 4.5 and 6 MeV is shown. The multiplets in the spectrum have been clearly resolved into its components in the deconvolved spectrum.

3.3 Energy Calibration

The accuracy of energy standards is often a constraint in (n,γ) spectroscopy by Ge detectors. The reaction $^{14}N(n,\gamma)^{15}N$ has been frequently used for energy calibration and there have been successive reports of the precise values for nitrogen lines (Gr74, Is74, St78,

Gr79, Gr80, Ke81, Gr80a), the last two reports deserving special attention. Kennett et al. determined a comprehensive set of energies for Cl transitions with an overall accuracy of 0.10 keV and on the basis of these they reproduced a set of energies for the $^{14}N(n,\gamma)^{15}N$ reactions. At about the same time Greenwood et al. (Gr80) reported another set of precise values for the nitrogen transitions which agree within 0.1 keV with those of Kennett et al. The consistency of these studies gives some confidence in the values of N and Cl lines.

The transitions in either $^{14}N(n,\gamma)^{15}N$ or $^{35}Cl(n,\gamma)^{36}Cl$ were used for energy calibration on different occasions. The energy scale in this work was found to be linear in two different regions, one greater and the other less than 5 MeV. For low energy calibrations, other reactions used were $^{1}H(n,\gamma)^{2}H$ and $^{12}C(n,\gamma)^{13}C$.

The various transitions used for energy calibration are presented in table 3.1. The centroid to energy transformation function was determined by a linear least-squares fit to the energies of suitable transitions.

TABLE 3.1

Energy Standards

Nitrogen[a] lines (keV)	Chlorine[a] lines (keV)	Other lines Energy (keV)	Identity	Ref.
1884.85	3061.80	4945.319	C	b
1999.71	3821.61	2223.25	H	b
2520.52	3981.06			
3532.01	4440.61			
3677.79	4944.61			
4508.72	4979.81			
5269.14	5517.38			
5297.78	5715.30			
5533.33	5902.96			
5562.04	6111.00			
6322.46	6628.02			
7299.06	6978.09			
	7414.17			

[a]Ref. Ke81
[b]Ref. Gr79
[c]Ref. Le78

3.4 Calibration of Detection Efficiency

To measure the intensity of transitions, it is necessary to know the variation in the system efficiency with energy. This is determined in general by the variation of the pair creation cross section in germanium modified by such factors as radiative energy loss and electron escape from the detector. In this study the beam is filtered with a plastic absorber that also introduces an energy-dependent transmission factor. The absolute efficiency at energy E_i is

$$\varepsilon_{abs}(E_i) = k\frac{A_i}{I_i}, \qquad 3.11$$

where A_i = area of the peak in the spectrum produced by photons with energy E_i having absolute intensity I_i,

k = overall normalizing factor involving the total number of captures that have produced the spectrum.

For our purpose, only knowledge of the relative efficiency is needed, and it is given by

$$\varepsilon_i = \frac{A_i}{I_i} \qquad 3.12$$

To arrive at a relative efficiency function for the

TABLE 3.2

Intensity Values from $^{14}N(n,\gamma)^{15}N$ Reaction Used for Efficiency Calibration

Energy (keV)	Absolute[a] Intensity (%)	Absolute Error
1885	19.7	1.0
2521	6.2	0.2
2831	2.0	0.1
3532	9.7	0.2
3678	14.9	0.3
4509	16.6	0.3
5269	30.1	0.4
5298	21.1	0.3
5533	20.0	0.3
5562	10.7	0.2
6322	18.8	0.3
7299	9.6	0.2

[a]Only for 1885 keV transition, Ref. Th67 was used and for the rest Ref. Ke80 were used.

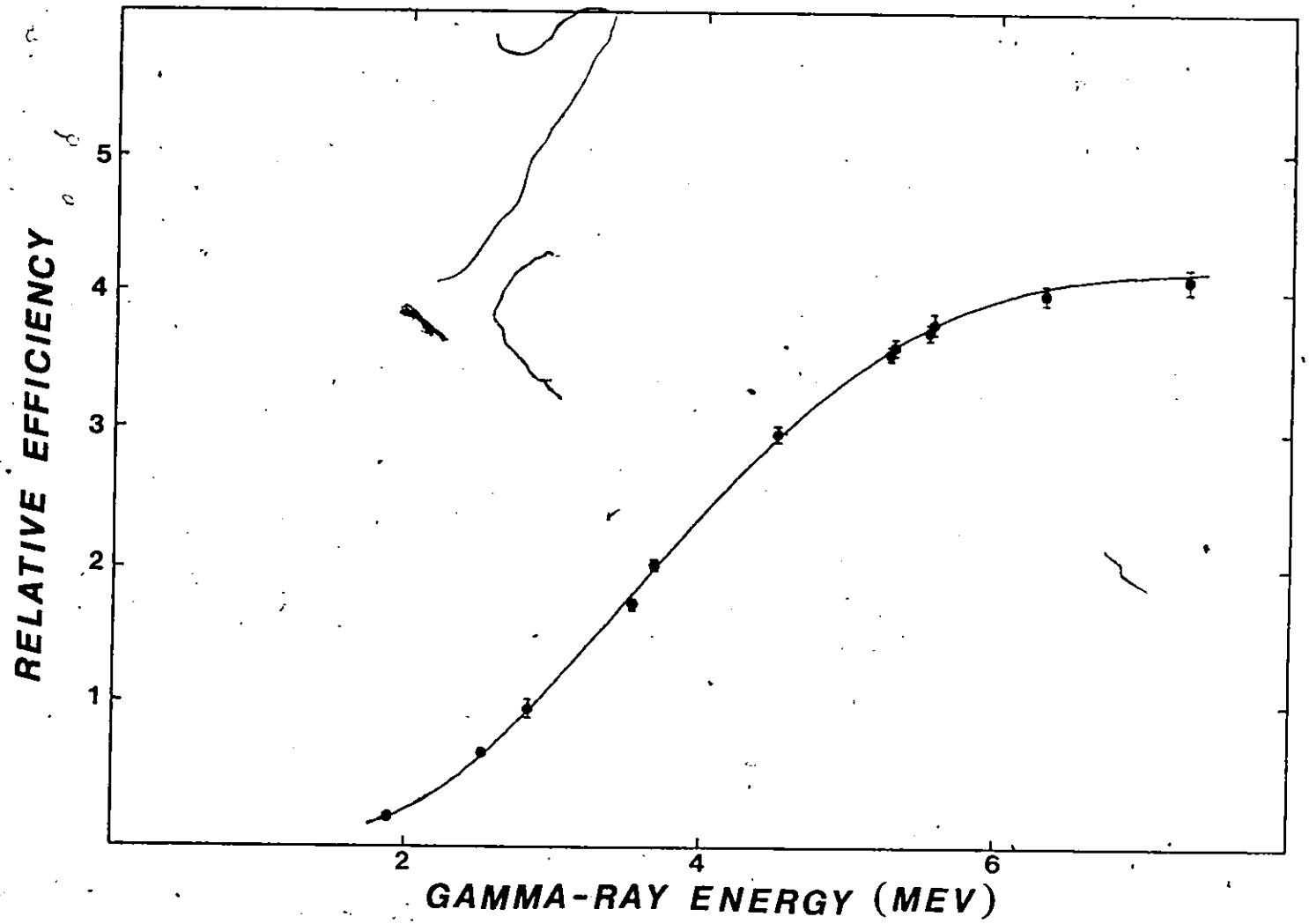

Figure 3.2. Variation of detection efficiency with incident energy

system, a standard with well-known intensities is needed. We used the reaction $^{14}N(n,\gamma)^{15}N$ for which precise values of intensities are available (Ke80, Th67). The transitions used for the calibration are presented in table 3.2. A smooth calibration curve is determined from a weighted linear least squares fit of the data points ε_i to the polynomial

$$\varepsilon_i(x) = a_1x + a_2x^2 + a_3x^3 + a_4x^4 \qquad 3.13$$

where $x = E - 2m_0c^2$ is the kinetic energy of the electron-positron pair. The analysis yielded a value of χ^2/f of 0.78. The variation of detection efficiency with incident energy is shown in figure 3.4.

A nitrogen spectrum accumulated over two days was used for this intensity calibration. Besides, the nitrogen transitions in different mixed calibration samples were exploited occasionally to search for changes in the efficiency profile of the system as a function of energy. No significant variation was noted during the series of experiments.

3.5 Reduction of Average-Resonance Data from Literature for E2 Strength Study

The Average-Resonance Method, developed by Bollinger and Thomas (Bo67, Bo68), involves many

resonances in the capture state and the intensities in the spectrum are essentially the averages of intensities due to individual resonances. Thus the P-T fluctuation is greatly reduced so that not only all the E1 and M1 primary transitions, but also the primary E2 transitions are likely to be detected. However in the case of average resonance capture, the E2 transition may be contaminated appreciably by p-wave capture followed by an E1 transition.

A complete literature survey shows several E2 primary transitions have been observed in average-resonance experiments. The transitions along with the references are displayed in table 3.3.

3.5.1 Normalizing Intensities of Average-Resonance Data

The intensities of transitions in all the average resonance data are given as relative intensities. To obtain the absolute intensities of E2 transitions, conversion factors were calculated in the present study. Each of the average spectra was compared with its corresponding thermal spectrum either from literature or from this work. It was assumed that a thermal spectrum is a sample from the spectra whose average is the average-resonance spectrum. This neglects the

TABLE 3.3

Average-Resonance Data from Literature

Final Nucleus	E (keV)	Populatd. level (keV)	Capture state spin	Final state spin	Ref.
^{106}Pd	9562	0	$2^+,3^+$	0^+	Bo70
	7856	1705		0^+	
^{150}Sm	6823	1166	$3^-,4^-$	1^-	Bu70
^{166}Ho	6161	82	$3^-,4^-$	1^-	Bo70
^{168}Er	7223	548	$3^+,4^+$	6^+	Bo70
	6507	1264		(6^+)	
^{180}Hf	7295	93	$4^+,5^+$	2^+	
	6189	1199		2^+	
	6128	1260		(2^+)	
	6088	1301		(2^+)	Bu74
	5751	1637		(2^+)	
	5664	1724		(2^+)	

possibility of significant p-wave capture in the resonance-averaged spectra. The primary E1 and M1 transitions in both spectra were used for the calculation. The relative intensities of all E1 and M1 transitions with energies between ~0.7 S_n to S_n were summed. The absolute intensities in the corresponding thermal spectrum were added. In the latter case, where the P-T fluctuation was present in an individual transition, the summation decreased the fluctuation reducing the relative standard deviation of the summed value to $(2/N)^{1/2}$, where N is the number of transitions (Bo70a). In the case of both thermal and average capture, the sum of the absolute intensities of the transitions was assumed to be equal. This equality gave the conversion factor for a nucleus. The factor was used to transform the relative intensities of the quadrupole transitions into absolute intensities. Since this conversion is crucial, a summary of the above treatment for the nuclei is given in table 3.4. The absolute intensities were then converted into partial widths.

TABLE 3.4

Summary of Conversion of Relative Intensity of Average Work into Absolute Intensity

Final Nucleus	Minimum energy of primary (keV)	No. of dipole primaries considered	Ref. for relative intensity of average work	Ref. for absolute intensity of thermal work
^{106}Pd	6971	17	Bo70	Co71[a]
^{150}Sm	5893	18	Bu70	Ba76
^{166}Ho	5684	18	Bo70	b
^{168}Er	6155	17	Bo70	b
^{180}Hf	5073	23	Bu74	b

[a]This is a resonance spectrum with E_n = 11.8 eV

[b]This work

3.5.2 Correction for P-wave Capture E1 Transition

As the intensities are averages over many resonances, the P-T fluctuation is greatly reduced. But because of the weakness of E2 transitions, any small contribution from E1 radiation following p-wave capture may be comparable in the case of average resonance capture. (To illustrate the p-wave contribution let us assume a target nucleus with spin 0^+. If the capture is S-wave, the capture state with spin $1/2^+$ will decay to a $5/2^+$ lower-lying level radiating an unmixed E2 transition. If there is p-wave capture, the initial state will have spins $1/2^-$ or $3/2^-$ and the $3/2^-$ state may decay to the same $5/2^+$ state through an E1 transition. Thus in the pulse-height spectrum, the E2 transition and the p-wave capture E1 transition will be superimposed). For the typical neutron energies at which these reactions occur, the penetrability factor for p-wave neutrons increases and thus p-wave capture is enhanced. In this section a working formula is developed and then applied to make corrections for p-wave capture E1 transitions which are mixed with the quadrupole transitions.

3.5.3 Theory

In the average resonance experiment, a ^{10}B filter reshapes the remaining 1/E neutron spectrum by cutting off the low energy neutrons. Although the ^{10}B filter has no effect on the high energy neutrons, the 1/E dependence causes this region to fall off in intensity. This essentially limits the band of neutron energies broad enough to contain many resonances but narrow enough to preserve the high resolution of the Ge(Li) detector and low enough to limit the capture to s-wave and p-wave. The neutron flux passing through the filter is (Lo73)

$$\phi(E) = \frac{\phi_0}{E} e^{-a/\sqrt{E}} \quad \text{(E is in eV)} \qquad 3.14$$

$$a = 36.7x$$

where x is the thickness of the ^{10}B filter in g/cm^2.

The total number of average resonance captures of ℓ-wave neutrons

$$Y_\ell = \int \bar{\sigma}_\ell(E)\,\phi(E)\,dE \qquad 3.15$$

where $\bar{\sigma}_\ell(E)$ is the average cross section of the ℓ-wave resonances at E.

The cross section $\bar{\sigma}_\ell(E)$ can be expressed in terms of resonance parameters as follows:

$$\bar{\sigma}_\ell(E) = \frac{1}{\Delta E}\int_{E-\Delta E/2}^{E+\Delta E/2} \sum_{Jr}\sum \pi\lambda^2 \frac{g_J \Gamma_{nr}\Gamma_{\gamma r}}{(E-E_r)^2+\frac{\Gamma_r}{4}^2}\, dE$$

$$= 2\pi^2\lambda^2 P_\ell(E) \sum_{Jr}\sum \frac{g_J \Gamma_{nr}^{\ell}\Gamma_{\gamma r}}{\Gamma_r \Delta E} \qquad 3.16$$

where $g_J = (J+1)/\,2(J_t+1)$, J and J_t being the spins of the capture state and target nucleus respectively. The penetrability factor $P_\ell(E)$ is given by

$$P_0 = \sqrt{E}$$

$$P_1 = \sqrt{E}\,\frac{K^2R^2}{1+K^2R^2} \qquad 3.17$$

where it can be shown that $(KR)^2 = 7.29\times10^{-8}E(eV)A^{2/3}$.

Equation 3.16 can be further reduced to

$$\bar{\sigma}_\ell(E) = F_\ell(E) \left\langle\frac{\Gamma_\gamma}{\Gamma}\right\rangle_\ell \sum_J g_J \frac{N_J \langle\Gamma_{\gamma J}\rangle}{\langle D_J\rangle N_J}$$

$$= F_\ell(E) \left\langle\frac{\Gamma_\gamma}{\Gamma}\right\rangle_\ell S_n^\ell \sum_J g_J \qquad 3.18$$

The partial cross section for a transition i is

$$\bar{\sigma}_{\ell i}(E) = F_\ell(E) \left\langle\frac{\Gamma_{\gamma i}}{\Gamma}\right\rangle_\ell S_n^\ell\, g_J \qquad 3.19$$

Thus the p-wave and s-wave yields are

$$Y_{1i} = \left\langle\frac{\Gamma_{\gamma i}}{\Gamma}\right\rangle_1 S_n^1 g_{J'} \int F_1(E)\,\phi(E)\,dE \qquad 3.20a$$

$$Y_{0i} = \left\langle\frac{\Gamma_{\gamma i}}{\Gamma}\right\rangle_0 S_n^0 g_J \int F_0(E)\,\phi(E)\,dE \qquad 3.20b$$

where J' and J are the initial state spins for the p-wave capture E1 and s-wave capture E2 transitions respectively.

The ratio of the p-wave to s-wave contribution is,

therefore,

$$Y_{1i} = \frac{\langle\Gamma_{\gamma i}\rangle_1}{\langle\Gamma_{\gamma i}\rangle_0} \frac{\langle\Gamma\rangle_0}{\langle\Gamma\rangle_1} \frac{S_n^1}{S_n^0} \frac{g_{J'}}{g_J} \frac{\int F_1(E)\phi(E)dE}{\int F_0(E)\phi(E)dE} \qquad 3.21$$

In the above equation,

$$\frac{\langle\Gamma_{\gamma i}\rangle_1}{\langle\Gamma_{\gamma i}\rangle_0} \equiv \frac{\langle\Gamma_{\gamma i}\rangle_{E1}}{\langle\Gamma_{\gamma i}\rangle_{E2}} = \frac{D_{J'}S(E1)}{D_J S(E2)} \approx \frac{(2J+1)}{(2J'+1)} \frac{S(E1)}{S(E2)}, \qquad 3.22$$

(where the exponential part of D is neglected)

$$\frac{\langle\Gamma\rangle_0}{\langle\Gamma\rangle_1} = \frac{\langle\Gamma_n+\Gamma_\gamma\rangle_0}{\langle\Gamma_n+\Gamma_\gamma\rangle_1} \approx \frac{\langle\Gamma_\gamma\rangle_0}{\langle\Gamma_\gamma\rangle_1}, \qquad 3.23$$

and

$$\frac{g_{J'}}{g_J} = \frac{(2J'+1)}{(2J+1)} \qquad 3.24$$

Thus finally the ratio of the p-wave to the s-wave contribution is

$$\frac{Y_{1i}}{Y_{0i}} = \frac{S(E1)}{S(E2)} \frac{S_n^1}{S_n^0} \frac{\langle\Gamma_\gamma\rangle_0}{\langle\Gamma_\gamma\rangle_1} \frac{\int F_1(E)\phi(E)dE}{\int F_0(E)\phi(E)dE} \qquad 3.25$$

The values of S_n^ℓ and $\langle\Gamma_\gamma\rangle$ were taken from Ref. Mu73 and Mu81. The value of S(E1)/S(E2) was estimated using the average resonance data. The integrals are evaluated in Appendix C. The quantity a present in the integrals is obtainable from equation 3.14 using the thickness of the ^{10}B filter in the individual average-resonance experiment.

The ratio of the partial to the total s-wave cross section is

$$\frac{\bar{\sigma}_{0i}(E)}{\bar{\sigma}_0(E)} = \frac{\left\langle\frac{\Gamma_{\gamma i}}{\Gamma}\right\rangle_0}{\left\langle\frac{\Gamma_\gamma}{\Gamma}\right\rangle_0} \frac{g_J}{\Sigma g_J},$$

from which the relation between I_γ and $\Gamma_{\gamma i}$ is found to be

$$\Gamma_{\gamma i} = I_\gamma \Gamma_\gamma \frac{\Sigma g_J}{g_J} \qquad 3.26$$

3.5.4 Corrected Widths of E2 Transitions in Average Capture

To estimate the correction for p-wave contribution to the E2 transitions in the average data from literature the quantity S(E1)/S(E2) was determined from the average-resonance spectrum of ^{166}Ho (Bo70) and ^{180}Hf (Bu74). In the first approximation, the contaminated E2 intensity was used to determine the ratio S(E1)/S(E2) which was used to estimate Y1/Y0. Then again the same procedure was carried out with the corrected E2 intensity. The process virtually converged after 2 iterations giving a value of 45 for S(E1)/S(E2). The thicknesses in g/cm^2 of ^{10}B filter for ^{106}Pd, ^{166}Ho and ^{168}Er were obtained directly from the literature (Bo70), while for ^{150}Sm (Bu70) and ^{180}Hf (Bu74) it was deduced from the given ^{10}B thickness in cm by using a density of 2.4 g/cm^3.

TABLE 3.5

P-Wave Correction for Average-Resonance Quadrupole Transitions

Final Nucleus	^{10}B thickness (g/cm^2)	$\frac{\langle \lambda^2 P_1 \rangle}{\langle \lambda^2 P_0 \rangle}$	$\frac{S_n^1}{S_n^0}$	$^b\frac{\langle \Gamma_\gamma \rangle S}{\langle \Gamma_\gamma \rangle P}$	Percentage[c] of p-wave contribution
^{106}Pd	0.27	0.021	12.5	1.1	93
^{150}Sm	0.76[a]	0.069	0.16	0.75	27
^{166}Ho	0.107	0.0093	0.6	0.9	18
^{168}Er	0.43	0.039	0.6	0.9	49
^{180}Hf	0.38[a]	0.036	0.2	0.9	22

[a] Density of 2.4 g/cm^3 assumed for ^{10}B

[b] Ref. Mu73

[c] A fixed value of 45 used for S(E1)/S(E2)

TABLE 3.6

Average-Resonance Widths

Final Nucleus	E_γ (keV)	[a] p-wave Corrected I_γ (per 10^4)	[b] Γ_γ (meV)	[c] $\Gamma_{\gamma i} = \Gamma_\gamma I_\gamma$ (meV)	$\frac{\Sigma g_J}{g_J}$
^{106}Pd	9562	<0.28	145	<0.0097	
	7856	<0.08		<0.0028	
^{150}Sm	6823	0.15	62	0.0022 (10)	
^{166}Ho	6161	0.23	75	0.0040 (20)	
^{168}Er	7223	<0.39	88	<0.0061	
	6507	<0.34		<0.0054	
^{180}Hf	7296	0.92	62	0.0127 (60)	
	6189	0.37		0.0051 (20)	
	6128	0.45		0.0062 (30)	
	6088	0.47		0.0064 (30)	
	5751	0.37		0.0051 (22)	
	5665	0.40		0.0056 (27)	

[a] Corrected and normalized in the present study.

[b] Ref. Mu73

[c] Sum in the numerator is over the two capture states and J is spin of the E2 decaying state.

The percentage of p-wave capture E1 transition in the average quadrupole transitions and the quantities used to estimate the percentage are presented in table 3.5. As expected, the contamination is by far the worst for ^{106}Pd as the p-wave neutron strength function is very high in this mass region. Due to the thin ^{10}B filter used for ^{166}Ho the p-wave contribution is least in this case. The p-wave contribution was then subtracted from the gamma-widths of all the average resonance quadrupole transitions. The corrected widths are presented in table 3.6.

3.5.5 Possibility of P-Wave Contribution to the Present Thermal Data

Since the ratio between the thermal and the epi-cadmium flux (ϕ_{th} and ϕ_0) of neutrons in our reactor is 1/20 (Ke82), there is a possibility that p-wave capture may contribute to the (n,γ) reaction in this study. It is, therefore, necessary to make a calculation for such a contribution. The worst case for the calculation was analyzed, so that if the contribution is negligible here, the same would hold true for the rest of the nuclides studied. This topic is discussed here instead of the place where our thermal data is discussed for two reasons. The most part of this section uses the concept

of section 3.5.3. More importantly, some concepts introduced here will be referred to in a subsequent section.

To begin with, one needs to know the resonance integral which, for the (n,γ) reaction, is defined by

$$I_R = \int_{Ec}^{\infty} \sigma_\gamma(E) \frac{dE}{E} \qquad 3.27$$

where E_c is determined by the cadmium cut-off energy. The resonance integral assumes that the dE/E neutron spectrum is not perturbed by the absorbing material. The value of I_R for a nuclide is, in general, a known quantity (Mu73). The ratio of the total p-wave and s-wave neutron capture is given by

$$\frac{Y_P}{Y_S} = \frac{\phi_{th}\bar{\sigma}^P_{th} + \phi_0 I^P_R}{\phi_{th}\bar{\sigma}^S_{th} + \phi_0 I^S_R}$$

$$= \frac{\bar{\sigma}^P_{th} + (1/20) I^P_R}{\bar{\sigma}^S_{th} + (1/20) I^S_R} \qquad 3.28$$

where $\bar{\sigma}^S_{th}$ and $\bar{\sigma}^P_{th}$ are the average thermal radiative capture cross sections of s-wave and p-wave neutrons; I^P_R and I^S_R resonance integrals due to p-wave and s-wave captures.

To assess the splitting of I_R into I^P_R and I^S_R for the target nucleus ^{162}Dy, a model similar to that in section 3.5.2 is used. The only difference here is the

absence of any ^{10}B filter and thus the presence of a simple ϕ_0/E neutron spectrum. The number of captures of ℓ-wave neutrons is given by equation 3.20

$$Y_\ell = \left\langle \frac{\Gamma_\gamma}{\Gamma} \right\rangle_\ell S_n^\ell \sum_J g_J \int_{0.5}^{\infty} F_\ell(E)\,\phi(E)\,dE$$

which may be written as

$$Y_\ell = \phi_0 \left\langle \frac{\Gamma_\gamma}{\Gamma} \right\rangle_\ell S_n^\ell \sum_J g_J \int \frac{F_\ell(E)}{E} dE$$

$$= \phi_0 \left\{ S_n^\ell \sum_J g_J \int \frac{F_\ell(E)}{E} dE \right\}$$

$$= \phi_0 \, I_R^\ell \qquad 3.29$$

where I_R^ℓ is the ℓ-wave resonance integral.

For s-wave capture,

$$\int \frac{F_0(E)}{E} dE \sim \int_{0.5}^{\infty} \frac{1}{E^{3/2}} dE = 2.83 \qquad 3.30$$

For p-wave capture,

$$\int \frac{F_1(E)}{E} dE \sim \int_{0.5}^{\infty} \frac{C_1 E}{1+C_1 E} \frac{1}{E^{3/2}} dE, \quad C_1 = 7.29 \times 10^{-8} A^{2/3}$$

$$= 4.6 \times 10^{-3} \qquad 3.31$$

The values of neutron strength functions for ^{162}Dy are (Mu73)

$$S_n^0 \approx 1.6\times10^{-4}$$

$$S_n^1 \approx 1\times10^{-4}$$

Thus

$$I_R^P \sim 1\times10^{-4}\times4.6\times10^{-3} = 1.4\times10^{-6} \qquad 3.32$$

and, $$I_R^S \sim 1.6\times10^{-4}\times2.83 = 4.5\times10^{-4} \qquad 3.33$$

Since the value of I_R for ^{162}Dy is 2730 b (Mu73),

$$I_R^P \sim 8 \text{ b} \qquad 3.34$$

$$I_R^S \sim 2730 \text{ b}$$

The average thermal cross section

$$\bar{\sigma}_\ell \propto \frac{\int \frac{\Gamma_\ell}{\Sigma\Gamma_\ell}\sigma(E)\phi(E)dE}{\int \phi(E)dE}, \qquad 3.35$$

where the total Γ is dropped assuming it to be equal for s-wave and p-wave captures. The expressions for Γ_ℓ are

$$\Gamma_P = P_1\langle S_n^1\rangle D_1 = \sqrt{E}\left(\frac{K^2R^2}{1+K^2R^2}\right)\langle S_n^1\rangle D_1$$

$$\Gamma_S = P_0\langle S_n^0\rangle D_0 = \sqrt{E}\langle S_n^0\rangle D_0$$

Assuming a 1/v variation for the cross section and the Maxwellian distribution, we have,

$$\sigma(E) \sim \frac{1}{E^{1/2}} \qquad 3.36$$

$$\phi(E)dE \sim E \exp(-E/\kappa T)dE \qquad 3.37$$

At this point the following plausible approximations may be made:

$$1 + K^2R^2 \approx 1 \qquad 3.38$$

$$\Sigma\Gamma_\ell = \Gamma_P + \Gamma_S \approx \Gamma_S \qquad 3.39$$

Thus,

$$\bar{\sigma}_S \alpha \int_0^{.5} \frac{1}{\sqrt{E}} E \exp(-E/\kappa T)dE$$

$$= \int_0^{.5} E^{1/2} \exp(-E/\kappa T)dE$$

$$= 3.5\text{x}10^{-3} \qquad 3.40$$

and,

$$\bar{\sigma}_p \alpha \frac{\langle S_n^1 \rangle D_1}{\langle S_n^0 \rangle D_0} \int_0^{.5} \sqrt{E}(C_1 E)\exp(-E/\kappa T)dE$$

$$= C_1 \frac{S_n^1 D_1}{S_n^0 D_0} \int_0^{.5} E^{3/2} \exp(-E/\kappa T)dE$$

$$= \frac{\langle S_n^1 \rangle D_1}{\langle S_n^0 \rangle D_0} 3\text{x}10^{-10} \qquad 3.41$$

$$\approx 10^{-9}$$

Since the thermal neutron capture cross section is 180b, it appears from equations 3.40 and 3.41 that

$$\bar{\sigma}_S = 180\,b \qquad 3.42$$

$$\bar{\sigma}_P \approx 0$$

Thus, using equations 3.34 and 3.42 in equation 3.28,

$$\frac{Y_P}{Y_S} = \frac{\frac{1}{20} I_R^P}{180 + (1/20) I_R^S} = 1.4 \times 10^{-3} \qquad 3.43$$

Thus the contribution of p-wave capture E1 transitions to the E2 transitions in ^{163}Dy is

$$4.7 \times 10^{-4} \frac{S(E1)}{S(E2)},$$

that is, 6%. The p-wave contamination in ^{163}Dy may, therefore, be neglected. Since the values of $\langle S_n^1 \rangle / \langle S_n^0 \rangle$ for other targets in this study are comparable and the ratios between the resonance integral and the thermal cross section are smaller than that of ^{162}Dy, the p-wave contamination is negligible in general.

CHAPTER 4

EXPERIMENTAL RESULTS AND DISCUSSIONS

4.1 Neutron Separation Energy

The content of this section has already been reported (Is82). To deduce an estimate of the neutron separation energy of a nucleus, the energy of a primary E1 or M1 transition was added to that of the populated level. The currently acceptable S_n value of a nucleus (Wap 77) was used to identify the final state associated with each high energy primary transition observed. Cases where the populated levels were not independently known with a precision of better than 0.1 keV were excluded from consideration. When the presence of a doublet was suspected or overlap interference between two nuclides was possible the case was rejected.

For each nuclide the mean separation energy was determined by

$$S_n = (1/N)\sum_k (E_k + E_k') \qquad 4.1$$

where E_k is the energy of a primary transition (photon energy plus recoil energy of the nucleus) which populates the level with energy E_k' and N is the number of cases

considered. The combinations taken for the estimation of the neutron separation energy of each nucleus are given in table 4.1. The references for the energy levels used are also given.

For the ith nuclide, the sample variance is

$$S_i^2 = \frac{\sum_{j=1}^{n_i} (x_{ij} - \bar{x}_i)^2}{n_i - 1}, \qquad 4.2$$

where x_{ij} is a member of n_i cases considered for the nuclide and $\bar{x}_i$ is the mean of its neutron separation energy. In this study, since all the data were collected with the same experimental arrangement and the energy scale was essentially the same, all nuclides were treated on an equal basis. There were a total of 15 nuclides each with cascades ranging in number from a minimum of 1 to a maximum of 10. Sample variances of 5 nuclides each with more than 5 cascades were chosen to calculate the joint sample variance

$$S^2 = \frac{\Sigma \nu_i S_i^2}{\nu}, \qquad 4.3$$

where ν_i is the degree of freedom and equals $(n_i - 1)$, and $\nu = \Sigma \nu_i$. This value of S, found to be 0.09 was used to estimate $\sigma_{mean} = S/\sqrt{n_i}$ of the neutron separation energy for each of the nuclides. In this treatment it

TABLE 4.1

Estimation of Neutron Separation Energy through Summation of Cascades

Final nucl.	Transition energy (keV)	Level energy (kev)	Ref. for level	S_n (keV)
^{143}Nd	4817.63	1306.00		6123.63
	5381.49	742.13	Tu78	6123.62
^{144}Nd	5612.45	2204.62		7817.06
	6256.22	1560.81		7817.03
	6306.53	1510.64	Ra73	7817.17
	6502.68	1314.50		7817.18
^{146}Nd	7111.51	453.77	Bu75	7565.28
^{156}Gd	7288.33	1248.00		8536.33
	6913.82	1622.47		8536.29
	6482.44	2054.06	Bu76	8536.50
	6429.77	2106.65		8536.42
^{158}Gd	6750.40	1187.097		7937.49
	6419.89	1517.401	Gr78	7937.29
	5784.30	2153.096		7937.39
^{162}Dy	7308.87	888.22		8197.09
	7233.86	963.00		8196.86
	7135.96	1061.05	Ba67	8197.00
	7048.80	1148.29		8197.09
	6986.78	1210.15		8196.93
^{163}Dy	5920.04	351.146		6271.18
	5881.28	389.747		6271.02
	5849.23	421.833		6271.06
	5533.28	737.641		6270.92
	5504.85	766.208	Sc67	6271.05
	5450.18	820.783		6270.96
	5411.65	859.280		6270.93
	5386.69	884.285		6270.47
	5335.74	935.109		6270.86
	5221.81	1049.061		6270.87
^{164}Dy	7415.80	242.23		7658.02
	6830.09	827.17	Sc64	7658.26
	6681.21	976.86		7658.07

TABLE 4.1 (Cont'd)

Final nucl.	Transition energy (keV)	Level energy (keV)	Ref. for level	S_n (keV)
^{165}Dy	5607.85	108.160		5716.01
	5557.37	158.591		5715.96
	5177.34	538.61	Bu76a	5715.95
	5145.59	570.25		5715.84
	5142.47	573.56		5716.03
	5110 88	605.10		5715.98
^{166}Ho	6072.55	171.074		6243.62
	6052.95	190.901		6243.85
	5988.04	260.661		6243.70
	5895.39	348.257		6243.64
	5871.66	371.984	Bu75a	6243.64
	5813.68	430.030		6243.71
	5772.80	470.839		6243.63
	5761.86	481.845		6243.70
	5685.11	558.562		6243.67
	6505.46	638.320		6243.77
^{168}Er	7507.24	264.08		7771.32
	6950.27	821.11		7771.38
	6875.74	895.71		7771.45
	6677.51	1093.90		7771.41
	6578.54	1193.06	Gr74a	7771.59
	6339.93	1431.54		7771.47
	6063.57	1708.03		7771.60
	5878.55	1893.00		7771.55
^{174}Yb	7388.19	76.480		7464.66
	7211.64	253.123		7464.76
	6146.19	1318.31		7464.50
	6028.81	1381.92	Mi73	7464.73
	5996.42	1468.12		7464.54
	5858.46	1606.25		7464.71
	5763.11	1701.41		7464.52
^{175}Yb	5266.12	556.085		5822.21
	5011.09	811.425	Br71	5822.35
	5830.09	992.263		5822.35
^{178}Hf	7319.85	306.61		7626.46
	6451.84	1174.64		7626.48
	6242.09	1384.53	Gr74b	7626.62
	6112.64	1513.64		7626.27
^{180}Hf	7080.64	308.58		7388.64
	6747.79	640.85	Bu74	7388.64

TABLE 4.2

Summary of Neutron Separation Energies from (n,γ) Reaction

	This work			Previous work
Final nucleus	S_n (keV)	Standard deviation (keV)	[a]Total absolute error (keV)	S_n by Wapstra and Bos[b] (keV)
^{143}Nd	6123.62	0.06	0.13	6122.6 ± 0.5
^{144}Nd	7817.11	0.05	0.12	7817.1 ± 1.0
^{146}Nd	7565.28	0.09	0.14	7564.78 ± 0.39
^{156}Gd	8536.39	0.05	0.12	8536.0 ± 0.9
^{158}Gd	7937.39	0.05	0.12	7937.4 ± 0.6
^{162}Dy	8196.99	0.04	0.12	8196.3 ± 1.6
^{163}Dy	6270.98	0.03	0.11	6272.5 ± 1.2
^{164}Dy	7658.11	0.05	0.12	7656.0 ± 1.8
^{165}Dy	5715.96	0.03	0.11	5715.4 ± 1.5
^{166}Ho	6243.69	0.03	0.11	6242.6 ± 0.7
^{168}Er	7771.47	0.03	0.11	7771.14 ± 0.39
^{174}Yb	7464.63	0.03	0.11	7465.1 ± 0.7
^{175}Yb	5822.35	0.05	0.12	5822.6 ± 0.5
^{178}Hf	7626.46	0.05	0.12	7626.3 ± 0.9
^{180}Hf	7388.64	0.06	0.13	7388.11 ± 0.39

[a] A combination of scale error and standard deviation. The energy scale is based upon a ^{15}N separation energy of 10833.30 (11) keV.

[b] Ref. Wa77.

was assumed that the variance σ_i^2 associated with each nuclide corresponds to a common population. To check the validity of the hypothesis Bartlett's test (Be54) was performed. The quantity

$$B = \frac{1}{c}(\nu \ell n S^2 - \Sigma \nu_i \ell n S_i^2) \qquad 4.4$$

was computed, where $c = 1 + \frac{\Sigma(1/\nu_i) - 1/\nu}{3(k-1)}$ and k is the number of sample variances considered which is 5. Using the fact that the distribution of B may be approximated by the χ^2-distribution with k-1 degrees of freedom, the value of B in our calculation was found to correspond to the validity of the hypothesis with a probability of 80%.

The values of the neutron separation energies observed are in general agreement with the systematics of Wapstra et al. (Wa77). The data presented here do represent a significant improvement in precision. A more recent value of 7464.8 ± 0.5 keV (Gr81) for ^{174}Yb has been reported and is in good agreement with our value of 7464.63 ± 0.11 keV. The S_n value of ^{165}Dy reported by Braumandl et al. (Br79) is 5716.60 ± 0.14 keV, which is much greater than our value of 5715.96 ± 0.11. However, their neutron binding energy for ^{13}C 4946.74 ± 0.30 keV, is also higher than our result of 4946.30 keV, the latter agreeing well with 4946.329 ± 0.024 keV reported by

Greenwood et al. (Gr80). There is agreement in the S_n-value of ^{168}Er between our value of 7771.47 ± 0.11 keV and that of Braumandl et al. which is 7771.33 ± 0.20 keV.

4.2 Absolute Intensity

4.2.1 Theory

The absolute intensity of a transition can be determined in different ways. If the complete decay scheme is derived or if all the primary transitions are identified one can use the fact $\Sigma_\gamma I_\gamma E_\gamma = 100$ Q. For most nuclei the complete decay scheme is not known and the extraction of all the primary transitions and their differentiation from the secondary transitions is extremely difficult.

Another way to determine the absolute intensity of a transition and the one that was adopted in this study is to normalize it to the known intensity of another nucleus. The count rate of a particular transition i is

$$A_i = \iiint_{VE} n(x)\sigma(E)\phi(x,E)\varepsilon_i I_i dE d^3x \qquad 4.5$$

where $n(x)$ = density of atoms of the target at position x,

$\sigma(E)$ = radiative capture cross-section of the target nucleus,

$\phi(x,E)$ = neutron flux,

ε_i = detection efficiency at the energy of transition,

I_i = intensity of transition.

If one assumes the target to have homogeneous density and the flux to be thermal only (the problem of contribution from resonance integral is discussed in section 4.3),

$$A_i = n\sigma\varepsilon_i I_i \int_V \phi(x)\, d^3x \qquad 4.6$$

It follows from equation 4.6 that if a sample 1 is mixed homogeneously with a standard 2 and is irradiated,

$$\frac{(A_i)_1}{(A_j)_2} = \frac{n_1\sigma_1\varepsilon_i(I_i)_1}{n_2\sigma_2\varepsilon_j(I_j)_2} \qquad 4.7$$

where the subscript j refers to a transition in the standard. Thus

$$(I_i)_1 = \frac{n_2\sigma_2\varepsilon_j(A_i)_1}{n_1\sigma_1\varepsilon_i(A_j)_2}\,(I_j)_2 \qquad 4.8$$

If the ratio of the number of atoms of the two nuclides, their cross sections, relative efficiencies, number of counts and the intensity of a line of the standard are known, the absolute intensity of a transition can be determined. It is evident from equation 4.8 that the precision in the intensity is dependent on the precision of the cross sections of the sample and the standard.

4.2.2 Radiative Capture Cross Section of ^{14}N

The results of this section have already been reported (Is81). The centroids of the prominent transitions were determined by the zero area filter method (Ro72) and they were transformed into energies in the way mentioned in section 3.3. With the help of the compilation of Rasmussen et al. (Ra69) impurities in the spectra were identified and a check was made to ensure that no interference existed for transitions to be analyzed. The intensities of nitrogen lines were used to calibrate the detection efficiency. However, to make the subsequent calculations almost insensitive to efficiency each of 9 lines of nitrogen was paired with its adjacent Cl and Al lines both higher and lower in energies. To minimize the error contribution from the efficiency correction and the error in the quoted intensities a maximum number of lines of the above category was chosen for analysis. The transitions and intensities utilized in this study for the Cl-mixture and Al-compound are presented in tables 4.3 and 4.4 respectively. The areas of all these peaks were determined by applying the zero-area filter (Ro72). To cross-check the possible bias from the method applied, areas were also determined by a weighted least-squares

TABLE 4.3

Data Used to Derive σ_γ of ^{14}N with Chlorine as Standard

Nitrogen (Ke81)		Chlorine (Ke81) = 43.6±0.4 b (Mu81)		
E_γ (keV)	I_γ (%)	E_γ (keV)	I_γ (%)	σ_γ of N (mb)
3522.01	9.7 (2)	3332.90	0.84	75.9
		3981.06	1.04	80.2
4508.72	16.6 (3)	4616.65	0.71	76.1
		4729.05	0.73	78.6
5269.14	30.1 (4)	4979.81	3.95	79.8
		5017.80	0.52	82.1
		5246.87	0.59	77.6
5533.33	20.0 (3)	5517.38	1.75	76.4
		5715.30	5.68	75.7
5562.04	10.7 (2)	5517.38	1.75	79.5
		5715.30	5.68	78.8
		5902.96	1.18	76.4
6322.46	18.8 (3)	6087.08	0.94	78.9
		6111.00	20.96	77.4
		6619.79	8.31	77.8
		6628.02	4.74	77.9
7299.06	9.6 (2)	6978.09	2.40	78.4
		7414.17	10.69	77.9
8310.12	4.2 (1)	7790.40	8.69	78.8
		8578.70	2.84	74.4
			Mean:	79.1
			Sample error	1.7
			Total error	1.8

TABLE 4.4

Data Used to Derive σ_γ of ^{14}N

with Aluminum as Standard

Nitrogen (Ke81)		Aluminum = 230±3 mb (Mu73)		
E_γ (keV)	I_γ (%)	E_γ (St78) (keV)	I_γ (Pr81) (%)	σ_γ of N (mb)
3522.01	9.7 (2)	3465.04	7.25 (15)	72.7
		3591.17	4.86 (10)	74.7
		3849.12	3.32 (7)	78.4
4508.72	16.6 (3)	4259.61	7.37 (15)	78.0
		4660.13	2.77 (6)	78.0
5297.78	21.1 (3)	5134.15	3.26 (6)	75.2
7299.06	9.6 (2)	7723.88	32.1 (0.6)	76.8
8310.12	4.2 (1)	7723.88	32.1 (0.6)	78.2
			Mean	76.7
			Sample error	2.2

TABLE 4.5

Values of σ_γ of ^{14}N

This Work			Previous	
σ_γ(mb) using Cl as standard	σ_γ(mb) using Al as standard	Average σ_γ(mb)	σ_γ(mb)	Ref.
79.1 ± 1.8	76.7 ± 2.7	78.4 ± 1.5	75 ± 7.5	Ju63
			80 ± 20	Ba57

fit to a Gaussian with polynomial background (Qu72). The peak areas with well-defined background were also determined by simple numerical integration (section 3.1). The ratios of the peak areas obtained by all three methods agreed with 0.5%. The σ_γ values used for Al and Cl were 230 ± 3 mb (Mu73) and 43.6 ± 0.4 mb (Mu81) respectively and intensities used were from Ref. Pr81 and Ke81.

The σ_γ value of ^{14}N using standards aluminum and chlorine are given in tables 4.3 and 4.4. The average value was found to be 78.4 ± 1.5 mb. This value along with those from the literature are presented in table 4.5. While this value agrees within error with those reported in the literature (Ju63, Ba57), the precision has been increased by more than a factor of three.

4.2.3 Experimental Value of Absolute Intensity

For each of the nuclides studied in this work, the absolute intensities of a few strong transitions were determined by normalizing them to nitrogen transitions and using the σ_γ of ^{14}N determined above. These values in turn were used to convert the relative intensities of all other transitions including the E2 transitions into absolute intensities. For the subsequent analysis, the E2 intensities were transformed into partial widths by multiplying them with the average of Γ_γ of many

resonances at the capture state, and dividing by fractional contribution from the spin state of interest. The absolute intensities of the E2 transitions measured in this study are given in section 4.4 while those of the other hundreds of high energy transitions are presented in section 4.3 and Appendix D.

4.3 Neutron Capture Gamma-Ray Spectra

Throughout the present study care has been taken to keep the errors in the experimentally measurable quantities minimal. One such quantity is the absolute intensity of a quadrupole transition. This was determined by normalizing to the strong primary dipole transitions in the same spectrum. The intensities of most of these strong transitions were determined by using ^{14}N as a standard and in the estimation the thermal cross section of ^{14}N was used. Complexities may arise due to the possibility of contribution from the resonance integral (see section 3.5.5). However, there are cases in which this effect may not be serious. If the thermal cross section is much higher than the resonance integral and the sample size is small, it may not be a problem. Conversely, if the resonance integral is dominant but the sample size is large, there may not be a problem either. The high resonance integral makes the mean free path of the fast neutrons very short and the bulk irradiation is

TABLE 4.6

Contribution of Resonance

Integral to Thermal Data

Target Isotope	Mass of sample (mg)	σ_γ (barn)	Resonance integral I_R (barn)	$\frac{I_R}{20}$ (barn)	Mean free path of thermal neutron (mm)	Mean free path of epi-cadmium neutron (mm)	Radius of[b] the sample size (mm)
^{143}Nd	148	325	140	7	2.4	5.6	2
^{162}Dy	310	180	2730	136	3.8	0.25	3
^{164}Dy	20	2700	377	19	0.29	2.1	1
^{165}Ho	400	66	700	35	9.6	0.9	3
^{167}Er	400[a]	670	2970	148	4.2	0.9	3
^{173}Yb	456	19	390	19	3.8	1.8	3
^{179}Hf	280	45	600	30	6.8	.5	3

[a]Mass of natural Er_2O_3.

[b]The sample size is crudely assumed to be spherical.

mainly due to thermal neutrons. Besides this skin effect, the weightage of the resonance integral is due to the ratio of 1/20 between the thermal and epicadmium flux of neutrons in our reactor. The factors determining the contribution from the resonance integrals for different targets are presented in table 4.6. It is apparent from the table that there is virtually no problem for the targets ^{143}Nd, ^{162}Dy and ^{164}Dy. For the rest there may be some problem, and among them ^{173}Yb seems to be a bad case. Thus it was necessary to determine the absolute intensities of the strong transitions of all the nuclides and compare them with previously reported values. A comparison of our results of absolute intensities with those in the literature for well moderated flux showed a general agreement.

The energies and intensities of the high energy transitions of most of the nuclides involved are tabulated in the present study. These are given in Appendix D. In this tabulation, because of the arbitrary intensity limits used, the E2 transitions given in section 4.4 are absent.

4.3.1 The ^{143}Nd(n,γ)^{144}Nd Reaction

The intensities of all the transitions in ^{144}Nd were normalized to the strong line at 6503 keV. The

absolute intensity of the 6503 keV line was determined with the help of the spectrum of the calibration sample of ^{143}Nd and chlorine. The transitions in chlorine used for the intensity calibration are at 6620 and 6628 keV with intensities 8.31 and 4.74% (Ke81). The cross sections used are 325 ± 10 b for ^{143}Nd and 43 ± 2 b for ^{35}Cl (Mu 73). The absolute intensity of the 6503 keV transition was found to be (8.1 ± 0.6)%. The absolute intensity of the same line is 7.0% as calculated from the intensity of natural Nd determined by Rasmussen et al. (Ra69). Groshev et al. (Gr69) reported a value of 5.8% and S. Raman (Ra67) compiled a value of 7.1%.

Although there have been many works on the levels of ^{144}Nd (Ra76 and Refs. therein) including the ^{143}Nd (n,γ) reactions, the intensities of most of the capture gamma-rays have never been reported. The energies and intensities of 116 transitions with energies above 3.8 MeV are presented in table D.1. The primary E1 transition at 7120 keV that populates the 2^+ first excited state is of particular interest (We72) because of its extremely low intensity. The intensity of the line found in this work is 0.005 ± 0.001 photons/100 n which is higher than the value of (0.0027 ± 0.0006)% reported by Raman et al. (Ra74). This may be due to different

normalization used to the absolute intensity determination.

The levels above 3461 keV populated by primary transitions (with few exceptions) in thermal and resonance capture gamma-rays are given in Ref. Ra74. We did not find 5 primary transitions above 4.36 MeV that Raman et al. found in resonance capture. We found several gamma-rays with comparable intensity in the same region that are absent in Raman's work. In addition to the lines presented in table D.1 many weaker lines were found in the present study. From their intensities it appears that there is a high probability that they are secondary (the possibility of quadrupole transitions cannot be ruled out). These weak transitions are presented separately in table D.6.

4.3.2 The $^{162}Dy(n,\gamma)^{163}Dy$ Reaction

The absolute intensity of the 5450 keV transition in ^{163}Dy was determined in the natural Dy spectrum where the isotopic ratio of ^{162}Dy and ^{164}Dy is known. The intensity of this line was normalized to the 5608 keV transition in ^{165}Dy with 3.78% (this work) intensity. The σ_γ of ^{162}Dy used in the calculation is 180 ± 20 b. The absolute intensity of the 5450 keV transition in ^{163}Dy was found to be (2.7 ± 0.4)% which is higher than

the value (2.08 ± .40)% obtained by Schult et al. (Sc67). The difference is due to the different value of the intensity of the ^{165}Dy transition used in their work.

In the spectrum of the separated isotope of ^{162}Dy, the only significant contaminant was from the accompanying 0.69% ^{164}Dy isotope. The spectrum of separated ^{164}Dy was, after proper normalization, subtracted from this spectrum and the spectrum consisting only of transitions in ^{163}Dy remained.

In table D.2, 327 transitions in ^{163}Dy between 2.36 to 5.92 MeV are presented. The comparison of the 56 populated levels with the literature shows that 16 levels are previously unknown and among the rest 4 levels were known only from (d,t) and (d,p) reactions.

4.3.3 The ^{164}Dy(n,γ)^{165}Dy Reaction

The absolute intensity of the electric dipole transition at 5608 keV was determined by normalizing with three transitions in nitrogen at 5269, 5533 and 6322 keV. The capture cross section of ^{164}Dy used in the calculation is 2700 ± 75 b (Mu73). The related quantities of nitrogen are given in section 4.2.2. The absolute intensity of the 5608 keV line was found to be (3.78 ± 0.19)%. The values of the same quantity reported in the literature are (3.00 ± 0.65)% (Sc67) and 3.9% (Ra69). All the transitions in

^{165}Dy were normalized to the 6508 keV line and our value of the absolute intensity was used to determine the conversion factor in finding all the absolute intensities.

The photon energies and intensities of 256 transitions between 2.38 to 5.61 MeV are presented in table D.3. The average absolute error of the energies is 0.15 keV and that of the intensities is estimated to be 5%. These energies and intensities were compared with those of the natural Dy spectrum to ensure that the correct assignment has been made. Many new transitions have been observed and many previously known singlets have been found to be doublets.

Possible Low-Lying Levels of ^{165}Dy

Although we found many new gamma-ray transitions for other nuclei, ^{165}Dy deserves special attention. Unlike in other nuclei many of the transitions in this nucleus seemed to be corresponding to new levels which are low-lying (<1650 keV) and it appeared to double the number of levels previously known (Ma67). We shall, therefore, discuss these levels in some detail and before accepting the new levels we shall investigate some of the alternative possibilities. For most of the other nuclides, we have just tabulated the energy and intensity of new transitions without referring to their new levels.

A comparison of the observed transitions in ^{165}Dy above 4069 keV with those of Markus et al. (Ma67) reveals that out of 32 transitions they reported, 15 are absent in this study. The number of events in the present work is about 500 times higher than that observed previously so that it is extremely unlikely that the lines would not have been observed. These 15 transitions would appear therefore to be either contaminants or artifacts. (Seven of these 15 transitions were considered uncertain, and out of the remaining 8 transitions, two were used to construct 2 new levels). As a result, we find no evidence for reported levels at 1449 and 1469 keV.

Above a photon energy of 4069 keV, 21 new gamma-rays have been observed in addition to the 14 previously established transitions. If these new transitions are primary gamma-rays from the ^{164}Dy(n,γ)^{165}Dy reaction, they populate 21 unreported levels. Before accepting these new lines the possibility that the lines are due to the (n,n'γ) reaction or to a contaminant in the sample must be explored.. The presence of (n,n'γ) due to high energy neutrons has been checked in two ways. The presence of γ-rays from the inelastic scattering of neutrons by ^{164}Dy is more probable in the low energy part of the spectrum. A comparison with a ^{164}Dy(n,n'γ)^{165}Dy

spectrum (Ba76) between energies 1.5 MeV and 2.4 MeV indicated the absence of such gamma-rays in the present spectrum. Rasmussen et al. (Ra69) used a well moderated flux having a Cd ratio >3000 to collect the (n,γ) spectrum of natural Dy. They observed 8 of the 21 transitions in question and the remaining 13 have intensities less than the detection limit in their work. Thus these 21 transitions are not due to $(n,n'\gamma)$. The possibility that these γ-rays result from (n,γ) reactions with contaminants has also been investigated.

Acceptance of the observed transitions as indicators of low-lying levels requires that these transitions be primaries. A probabilistic calculation (Ke82) shows it is highly probable that 15 of the new 21 transitions may be primary. Thus, we believe, we have found 29 levels in total below 1648 keV of which 15 are new.

Using our S_n value of 5715.96 ± 0.11 keV, the energies of the levels found in this work along with the previous work are presented in table D.7. The general absolute error of the level energies is 0.18 keV. Out of the 26 levels given in table D.7, 15 levels are new.

The $1/2^+$ state formed by S-wave capture, dominated by the -1.9 eV resonance, decays to low-lying levels mainly by electric or magnetic dipole transitions. All

the newly reported levels are most likely, therefore, to have spin 1/2 or 3/2 with either parity. Such states would represent either rotational band heads or the first members of the rotational bands.

4.3.4 The $^{165}Ho(n,\gamma)^{166}Ho$ Reaction

The absolute intensity of the 5814 keV line was determined by normalizing to the nitrogen transitions at 5533, 5562 and 6322 keV and the value was found to be 7.8 ± 0.4 per 1000 n captures. The cross section of ^{165}Ho used is 200 ± 20 b (Mu73). The values of I_γ previously reported are 7.6 ± 1.2 (Mo67) and 7.1 (Ra69) per 1000 captures.

A total of 440 transitions have been found between 3.1 to 6.2 MeV in the ^{166}Ho spectrum. The energies and intensities of the photons are presented in table D.4. A large number of lines absent in the previously known thermal ^{166}Ho spectra has been detected. For example, while only 25 lines above 4.9 MeV have been reported by Motz et al. (Mo67), we obtained 90 lines in the same energy range. But a comparison between our thermal spectrum with the average resonance spectrum (Bo70) shows that above 5 MeV, there are 30% more dipole transitions in the latter. This is obviously due to P-T fluctuation in thermal intensity.

4.3.5 The $^{167}Er(n,\gamma)^{168}Er$ Reaction

As the cross section of ^{167}Er is much higher than its accompanying isotopes and the expected E2 transition is at a high energy, it was decided to run a natural sample instead of a separated one. For this sample the desired quadrupole transition was observed in a relatively short period of time and the sample was not irradiated further. The use of the natural sample coupled with the short period of run left little possibility of producing new transitions and no effort was taken to extract a comprehensive list of the lines of the $^{167}Er(n,\gamma)$ reaction. However, the energies of some of the strong isolated lines were determined and they have been used to find the neutron separation energy of ^{168}Er. The absolute intensity of the strong line at 6229 keV was found to be (0.88 ± .05)% following the normalization with the 6322 keV nitrogen transition. The σ_γ of ^{167}Er used in the calculation is 670 ± 30 b (Mu73). The I_γ value of the 6229 keV line agrees with 0.93 as found from the compilation of Lone et al. (Lo81) after converting their value of natural erbium into that of ^{168}Er. The other value in the literature is 0.59% (Gr66).

4.3.6 The $^{173}Yb(n,\gamma)^{174}Yb$ Reaction

The transitions in ^{174}Yb were all normalized to the 7388 keV transition. The absolute intensity of this strong line was determined using a calibration spectrum of ^{174}Yb and melamine in a known ratio. The 7388 keV line was normalized to the 7299 keV transition in ^{15}N. The σ_γ of ^{173}Yb used in the calculation is 19 ± 2 b (Mu73). The absolute intensity of the 7388 keV transition of ^{174}Yb was found to be (1.41 ± 0.15)% which agrees well with 1.44% reported by Greenwood et al. (Gr81).

It was very difficult to identify the γ-rays of ^{174}Yb as there were many lines of $^{172,173,175}Yb$ present in the spectrum. Besides, the lines of the impurity Gd also posed a problem. These difficulties were coupled with the appearance of many new lines previously undetected. The lines of Gd and three isotopes of Yb were identified with the help of their energies and reported intensities (Ra69, Gr75, Al71, Mi76). The remaining transitions were compared with the thermal and 2 keV neutron capture spectra reported recently by Greenwood et al. (Gr81). Many lines observed in the present work are absent in that thermal spectrum but present in the 2 keV spectrum which is effectively averaged over many

resonances. This is understandably possible by the improved statistics in the present study. But we observed some lines which were not present even in the average spectrum and could not be attributed to any impurity. This may be feasible because of the better resolution and again the excellent statistics. The photon energies and intensities of the $^{173}Yb(n,\gamma)^{174}Yb$ reaction are presented in table D.5. The previously unknown lines with intensities lower than 0.15 per 1000 are not listed. Some of the lines are interfered with by impurity lines, but no correction was made; instead, they are simply marked in the table.

4.3.7 The $^{179}Hf(n,\gamma)^{180}Hf$ Reaction

In the spectrum of this reaction, there is 25% contribution from the target ^{177}Hf and 8% contribution from ^{178}Hf. We did not make any effort to identify all γ-rays of ^{180}Hf. The absolute intensity of the strong transition at 5847 keV was determined by normalizing it to the nitrogen lines at 5562 and 6322 keV, and the value was found to be 0.26 ± 0.03 per 100 n captures. The only other previously reported value is 0.19% (Na66).

4.4 Possible Primary E2 Transitions Found in This Work

In total 8 possible E2 primary transitions were observed in the present study. In addition to these, the upper limits of the intensities of 4 probable E2 transitions were determined. A detection limit corresponding to 95% probability has been adopted in this study. The areas of the peaks were corrected for detection efficiency and then normalized to the intensities of strong dipole transitions in their respective spectra (section 4.3). The absolute intensities of the E2 transitions are presented in table 4.7. The quoted errors are 1 standard deviation.

The 5490 keV transition of ^{163}Dy was interfered with by a 0.12% intensity line (Ra69) of the impurity samarium. Using the 0.75% line (7213 keV) of samarium in the same spectrum, a correction was made for the contribution of this element to the 5490 keV transition. This correction amounted to only 5%. Partially overlapped with the 7296 keV transition of ^{180}Hf, there was the 7299 keV transition of nitrogen, a weak (n,γ) background of the system. This problem was handled in two different ways and the net areas of the E2 transition in ^{180}Hf found were in agreement. First, a least-squares fit of the doublet was performed and the background and nitrogen component were subtracted. Secondly, the area of the Hf-nitrogen

TABLE 4.7

Primary E2 Transitions Found in this Work

Final Nucleus	E_γ (keV)	I_γ (per 10^4)	$a\Gamma_\gamma$ (meV)	$c\Gamma_{\gamma i}=\Gamma_\gamma I_\gamma/f$
^{144}Nd	4573	0.28 ±0.12	[b] 8	0.0022 ±0.001
^{163}Dy	6020	<0.16		<0.0025
	5490	0.9 ±0.3	155	0.014 ±0.005
	5322	<0.23		<0.0036
^{165}Dy	5132	0.18 ±0.008	58	0.001 ±0
^{166}Ho	6161	0.07 ±0.03	75	0.00074±0.00037
^{168}Er	7223	1.9 ±0.2	88	0.025 ±0.003
^{174}Yb	5086	<0.14	76	<0.0015
^{180}Hf	7296	0.062±0.026	62	0.00048±0.00024
	6088	0.38 ±0.11		0.0030 ±0.0010
	5751	<0.13		<0.001
	5664	0.46 ±0.13		0.0036 ±0.0012

[a] Ref. Mu73 for all but ^{144}Nd.

[b] Ref. Mu81.

[c] Symbol f is the fractional contribution of the spin states of interest.

complex was determined by simple numerical integration and the contribution of the nitrogen line was extracted by normalizing with the intensity (Ke81) of an isolated nitrogen peak at 6322 keV in the same spectrum. The correction for the nitrogen line was only 20%.

The detection of the 8 possible primary E2 transitions increases the number of such transitions observed in thermal capture by 50% and the number in both thermal and discrete resonance capture by 30%. The upper limit values of 4 probable E2 transitions represent a further addition to the present knowledge. Subsequently, this study removes the existing gap in data in the literature in the mass region $143 < A < 181$.

CHAPTER 5

STUDY OF RADIATIVE ELECTRIC QUADRUPOLE STRENGTH

The properties of the E2 transitions of the highly excited states are discussed in this chapter. The existence of the giant quadrupole resonances for nuclei spanning the whole periodic table is well-known (Be76). It is possible that the GQR may contribute to the transition strength near the neutron threshold, (Ko81). To investigate the influence rigorously we have deduced a theoretical quantitative expression for the strength function $\langle \Gamma_{\gamma i}/D \rangle$ on the basis of the GQR model, and also assuming the equivalence between the radiative capture and the photonuclear reaction. The combined effect of the isoscalar and the isovector GQR is taken into account. The observed values of $\Gamma_{\gamma i}/D$ has been compared with the corresponding theoretical values to examine the validity of the theoretical model.

The dependence of the E2 radiation width on the transition energy and the nuclear mass number has been deduced. Quantities such as the reduced transition probability and the average quadrupole strength have been calculated.

5.1 Influence of Giant Resonance on Quadrupole Strength Function

5.1.1 Theory

The linearly energy-weighted sum rule is (Bo69)

$$S_L = \sum_n (E_n - E_0)|\langle n|Q_{L0}|0\rangle|^2$$
$$= \frac{1}{2}\langle 0|[Q_{L0},[H,Q_{L0}]]|0\rangle, \qquad 5.1$$

where n is the complete set of excited states that can be reached by operation with the electric multipole operator Q_{L0} on the ground state. If the Hamiltonian H does not explicitly depend on the momenta of the particles the commutator in equation 5.1 receives contribution only from the kinetic energy, and one obtains

$$S_L = \frac{\hbar^2}{2m}\langle 0||\nabla Q_{L0}|^2|0\rangle \qquad 5.2$$

The electric multiple operator for a system of nucleons

$$Q_{L0} = e\sum_i \frac{1}{2}[1+\tau_3^{(i)}] r_i^L Y_{L0}(i) \qquad 5.3$$

Assuming that the Hamiltonian contains no charge dependence and thus commutes with the charge operator $[1+\tau_3(i)]$, the sum rule can be reduced to

$$S_L = \frac{L(2L+1)}{4\pi}\frac{\hbar^2}{2m} Ze^2 \langle r^{2L-2}\rangle_{proton}, \quad L>2 \qquad 5.4$$

Equation 5.4, for quadrupole transitions, is

$$S_2 = \frac{5\hbar^2}{4\pi m} e^2 Z \langle r^2 \rangle_{proton} \qquad 5.5$$

where $\langle r^2 \rangle$ is the mean-square radius for the protons in the initial state.

The sum rule includes both the isoscalar (T = 0) and the isovector (T = 1) transitions. The first term in the operator in equation 5.3 describes the isoscalar transition and the second term, the isovector transition. If there is no interference between these two kinds of transitions, then the sum rule for the quadrupole transition for each kind can be written as (Wa69)

$$S_2^T = \frac{5\hbar^2 e^2}{4\pi m} O_T \langle r^2 \rangle \qquad 5.6$$

where $O_T = Z^2/A$ for T = 0, and $O_T = NZ/A$ for T = 1. It is assumed here that $\langle r^2 \rangle_{proton} = \langle r^2 \rangle_{nucleon}$.

Now the photonuclear cross-section with a target of spin zero (B152)

$$\sigma_\gamma^T = \frac{4\pi^3 (L+1)(2L+1)}{L[(2L+1)!!]^2} \frac{k^{2L-1}}{D_L} \left\langle |Q_{L,1}|^2 + |Q_{L,-1}|^2 \right\rangle_{av} \qquad 5.7$$

where D_L is the level spacing at the final state and average is that of the square of the multipole matrix elements between the lower level and a large number of upper levels. The sum rule

$$\int_0^\infty \frac{\sigma_\gamma^T}{E^2}dE = \frac{4\pi^3(L+1)(2L+1)}{L[(2L+1)!!]^2\hbar^3c^3}\int_0^\infty E\frac{\langle|Q_{L,1}|^2+|Q_{L,-1}|^2\rangle_{av}}{D_L(E)}\cdot dE$$

$$= \frac{8\pi^3(L+1)(2L+1)}{L[(2L+1)!!]^2\hbar^3c^3}\int_0^\infty E\langle|Q_{L,0}|^2\rangle\frac{dE}{D_L(E)} \qquad 5.8$$

where the fact $\langle IQ_{LM}I^2\rangle$ is independent of M has been used. The integral on the right hand side of equation 5.8 is essentially the sum rule in equation 5.1. Therefore

$$\int_0^\infty \frac{\sigma_\gamma^T}{E^2}dE = \frac{8\pi^3(L+1)(2L+1)}{L[(2L+1)!!]^2\hbar^3c^3}S_L^T \qquad 5.9$$

For the quadrupole transition, equation 5.9 reduces to

$$\int_0^\infty \frac{\sigma_\gamma^T}{E^2}dE = \frac{1}{3}\pi^2\left(\frac{e^2}{\hbar c}\right)O_T\frac{\langle r^2\rangle}{mc^2}$$

$$= \frac{1}{3}\pi^2\alpha O_T\frac{\langle r^2\rangle}{mc^2} \qquad 5.10$$

The mean square radius

$$\langle r^2\rangle = \frac{3}{5}R^2 = \frac{3}{5}r_0^2A^{2/3},\ r_0 = 1.233\ \text{fm} \qquad 5.11$$

where R is the equivalent uniform radius. The compilation of the values of R given in Ref. Pr75 for 20 nuclides spanning the whole mass range was used in the present study to determine the value of r_0. Substituting the numerical values in equation 5.10.

$$\int_0^\infty \frac{\sigma_\gamma^T}{E^2}dE = 2.35\times10^{-4}O_TA^{2/3}\ \text{mb/MeV} \qquad 5.12$$

The energy dependence of a giant resonance may be approximated by a Lorentz-shaped resonance line and thus another expression for the photonuclear cross section is

$$\sigma_\gamma^T = \sigma_0^T \frac{\Gamma^2 E^2}{(E^2 - E_0^2)^2 + \Gamma^2 E^2} , \qquad 5.13$$

where σ_0^T is the peak resonance cross section, Γ and E_0 are the width and energy of the resonance corresponding to the transition T. The integral

$$\int_0^\infty \frac{\sigma_\gamma^T}{E^2} dE = \frac{\pi\Gamma}{2E_0^2}\sigma_0^T . \qquad 5.14$$

Thus a comparison between equations 5.12 and 5.14 readily gives

$$\sigma_0^T = 1.50 \times 10^{-4} O_T A^{2/3} E_0^2 / \Gamma \text{ mb} \qquad 5.15$$

At this point, it is interesting to compare this result with the literature. The value of σ_0^T obtained by Fubini et al. (Fu72) is 2 times higher, because the value used by them for the sum rule, equation 5.12, is twice as large as obtained in the present work. The expression in equation 5.12 is consistent with that deduced by Iu. K. Khokhlov (Kh57) by a different method. Fubini et al.'s value would agree with ours if it were corresponding to that before splitting into isoscalar (T = 0) and iso-

vector (T = 1) parts.

Using equation 5.15 in equation 5.13 and writing the isoscalar and isovector parts separately

$$\sigma_\gamma^{+} = 1.50\times10^{-4}\frac{NZ}{A}A^{2/3}E_0^{+2}\frac{\Gamma^{+}E^2}{(E^2-E_0^{+2})^2+\Gamma^{+2}E^2}\ \text{mb} \qquad 5.16$$

$$\sigma_\gamma^{-} = 1.50\times10^{-4}\frac{NZ}{A}A^{2/3}E_0^{-2}\frac{\Gamma^{-}E^2}{(E^2-E_0^{-2})^2+\Gamma^{-2}E^2}\ \text{mb} \qquad 5.17$$

The superscripts + and - stand for the isoscalar and the isovector giant resonances respectively.

It can be shown that the average photonuclear cross section (Ax62)

$$\langle\sigma_\gamma^{J}(EL)\rangle = 2\pi^2\lambda\!\!\!^{-2}g_J\left\langle\frac{\Gamma_{\gamma 0}}{D}\right\rangle_J , \qquad 5.18$$

where $g_J = (2J+1)/[2(J_0+1)]$, J_0 and J being the spins of the ground and final states, and $\Gamma_{\gamma 0}$ is the partial width for de-excitation to the ground state. The average total photonuclear cross section

$$\langle\sigma_\gamma(EL)\rangle = 2\pi\lambda\!\!\!^{-2}\sum_J g_J\left\langle\frac{\Gamma_{\gamma 0}}{D}\right\rangle_J \qquad 5.19$$

Assuming the strength function $\langle\Gamma_\gamma/D\rangle$ to be independent of J,

$$\langle\sigma_\gamma(EL)\rangle = \pi^2\lambda\!\!\!^{-2}\left\langle\frac{\Gamma_{\gamma 0}}{D}\right\rangle\sum_{J=J_0-L}^{J_0+L}\frac{(2J+1)}{(2J_0+1)}$$

which is reduced to

$$\langle\sigma_\gamma(EL)\rangle = (2L+1)\pi^2\lambda\!\!\!^{-2}\left\langle\frac{\Gamma_{\gamma 0}}{D}\right\rangle \qquad 5.20$$

It is to be noted here that $\Gamma_{\gamma 0}$ is a ground state transition from a particular spin state and D is the level spacing of the same spin states.

Although equation 5.20 is applicable to the ground state transition, it can be extended to transitions to excited states following the Brink hypothesis (Br55). Therefore the quadrupole strength function

$$\left\langle\frac{\Gamma_{\gamma i}}{D}\right\rangle = \frac{1}{5\pi\lambda\!\!\!^{-2}}\langle\sigma_\gamma(E2)\rangle$$

$$= 5.2\times10^{-8}E^2\langle\sigma_\gamma(E2)\rangle$$

(E is in MeV) 5.21

Using equations 5.16 and 5.17 in equation 5.21, the final expressions for the strength functions are

$$\left\langle\frac{\Gamma_{\gamma i}}{D}\right\rangle_{T=0} = 7.77\times10^{-12}E^4E_0^{+2}Z^2A^{-1/3}\frac{\Gamma^+}{(E^2-E_0^{+2})^2+\Gamma^{+2}E^2} \qquad 5.22a$$

$$\left\langle\frac{\Gamma_{\gamma i}}{D}\right\rangle_{T=1} = 7.77\times10^{-12}E^4E_0^{-2}NZA^{-1/3}\frac{\Gamma^-}{(E^2-E_0^{-2})^2+\Gamma^{-2}E^2} \qquad 5.22b$$

Thus the total quadrupole strength function

$$\left\langle\frac{\Gamma_{\gamma i}}{D}\right\rangle = \left\langle\frac{\Gamma_{\gamma i}}{D}\right\rangle_{T=0} + \left\langle\frac{\Gamma_{\gamma i}}{D}\right\rangle_{T=1} \qquad 5.23$$

5.1.2 Comparison between Experimental and Theoretical Results

The values of $\langle \Gamma_{\gamma i}/D \rangle$ predicted by equation 5.23 were compared with the experimental values both from the literature and this work. Since the quantities depend on energy and mass number in a rather complex way, corresponding to each experimental data point the theoretical value was calculated and the ratio was taken. Finally the proper average of these ratios were taken.

Computation of Theoretical Values

In equations 5.22a and 5.22b, the atomic number Z was replaced by the expression corresponding to maximum stability (Bu73)

$$Z = \frac{A}{1.98+0.015A^{2/3}} \qquad 5.24$$

The resonance energies are given by (Be76)

$$E_0^{+} = 63A^{-1/3}$$
$$E_0^{-} = 120A^{-1/3} \qquad 5.25$$

To obtain the width of the giant quadrupole resonance of each of the nuclei, the systematics compiled by F.E. Bertrand (Be76) were used. The data was provided by inelastic scattering of medium-energy electrons and nuclear projectiles. The values of the isoscalar GQR

widths spanning the whole mass number range were given. A least-squares fit of the data of 32 nuclides was performed with equal weighting as all the errors were comparable. The best fit for the isoscalar resonance width was a straight line with a negative slope:

$$\Gamma^{+} = 6.11-0.01214xA \text{ MeV} \qquad 5.26$$

For the isovector GQR, widths of only 4 nuclei, all from (e,e') measurements were available. Since the subsequent calculation is not very sensitive to the isovector resonance width, a linear fit of these four values was accepted. The function was

$$\Gamma^{-} = 10.64-0.0270xA \text{ MeV} \qquad 5.27$$

Using equations 5.24, 5.25, 5.26 and 5.27 in equation 5.23, we obtain an expression for the quadrupole strength function which only contains 2 variables, the energy (MeV) and mass number. In table 5.1 the isoscalar, isovector and total strength functions (Sϕ), (S1) and S(theo) are given in the seventh, eighth and ninth columns.

Experimental Results and Theoretical Values

The experimental widths $\Gamma_{\gamma i}$ of all the acceptable E2 transitions, observed in thermal, resonance and average-resonance experiments are presented in table 5.1.

In this list, ^{109}Pd was not included for the lack of information about its level density. Also excluded was the set of resonance capture transitions in ^{208}Pb because there is prominent structure in the GQR of this nucleus (Ra78) and consequently our simplified model of one isoscalar and one isovector GQR does not hold. It is true that there may be such structure effects in some other nuclei as well, and since a gross average of the ratios of experimental and theoretical strength functions is sought its inclusion may be justified. But as there are 27 E2 transitions in ^{208}Pb it bears much weight and again it is complicated by the fact that three widely different values of the level spacing of the initial 2^+ states of 5 (Ra78), 8 (Ho78) and 14 keV (Mu73) have been reported in the literature. For the sake of simplicity, the E2 transitions of ^{208}Pb have been listed separately in tables D.8 and D.9, and the results are discussed later in a qualitative way.

The ratio $\Gamma_{\gamma i}/D$ for each transition in table 5.1 was calculated. The average level spacing, D at the capture state of a nucleus with a particular spin was generally obtained from the literature (Mu73). This quantity was calculated when only the level spacing irrespective of spins was known. For the calculation,

TABLE 5.1 Comparison between Observed $\langle \Gamma_{\gamma i}/D \rangle$ and the Theoretical Prediction Based on the GQR Model

No.	Mass	Energy (keV)	Width (meV)	Level Spacing(eV)	S(exp) x1E7	S0(theo) x1E7	S1(theo) x1E7	S(theo) x1E7	Ratio (exp/theo)
1	21	6410	4.5000	574000	0.08	0.06	0.03	0.09	0.8531
2	26	11093	4.3000	43000	1.00	1.40	0.47	1.87	0.5340
3	33	6676	11.0000	270000	0.41	0.21	0.10	0.31	1.3079
4	33	5754	1.3000	270000	0.05	0.11	0.05	0.16	0.2938
5	34	6728	0.1400	30000	0.05	0.24	0.11	0.35	0.1351
6	46	8618	2.0000	2700	7.41	1.60	0.60	2.20	3.3656
7	57	7511	14.5000	22700	6.39	1.34	0.54	1.89	3.3825
8	74	9606	0.0720	163	4.42	9.95	2.83	12.79	0.3455
9	74	8998	0.0140	163	0.86	6.72	2.12	8.84	0.0972
10	92	8635	0.1500	1200	1.25	9.23	2.84	12.08	0.1035
11	93	8067	9.0000	2100	42.86	6.39	2.16	8.54	5.0166
12	93	8067	4.5000	2100	21.43	6.39	2.16	8.54	2.5083
13	93	6375	0.9000	2100	4.29	1.85	0.78	2.63	1.6275
14	94	7229	0.2600	90	28.89	3.60	1.37	4.97	5.8147
15	94	6833	0.2300	90	25.56	2.69	1.08	3.76	6.7945
16	104	6948	0.2600	62	41.94	3.69	1.42	5.11	8.1987
17	104	6731	0.0900	32	28.12	3.13	1.24	4.37	6.4341
18	104	6731	0.0110	32	3.44	3.13	1.24	4.37	0.7864
19	109	6153	0.0850	173	4.91	2.20	0.93	3.14	1.5669
20	109	5613	0.0690	173	3.99	1.41	0.63	2.04	1.9544
21	109	5172	0.2300	173	13.29	0.96	0.45	1.41	9.4521
22	136	9107	0.3700	72	51.39	36.94	8.20	45.14	1.1385
23	144	4573	0.0022	80	0.27	0.94	0.46	1.40	0.1965
24	150	6823	0.0022	5	4.40	7.66	2.69	10.35	0.4250

TABLE 5.1 (cont'd.)

No.	Mass	Energy (keV)	Width (meV)	Level Spacing(eV)	S(exp) x1E7	S0(theo) x1E7	S1(theo) x1E7	S(theo) x1E7	Ratio (exp/theo)
25	163	6020	0.0025	72	0.35	4.63	1.81	6.44	0.0539
26	163	5490	0.0140	72	1.94	2.88	1.22	4.10	0.4744
27	163	5322	0.0036	72	0.50	2.47	1.07	3.53	0.1415
28	165	5132	0.0010	200	0.05	2.11	0.93	3.05	0.0164
29	166	6161	0.0007	6	1.23	5.44	2.06	7.50	0.1645
30	166	6161	0.0040	6	6.67	5.44	2.06	7.50	0.8892
31	168	7223	0.0250	9	27.78	13.84	4.23	18.06	1.5378
32	174	5086	0.0015	17	0.88	2.23	0.98	3.21	0.2746
33	180	7296	0.0005	9	0.53	17.30	4.96	22.26	0.0240
34	180	6088	0.0030	9	3.33	6.02	2.23	8.25	0.4040
35	180	5751	0.0010	9	1.11	4.44	1.74	6.19	0.1796
36	180	5664	0.0036	9	4.00	4.10	1.63	5.74	0.6974
37	180	7296	0.0127	9	14.11	17.30	4.96	22.26	0.6339
38	180	6189	0.0051	9	5.67	6.59	2.40	8.98	0.6308
39	180	6128	0.0062	9	6.89	6.24	2.30	8.53	0.8072
40	180	6088	0.0064	9	7.11	6.02	2.23	8.25	0.8618
41	180	5751	0.0051	9	5.67	4.44	1.74	6.19	0.9161
42	180	5664	0.0056	9	6.22	4.10	1.63	5.74	1.0849
43	208	4753	5.5000	58000	0.95	2.20	0.95	3.15	0.3009
44	210	4285	2.1000	14000	1.50	1.36	0.62	1.98	0.7571
45	210	4171	17.7000	14000	12.64	1.20	0.56	1.75	7.2099
46	235	5246	0.0200	12	16.67	4.44	1.65	6.10	2.7344
47	239	4610	0.0400	18	22.22	2.36	0.97	3.33	6.6818
48	239	4610	0.0100	18	5.56	2.36	0.97	3.33	1.6704

the spin dependence (Er58) of the level density

$$F(J) \sim (2J+1)\exp\left\{-\frac{J(J+1)}{2\sigma^2}\right\} \qquad 5.28$$

was used. A value of 4.5 was used for the spin dependence parameter σ (Gi65).

The ratio of the experimental to theoretical value of $\Gamma_{\gamma i}/D$ for each transition is given in the 10th column of table 5.1. To display the ratios as a function of the mass number, the values for the same A were averaged thereby reducing statistical fluctuations. For the average-resonance data, only experimental errors are shown in figure 5.1, while for the rest confidence limits of 66% are given. If T has a χ^2-distribution with ν degrees of freedom, one can determine the value of x such that $Pr(T<t) = P$. The probability

$$P = \int_0^{\chi^2} f(t)dt \quad \text{where}$$

$$f(t) = \frac{t^{\frac{\nu}{2}-1} e^{-t/2}}{2^{\nu/2}\Gamma(\nu/2)}, \quad 0<t<\infty \qquad 5.29$$

is the chi-squared probability density function. The values of χ^2 for degrees of freedom ν, were determined corresponding to P = 0.17 and 0.83. As the quantity $t = \nu x/\bar{x}$, the lower confidence limit for the value x is

$\chi^2_{\bar{x}}/\nu$ for P = 0.17 and the upper confidence limit is given by the same expression for P=0.83. To determine the confidence limits of the ratios in table 5.1, the ratios themselves were assumed to be the mean of each χ^2- distribution.

The horizontal line in figure 5.1 at the ratio 1 is corresponding to complete agreement between the experiment and theory. A rough overall agreement between the observed and theoretically predicted values is apparent. To compare more quantitatively, a gross average of the ratios of all the nuclei in table 5.1 was sought. But there seems to be a dip in the ratios for the nuclides $143<A<181$, and the model of a constant strength function may be erroneous. However, we at first made a rough estimation of the gross average and then treated the entire data in a few subgroups separately.

Assuming crudely a Gaussian distribution of all the data, the average was searched. The weighted average was determined by the relation

$$\bar{R} = \frac{\Sigma R_i/\sigma_i^2}{\Sigma 1/\sigma_i^2} \qquad 5.30$$

where σ_i's for the thermal and discrete resonance were

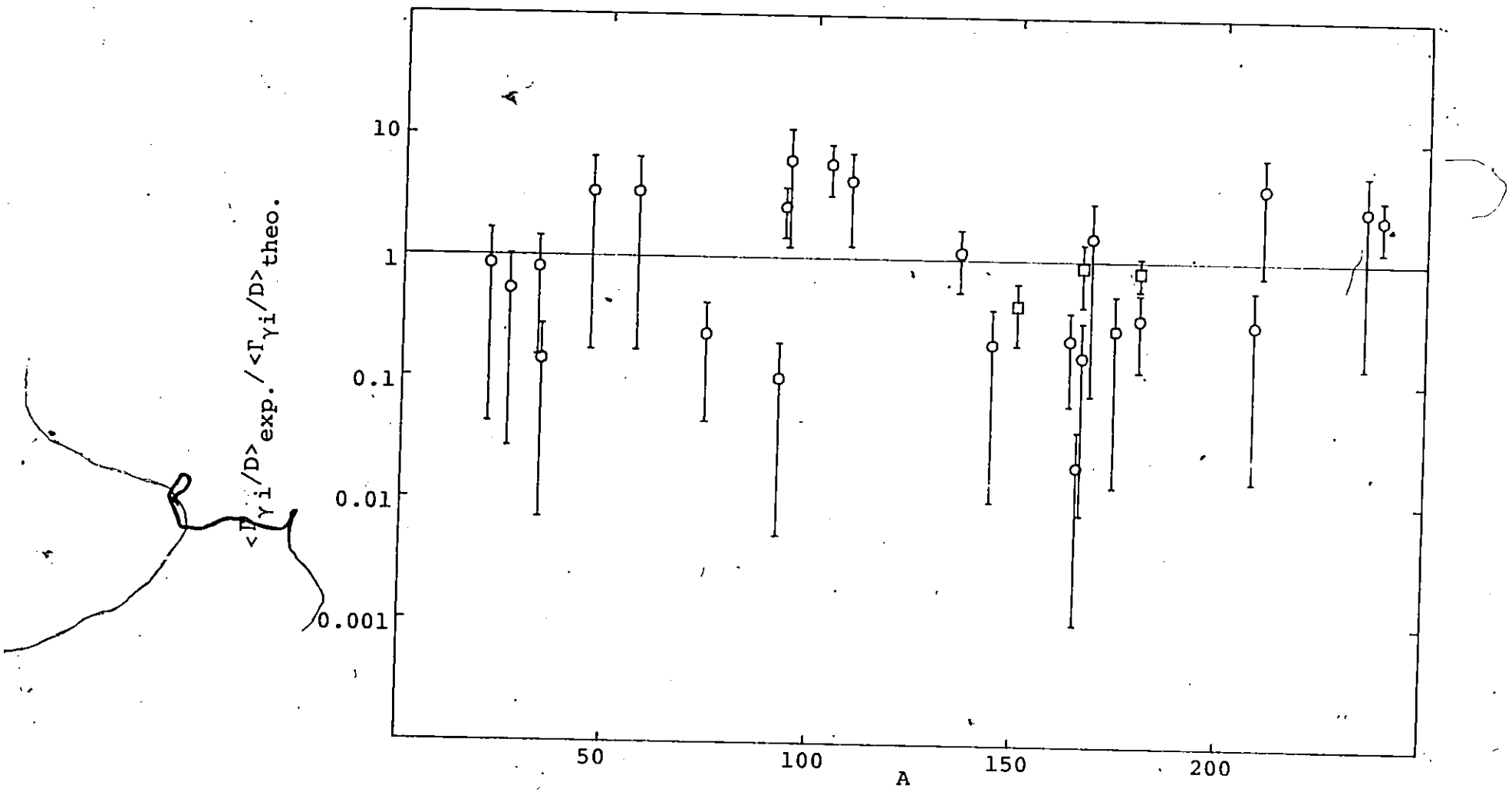

Figure 5.1. The ratio of the experimental to theoretical values of $\langle\Gamma_{\gamma i}/D\rangle$. The theoretical value is based on the giant resonance model. The horizontal line corresponds to the equality of experimental and theoretical values.

due to P-T fluctuations and those for the average-resonance data were mainly of experimental origin. To calculate the σ_i's for the first group, the average was intuitively assumed to be between 0.3 to 1. The above treatment gave a reduced $\chi^2>22$ which was unacceptable and it showed that the model of a constant strength function was not valid. The high value of the reduced χ^2 demonstrated the presence of structures in the strength function. The possibility of the presence of structures led to the assumption of an additional error in all the data. A constant error σ_c was added in quadrature with each of the σ_i's. The σ_c was varied to obtain a reduced χ^2 of 1. The corresponding gross average was found to be 1.7 ± 0.4. This value roughly equals the average if determined with equal weightage. The value 1.7, although higher than 1, indicates tentatively an overall agreement of the observations with the prediction of the theory.

The average of the ratios for the nuclei outside the range 143<A<181, was determined separately. The average $\bar{R}$ was found by minimizing

$$y = \sum_j \frac{(\bar{R}T_j - x_j)^2}{\sigma_j^2} \qquad 5.31$$

with respect to $\bar{R}$. The quantities T_j and x_j are theoretical and experimental $\Gamma_{\gamma i}/D$ respectively. The weightage σ_j^2 may be assessed for different x_j's. The relation

$$\frac{\delta Y}{\delta \bar{R}} = 0$$

gives the expression for the average:

$$\bar{R} = \frac{\sum_j \frac{x_j T_j}{\sigma_j^2}}{\sum_j T_j^2/\sigma_j^2} \qquad 5.32$$

To determine the weightage of the thermal and discrete resonance data, let us consider the likelihood function corresponding to χ^2-distributions with degrees of freedom ν_i,

$$L = \prod_i \bar{x}^{-\frac{\nu_i}{2}} e^{-\frac{\nu_i}{2}\left(\frac{x_i}{\bar{x}}\right)}, \qquad 5.33$$

where all factors independent of the average $\bar{x}$ of x_i have been dropped. Since ℓnL attains its maximum for the same value of $\bar{R}$ as L, we consider the equation

$$\frac{\delta \ell nL}{\delta \bar{R}} = 0 \qquad 5.34$$

Substituting L from equation 5.33 in equation 5.34, we get

$$\bar{x} = \frac{\Sigma \nu_i x_i}{\Sigma \nu_i} \qquad 5.35$$

Using the averaging process in equation 5.35 in equation

5.32 the expression of $\bar{R}$ for the thermal and discrete resonance data:

$$\bar{R} = \frac{\Sigma x_i T_i \nu_i}{\Sigma T_i^2 \nu_i} \qquad 5.36$$

The corresponding uncertainty (Ba73) for such a quantity is

$$\Delta\bar{R} = \bar{R}\sqrt{\frac{2}{m}}\ , \qquad 5.37$$

where m is the total number of degrees of freedom.

The average of the ratios for the region outside the dip was found to equal 1.3 ± 0.2.

For the region 143<A<181, the average was at first determined with the average-resonance data alone. The weighted average was found to 0.7 ± 0.2. This value is clearly much smaller than 1.3 ± 0.2 determined for the rest of the nuclei. The value 0.7 raises the possibility of a depression in the transition strength in the mass region. To ascertain the dip we searched for a similar average in our thermal data in this region. The average was determined using equation 5.36. The value for our data was found to be 0.5 ± 0.2 which supported the result of the average-resonance data.

The above results show that there may be a dip in the strength function in the mass region 143<A<180.

Since most of the nuclides in this region are well-deformed, there may be broadening of the giant resonances (Lo79) for them. But such broadening should increase the ratio of experimental to theoretical values instead of decreasing it. This reduction in quadrupole strength function in the region is due to some other reasons. There is a possibility that in the GQR for this region, there may be such structures in the low energy tail which may cause the dip in the strength function.

Strength Function of ^{208}Pb

The ratios of the observation and the theoretical prediction are shown in table D.8 and table D.9 with the level spacing 8 keV (Ho78) and 14 keV (Mu73) respectively. The averages are 5.1 ± 1.4 and 2.9 ± 0.8. In either case it is much greater than 1. This high value is possible as there is prominent structure in the GQR of ^{208}Pb (Ra78) capable of enhancing the radiation strength in the energy region of interest.

5.2 Dependence of Quadrupole Radiation Width on E and A

It has been indicated in the previous section that possibly there is the influence of the GQR on the E2 radiation width. Another way of investigating the decay process is to find the dependence of the transition width on the energy and the nuclear mass number. The commonly used procedure to do this is to assume a model for the average width

$$\langle\Gamma(E2)\rangle = kA^{p}E^{q}\langle D\rangle, \qquad 5.38$$

and then find the parameters k, p and q by using the experimental data.

It was mentioned in section 1.2.3 that the single-particle model (Bl52) predicts a dependence of the form

$$\langle\Gamma(E2)\rangle = kA^{4/3}E^{5}\langle D\rangle. \qquad 5.39$$

The expression of the GQR model prediction discussed in detail in section 5.1 can be reduced to the form of equation 5.38 when only the isoscalar GQR is considered and certain plausible approximations are made. If the values of E = 7 MeV and A = 100 are used to represent the global properties of the whole mass range, the following expression for the E2 giant resonance model holds (Ax62, Ko81)

$$\langle \Gamma(E2) \rangle = kA^{2.7}E^{5.2}\langle D \rangle \qquad 5.40$$

which deviates from the single-particle estimate mainly in an additional mass dependence.

To test the single-particle prediction, the quantities

$$k(E2) = \frac{\Gamma(E2)}{A^{4/3}E^{5}\langle D \rangle}, \qquad 5.41$$

where E is in MeV and Γ and D are in eV, were calculated for our thermal data and other thermal, resonance and average-resonance data. The values as a function of A are plotted on a logarithmic scale in figure 5.2. Some of the points in the plot resulted from the average over the same mass number. Except for the presence of a dip around A~160, an overall increase in the value of k with the mass number is apparent.

To arrive at the best estimate of k, p and q, the method of maximum likelihood (Ke61) was applied to the experimental data. In this treatment the inclusion of the average-resonance data would be complicated because of the combined effect of its low value and the Gaussian nature of its distribution. Therefore, the average-resonance data was ignored. The thermal and discrete resonance data from the literature, and our thermal values including the upper limits were sub-

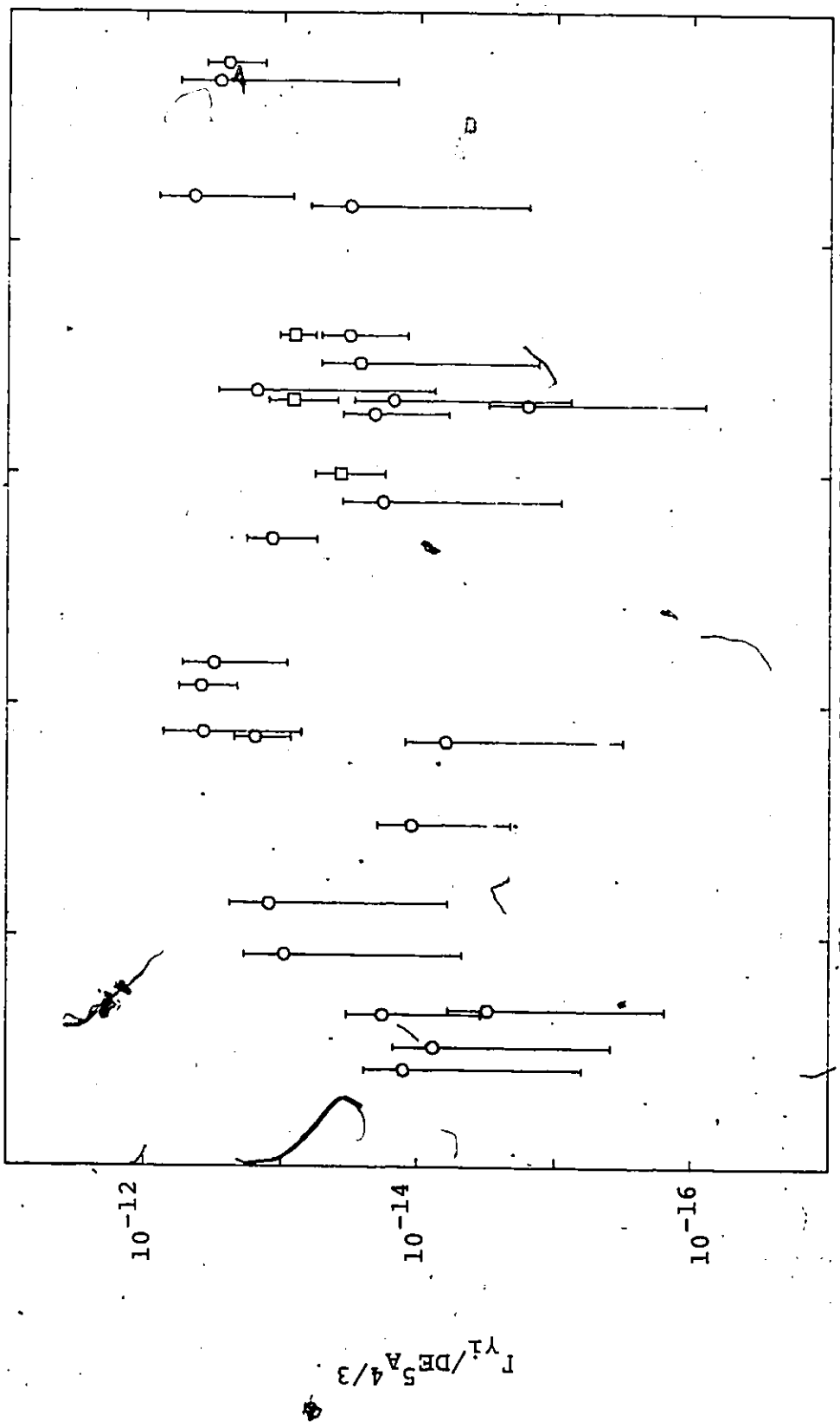

Figure 5.2. The quadrupole strength shown as a function of mass number.

jected to the treatment.

The likelihood of observing a particular value of the thermal or discrete resonance data

$$L_i = c\bar{\Gamma}_i^{-\frac{\nu_i}{2}} e^{-\frac{\nu_i}{2}\left(\frac{\Gamma_i}{\bar{\Gamma}_i}\right)} \qquad 5.42$$

where c contains terms involving functions of ν_i and Γ_i. The likelihood of observing a value less than or equal to an upper limit X_i (for a χ^2 distribution of 1 degree of freedom)

$$L_j = \int_0^{x_0} \frac{1}{\sqrt{2\pi x}} e^{-x/2} dx \qquad 5.43$$

where $x_0 = X_i/\bar{\Gamma}_i$ and $x = \Gamma_i/\bar{\Gamma}_i$. Substituting

$$y^2 = x/2,$$

$$L_j = \frac{2}{\sqrt{\pi}} \int_0^{Y_0=\sqrt{\frac{x_0}{2}}} e^{-y^2} dy \qquad 5.44$$

Equation 5.44 is called error function of y_0

$$\text{erf } y_0 = \frac{2}{\sqrt{\pi}} \int_0^{Y_0} e^{-y^2} dy \qquad 5.45$$

Using approximations from Ref. Ha55,

$$\text{erf } y_0 = 1-(a_1t+a_2t^2+a_3t^3)e^{-y_0^2}+\epsilon(y_0) \qquad 5.46$$

$$t = \frac{1}{1+py_0}, \quad p = 0.471 \quad |\epsilon(y_0)| \leq 2.5\times10^{-5}$$

$$a_1 = 0.348$$

$$a_2 = -0.096$$

$$a_3 = 0.748$$

Neglecting $\epsilon(y_0)$ in equation 5.46,

$$\text{erf } y_0 = 1-(a_1t+a_2t^2+a_3t^3)e^{-y_0^2} \qquad 5.47$$

Equation 5.47 gives the likelihood of observing a value less than or equal to an upper limit X_i. Thus the total likelihood of a combined set of N values and M upper limits

$$L = \prod_{i=1}^{N} c\bar{\Gamma}_i^{-\frac{\nu_i}{2}} e^{-\frac{\nu_i}{2}\left(\frac{\Gamma_i}{\bar{\Gamma}_i}\right)} \prod_{j=1}^{M} \left\{1-(a_1t_j+a_2t_j^2+a_3t_j^3)e^{-y_0^2}\right\} \qquad 5.48$$

where $t_j = \frac{1}{1+0.47\sqrt{\frac{X_i}{2\bar{\Gamma}_j}}}$ and $y_0 = \sqrt{\frac{X_i}{2\bar{\Gamma}_i}}$

and $\bar{\Gamma}_i = kA_i^pE_i^qD_i$.

The value of ℓnL, determined by the values of A_i, E_i and D_i, was maximized with respect to a set of values of the parameters k, p and q. For the thermal data, ν_i was assumed to be 1. The number of resonances was taken to equal ν_i for the discrete resonance values.

To determine the error in k, p and q, the second derivatives of ℓnL were derived with respect to the

the parameter. In the error analysis, for the sake simplicity, the upper limits were treated as actual values. The second derivatives are

$$\frac{\delta^2}{\delta p^2}(\Sigma \ell n L_i) = -\sum \frac{\nu_i}{2} \frac{\Gamma_i (\ell n A_i)^2}{k E_i^{q_{A_i}} P_{D_i}} \qquad 5.49$$

$$\frac{\delta^2}{\delta q^2}(\Sigma \ell n L_i) = -\sum \frac{\nu_i}{2} \frac{\Gamma_i (\ell n E_i)^2}{k E_i^{q_{A_i}} P_{D_i}} \qquad 5.50$$

$$\frac{\delta^2}{\delta k^2}(\Sigma \ell n L_i) = \sum \left\{ \frac{\nu_i}{2} \frac{1}{k^2} - \frac{\nu_i \Gamma_i}{k^3 A_i P_{E_i}^{q_{D_i}}} \right\} \qquad 5.51$$

The variances, therefore, are (Ke61)

$$\sigma_p^2 = \frac{1}{\sum \frac{\nu_i}{2} \frac{\Gamma_i (\ell n A_i)^2}{D_i k E^{q_A} P}} \qquad 5.52$$

$$\sigma_q^2 = \frac{1}{\sum \frac{\nu_i}{2} \frac{\Gamma (\ell n E)^2}{D_i k E^{q_A} P}} \qquad 5.53$$

$$\text{and, } \sigma_x^2 = \frac{1}{\sum \frac{\nu_i \Gamma_i}{k^3 A_i P_{E_i}^{q_{D_i}}} - \frac{\nu_i}{2} \frac{1}{k^2}} \qquad 5.54$$

The above analysis was performed twice: once with the values from the literature only (thus ignoring the region

of depressed strength) and then with all our thermal values included. With the former set, the best fitted values are

$$p = 2.5 \pm 0.1$$
$$q = 4.9 \pm 0.1 \qquad 5.55$$
$$\text{and } k = (9.6 \pm 2.0) \times 10^{-16}$$

When our data is included,

$$p = 2.2 \pm 0.1$$
$$q = 5 \pm 0.1 \qquad 5.56$$
$$\text{and } k = (2.7 \pm 0.5) \times 10^{-15}$$

The values of p and q, excluding the region $143<A<181$ agree well with that predicted by the GQR model. The inclusion of the region of dip was expected to bring down the overall dependence of A. Therefore, when it was included, the power of A was found to equal 2.2 which is less than 2.5. The functions $\Gamma_i/A^p E^q$ <D> in the two cases are plotted in figures 5.3 and 5.4. The solid horizontal line in each plot represents the fitted value of k.

In both the cases discussed above, the dependence on the mass number is clearly higher than 4/3 predicted by the single-particle model. This extra dependence may be due to the collective nature of the transition. It may therefore be concluded that the giant quadrupole

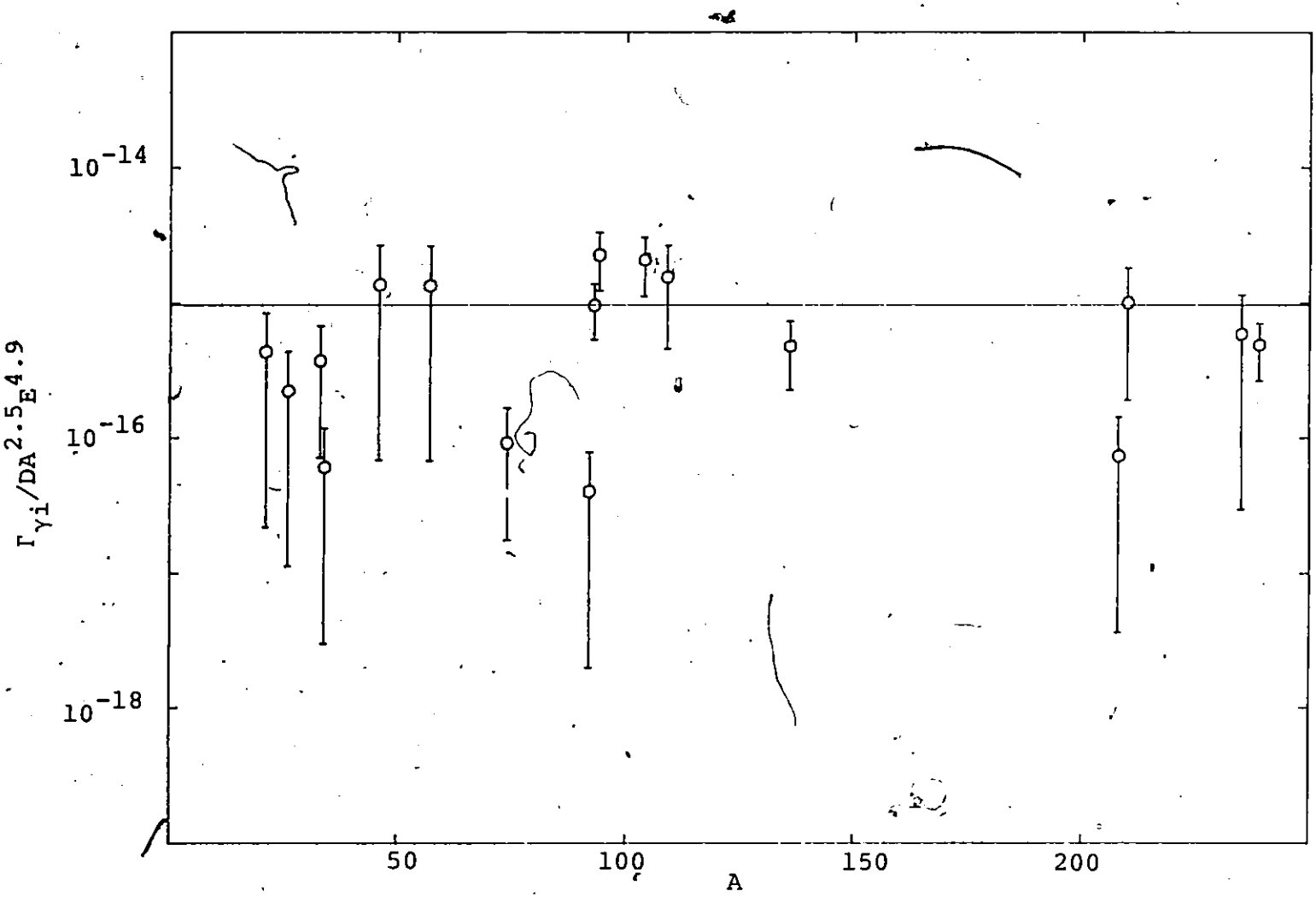

Figure 5.3. The reduced E2 strengths, defined as shown, as a function of mass number. The results are the thermal and discrete resonance data from the literature. The horizontal line corresponds to the mean.

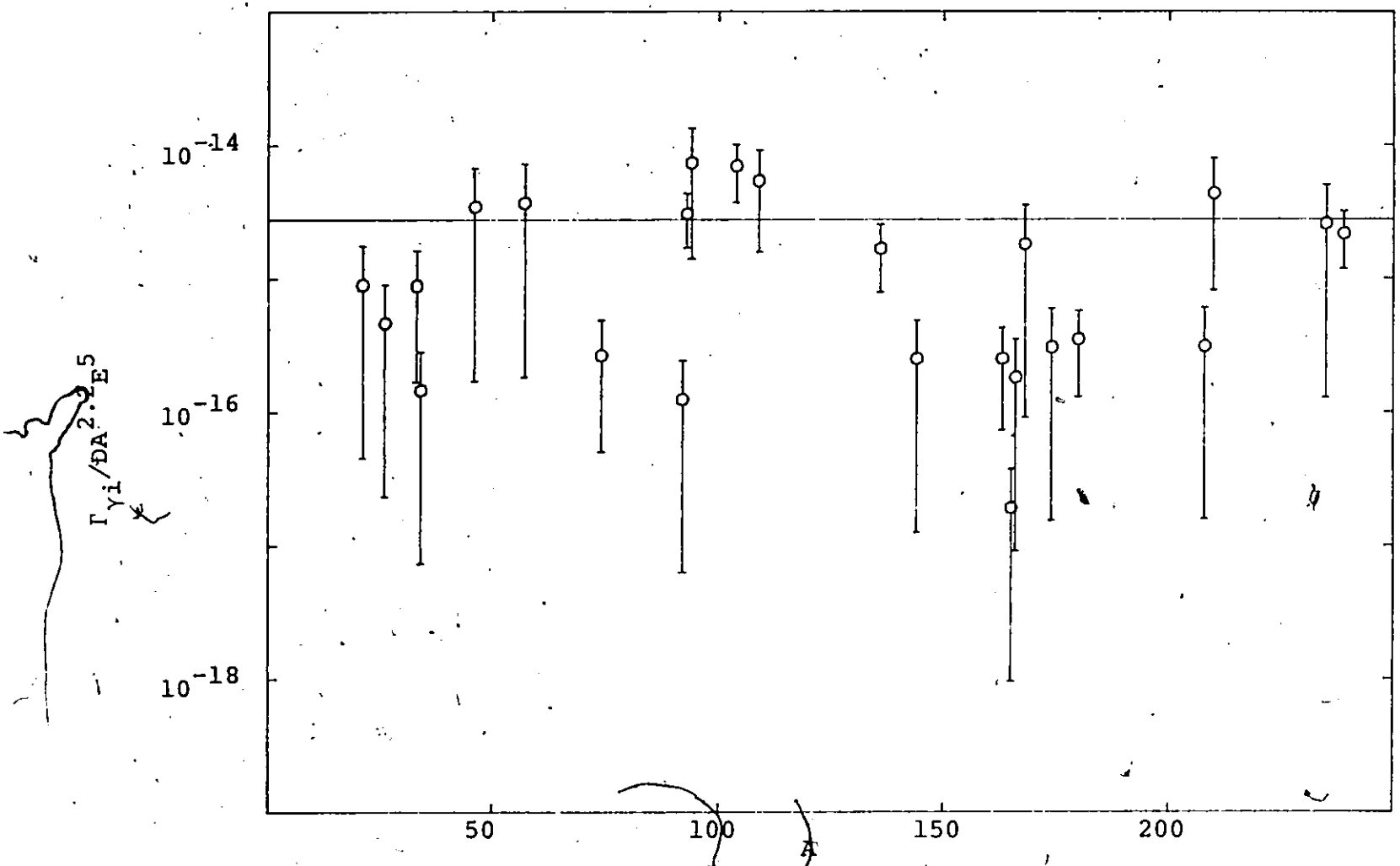

Figure 5.4. The reduced E2 strengths, defined as shown, as a function of mass number. The data includes thermal and discrete resonance works from literature, and our thermal data. The drawn line corresponds to the mean.

resonance is to a large extent responsible for the transition properties of the E2 radiation near the neutron threshold.

5.3 Reduced Transition Probabilities

The reduced transition probabilities $\bar{B}E2$ (per MeV) were determined for several masses or mass regions. They were then expressed in the Weisskopf single particle unit. To estimate $\bar{B}E2$ (per MeV), the functions

$$f_{E2}(E) = \left\langle \frac{\Gamma_{\lambda\gamma f}^{E2}(eV)}{D_{\lambda}(eV)E^{5}(MeV)} \right\rangle \qquad 1.23$$

were determined. The average was taken over several nuclides and/or several resonances. Averaging over adjacent nuclides did not introduce more than 4% error which is much smaller than the P-T fluctuation even after its reduction. As before, the degree of freedom of a thermal E2 transition, as well as that of a single resonance capture E2 transition, was taken to be 1. The average was determined by the relation

$$\bar{x} = \frac{\Sigma \nu_i x_i}{\Sigma \nu_i} \qquad 5.35$$

and the error was determined on the basis of P-T fluctuation alone. The function $f_{E2}(E)$ was transformed into $\bar{B}E2$ (per MeV) by equation 1.2.4. The values of $\bar{B}E2$ (per MeV) and $\bar{B}E2/B_W(E2)$ (per MeV) are presented in table 5.2. For the average-resonance values of ^{150}Sm,

^{166}Ho and ^{180}Hf, the errors are due to experimental origins and various factors involved. The errors of most of the results in table 5.2 are too high to make any definite conclusion. Nevertheless it is apparent that for nuclei 150<A<180 a fraction of the single particle transition strength is spread over 1 MeV.

The quadrupole strengths

$$K(E2) = \frac{\Gamma_{\gamma i}}{D_\lambda E^5 A^{4/3}} \qquad 1.28$$

averaged over several transitions in a nucleus, or nuclei with adjacent mass numbers were determined. These values are presented in table 5.2.

TABLE 5.2

Reduced Transition Probability per MeV and the Average Quadrupole Strength

Mass No.	ν	$\bar{B}E2$ (per MeV) ($e^2fm^4MeV^{-1}$)	$\frac{\bar{B}E2}{B_W(E2)}$ (MeV^{-1})	$\bar{k}(E2)$ ($10^{-13}MeV^{-5}$)
92- 94	12	94± 38	3.7 ±1.5	1.8 ±0.7
104-109	11	226± 96	7.7 ±3.3	3.7 ±1.6
136	6	102± 55	2.5 ±1.4	1.2 ±0.7
150	a	37± 19	0.79±0.40	0.37±0.19
163-166	5	18± 11	0.33±0.20	0.16±0.09
166	a	94± 49	1.7 ±1.0	0.82±0.40
180	4	40± 28	0.66±0.47	0.32±0.22
180	a	102± 35	1.7 ±0.7	0.81±0.29
208-210	3	477±358	6.4 ±4.8	3.1 ±2.3
235-239	9	466±210	5.3 ±2.4	2.5 ±1.2

[a]Average resonance capture. The errors in BE2 are of pure experimental origin.

CHAPTER 6

CONCLUSIONS

This work has increased the number of known primary E2 transitions following thermal neutron capture by 50%. In total 8 primary E2 transitions in 6 nuclei have been detected and their intensities have been determined. The upper limits of the intensities of 4 transitions have been estimated. This data removes the gap in the existing knowledge of E2 intensities in the mass region $143<A<181$.

The data obtained in the present study along with those from the literature is analyzed to study the radiative quadrupole strength in neutron capture. A quantitative expression for the strength function $\langle \Gamma_{\gamma i}/D \rangle$ has been derived on the basis of the influence of the giant quadrupole resonances (isoscalar and isovector) on the transition strength. All the experimental values of $\Gamma_{\gamma i}/D$ are compared with their corresponding theoretical prediction. It is found that the experimental values on an average are higher than the theoretical values. Nevertheless there is an overall agreement between the two. Thus the GQR seems to contribute to the E2 strength. We have found a depression in the strength function in the

mass region $143<A<181$. This deficiency is supported both by the average-resonance data and our thermal data. The probable reason behind this dip may be the presence of such structures in the giant resonances in this mass region that depletes the strength. Since this region consists mainly of the deformed nuclei a theoretical investigation of the low value of the strength function may be worthwhile.

The method of maximum likelihood has been applied to data acquired in the present study along with the previous thermal and discrete resonance data in order to find the best estimate of the energy and mass number dependence of the quadrupole radiation width. If the region of dip is not included, the power of A is found to be 2.5 ± 0.1 and the power of E equals 4.9 ± 0.1. These values agree with the giant resonance prediction (Ax62, Ko81) of 2.7 and 5.2. The previously reported (Ko81) mass dependence, derived by slightly different set of data and by the method of least squares, was $A^{(3.0\pm0.3)}$ which agrees within error with our result. But when the region $143<A<181$ is included in our analysis, a mass dependence of $A^{(2.2\pm0.1)}$ is found. Obviously the low values of the radiation widths in the region have brought down the value of the power of A. It seems more reasonable to assume a

smooth function with the higher power of A superimposed with a dip in the region 143<A<181 rather than the overall decrement in the dependence of A.

It may be concluded that the giant quadrupole resonance does influence the radiative strength in neutron capture. The single-particle prediction of the mass dependence $A^{4/3}$ is too low to adequately describe the data.

The reduced transition probabilities in Weisskopf unit and the average quadrupole strengths of some mass numbers have been calculated in this work. These quantities for the quadrupole transition are new of its type in the literature. To use them for studying nuclear properties (Lo79), more such numbers are required and in most of the cases the improvement in precision is needed.

To have more understanding of the influence of the giant quadrupole resonances at the neutron threshold and to identify the presence of structures, more E2 data for many of the missing nuclides is to be acquired. One way to enrich the knowledge of the E2 intensities is to look for E2 transitions in (n,γ) reactions even though it may be meant for some other investigations and if the E2 radiation is not detected it is sometimes possible to assign the upper limit of its intensity. These upper

limits may be useful in the subsequent analysis.

In the course of detecting and analyzing the E2 transitions, the neutron separation energies of 15 nuclides have been determined. These values agree in general with those reported in the literature (Wa77), but the precision in our values has been increased by more than a factor of 20 in many cases. The radiative capture cross section of the calibration standard ^{14}N has been found to be 78.4±1.5 mb. This is a marked improvement in the precision over the previously known value of 75.0±7.5 mb (Ju63). A large number of new gamma-ray transitions in the (n,γ) reactions has been found, and their intensities and energies are presented. Some of these transitions are indicative of new nuclear levels. The number of possible levels in ^{165}Dy below 1650 keV has been increased by a factor of 2.

APPENDIX A

TABLE A.1

Survey of the Primary E2 Transitions in

(n,γ) Reactions

Final Nucleus	E_n (keV)	E_γ (keV)	Transition	Ref.	I_γ (per 10^4)	a_{Γ_γ} (meV)	$b_{\Gamma_{\gamma i}}$ (meV)
^{21}Ne	th	6410	$1/2^+ \rightarrow 5/2^+$	Be71	80±40	560	4.5±2.3
^{26}Mg	th	11093	$2^+ \rightarrow 0^+$	Se69	11±5	3900	.4.3±2.2
^{33}S	th	6676	$1/2^+ \rightarrow 5/2^+$	Ke67	60±20	1900	11±5
^{33}S	th	5754	$1/2^+ \rightarrow 5/2^+$	Ra81	7±3	1900	1.3±0.6
^{34}S	th	6728	$2^+ \rightarrow 4^+$	Ra81	2±1	680	0.14±0.07
^{35}S	th	4269	$1/2^+ \rightarrow 5/2^+$	Ra81	34±5	1900	6.5±1.0
^{46}Sc	th	8618	$3^- \rightarrow 1^-$	Ti82	24±8	840	2.0±0.8
^{57}Fe	1.1(P)	7511	$1/2^- \rightarrow 5/2^-$	Ch73			14.5±5
^{74}Ge	th	9606	$4^+ \rightarrow 2^+$	We66	3.6±0.4	200	0.072±0.008
^{74}Ge	th	8998	$4^+ \rightarrow 2^+$	We66	0.7±0.2	200	0.014±0.004
^{92}Zr	th	8635	$2^+ \rightarrow 0^+$	Or70	11±3	140	0.15±0.05
^{93}Mo	0.35(S)	8067	$1/2^+ \rightarrow 5/2^+$	Wa73			9±1
^{93}Mo	$\langle S \rangle_6$	8067	$1/2^+ \rightarrow 5/2^+$	Wa73			4.5±2.6
^{93}Mo	$\langle S \rangle_2$	6375	$1/2^+ \rightarrow 5/2^+$	Wa73			0.9±0.6
^{94}Nb	0.106(S)	7229	$4^+ \rightarrow 6^+$	Ch71			0.26±0.2
^{94}Nb	0.036(P)	6833	$5^- \rightarrow (3^-)$	Ch71			0.23±0.31

TABLE A.1 (Cont'd)

Final Nucleus	E_n (keV)	E_γ (keV)	Transition	Ref.	I_γ (per 10^4)	$a\Gamma_\gamma$ (meV)	$b\Gamma_{\gamma i}$ (meV)
^{104}Rh	th	6731	$1^- \rightarrow 3^-$	Ke81b	0.7±0.2	160	0.011±0.004
^{104}Rh	$\langle S \rangle_1$	6948	$0^- \rightarrow 2^-$	Ri70	16.1±6	160	0.26±0.13
^{104}Rh	$\langle S \rangle_6$	6731	$1^- \rightarrow 3^-$	Ri70	5.8±2.8	160	0.09±0.04
^{109}Pd	th	6153	$1/2^+ \rightarrow 5/2^+$	Ca80	11±2	77	0.085±0.017
^{109}Pd	th	5613	$1/2^+ \rightarrow 5/2^+$	Ca80	9±6	77	0.069±0.034
^{109}Pd	th	5172	$1/2^+ \rightarrow 5/2^+$	Ca80	30±12	77	0.23±0.10
^{136}Ba	$\langle S \rangle_6$	9107	$2^+ \rightarrow 0^+$	Ch74			0.37±0.21
^{208}Pb	th	4753	$1^- \rightarrow 3^-$	Ma72	11±3	5000	5.5±1.8
^{208}Pb[d]	$\langle P \rangle_{27}$	7371-8167	$2^+ \rightarrow 0^+$	Ra78			
^{210}Bi	th	4285	$4^- \rightarrow 2^-$	Ts82	109±21	45	[e] 2.1±0.5
^{210}Bi	th	4171	$5^- \rightarrow 7^-$	Ts82	3020±40	45	[e] 17.7±0.4
^{235}U	th	5246	$1/2^+ \rightarrow 5/2^+$	Ju69	8±2	25	0.02±.006
^{239}U	th	4610	$1/2^+ \rightarrow 5/2^+$	Bo72	16±2	25	0.04±.005
^{239}U	$\langle S \rangle_7$	4610	$1/2^+ \rightarrow 5/2^+$	Pr68			0.01±0.001

[a] For A≤109, Ref. Mu81; For the rest, Ref. Mu73.

[b] Those $\Gamma_{\gamma i}$ for which no corresponding I_γ was given, were determined directly.

[c] Spins of resonances taken from Ref. Ha75.

[d] Partial widths of 27 transitions can be obtained directly from Ref. Ra78.

[e] Correction done for spin states at neutron capture.

APPENDIX B

TABLE B.1

[a]Contents of the Separated Isotope Samples

Separated isotope	Element	Mass Number	Atomic percent	σ_γ [b] (barn)
^{143}Nd	Nd	142	2.92	19
		143	91.68	325
		144	4.27	4
		145	0.46	42
		146	0.52	1
		148	0.09	3
		150	0.06	1
	Gd		<0.02	49000
	Sm		<0.05	5800
	Cd		<0.05	2450
^{162}Dy	Dy	156	<0.02	930
		158	<0.02	43
		160	0.08	61
		161	1.22	585
		162	96.26	180
		163	1.75	130
		164	0.69	2700
	Sm		<0.05	
	Gd		<0.02	
	Cd		<0.05	
^{164}Dy	Dy	156	<0.01	930
		158	<0.01	43
		160	0.01	61
		161	0.15	585
		162	0.35	180
		163	1.05	130
		164	98.43	2700
	Sm		<0.05	
	Gd		<0.02	
	Cd		<0.05	

TABLE B.1 (Cont'd.)

Separated isotope	Element	Mass Number	Atomic percent	σ_γ [b] (barn)
^{173}Yb	Yb	168	<0.02	37
		170	0.08	
		171	0.62	
		172	2.44	
		173	92.08	
		174	4.46	
		176	0.32	
	Gd		<0.02	
	Sm		<0.05	
	Cd		<0.05	
	Dy		<0.1	930
^{179}Hf	Hf	174	<0.05	102
		176	0.56	38
		177	3.42	365
		178	5.42	86
		179	81.85	45
		180	8.74	44
	Gd		<0.02	
	Sm		<0.05	
	Dy		<0.1	
	Cd		<0.05	

[a] Supplied by Union Carbide Corporation Nuclear Division. Spectrographic analysis.

[b] Ref. Mu73.

APPENDIX C

Calculation for P-Wave Correction in Average Resonance Data

The wave number for a neutron

$$K = 2.18\times10^{11}\sqrt{E(eV)}\ m^{-1} \qquad C.1$$

The quantity

$$(KR)^2 = 7.23\times10^{-8}E(eV)A^{2/3}, \text{ where } R=1.233\times10^{-15}A^{1/3}\ m \qquad C.2$$

The integral in equation 3.20 b can be replaced by

$$I_0 = \int_0^\infty \frac{e^{-a/\sqrt{E}}}{E^{3/2}}dE$$

Using $E = \frac{1}{x^2}$, $I_0 = 2\int_0^\infty e^{-ax}dx = \frac{2}{a}$ C.3

Similarly, the integral in equation 3.20 a can be replaced by

$$I_1 = \int_0^\infty \frac{e^{-a/\sqrt{E}}}{E^{3/2}} \frac{C_2E}{1+C_2E}dE \quad [C_2=7.29\times10^{-8}A^{2/3}]$$

Using $E = \frac{1}{x^2}$

$$I_1 = 2C_2\int_0^\infty \frac{1}{x^2+(\sqrt{C_2})^2}e^{-ax}dx \qquad C.4$$

Using the Table of Integrals (Gr65),

$$I_1 = 2\sqrt{C_2}\left\{C_i(a\sqrt{C_2})\sin(a\sqrt{C_2}) - Si(a\sqrt{C_2})\cos(a\sqrt{C_2})\right\}$$

Let $a\sqrt{C_2} = y$

$$I_1 = 2\,C_2\left\{Ci(y)\sin(y) - Si(y)\cos(y)\right\} \qquad C.5$$

$$Ci(y) = C - \ell n(y) + \sum_{k=1}^{\infty} (-1)^k \frac{y^{2k}}{2k(2k)!} \qquad C.6$$

Euler's constant C = 0.5772. The third term in equation 3.6 is negligible.

$$Si(y) = -\frac{\pi}{2} + \sum_{k=1}^{\infty} \frac{(-1)^{k+1} y^{2k-1}}{(2k-1)(2k-1)!} \qquad C.7$$

where the second term is negligible.

APPENDIX D

TABLE D.1

PHOTON ENERGIES AND INTENSITIES OBSERVED IN THE $^{143}Nd(n,\gamma)^{144}Nd$ REACTION

NO.	ENERGY keV	INTENSITY per 1000	NO.	ENERGY keV	INTENSITY per 1000	NO.	ENERGY keV	INTENSITY per 1000	NO.	ENERGY keV	INTENSITY per 1000
1	7120.42	0.05	30	4829.41	0.21	59	4340.32	1.18	88	4046.92	1.40
2	6502.64	80.78	31	4790.54	12.40	60	4322.95	0.75	89	4037.07	1.22
3	6306.88	0.43	32	4774.33	4.69	61	4317.87	0.24	90	4021.83	0.91
4	6256.26	34.27	33	4752.41	1.29	62	4310.90	0.38	91	4018.01	0.23
5	5744.37	1.17	34	4746.51	3.61	63	4300.45	0.21	92	4010.40	2.11
6	5723.93	0.66	35	4737.34	0.17	64	4298.83	0.39	93	4002.66	3.51
7	5707.31	4.74	36	4716.82	0.48	65	4293.72	0.74	94	3994.62	1.08
8	5638.40	3.88	37	4690.71	6.48	66	4282.54	0.23	95	3982.44	0.31
9	5612.42	0.41	38	4669.57	6.52	67	4267.29	1.13	96	3980.32	0.74
10	5521.77	13.26	39	4615.00	4.39	68	4265.60	0.37	97	3973.29	0.51
11	5448.59	16.96	40	4595.20	2.05	69	4256.00	3.62	98	3962.96	0.90
12	5252.84	0.49	41	4564.91	1.44	70	4238.01	0.32	99	3957.75	0.57
13	5224.71	1.40	42	4562.49	4.01	71	4215.20	1.12	100	3948.50	2.41
14	5216.39	0.26	43	4543.68	0.29	72	4211.14	0.49	101	3938.69	0.27
15	5211.21	1.20	44	4535.11	4.54	73	4204.55	0.36	102	3924.16	0.52
16	5161.57	0.39	45	4526.61	0.24	74	4185.73	0.55	103	3910.96	0.67
17	5124.54	0.21	46	4515.37	0.32	75	4179.45	1.15	104	3901.84	0.29
18	5101.59	0.16	47	4501.57	3.76	76	4170.21	0.50	105	3893.32	3.57
19	5039.46	0.19	48	4474.48	0.48	77	4155.96	0.32	106	3885.87	0.99
20	5008.30	0.20	49	4466.56	0.27	78	4150.90	1.01	107	3864.92	0.38
21	4988.50	0.19	50	4456.52	0.36	79	4148.67	0.75	108	3854.41	0.73
22	4982.47	1.34	51	4439.86	0.63	80	4130.55	2.92	109	3850.59	0.39
23	4948.93	10.73	52	4435.46	4.53	81	4122.87	1.94	110	3844.56	0.91
24	4929.66	0.55	53	4421.94	2.98	82	4114.14	1.90	111	3843.22	0.58
25	4915.61	3.61	54	4414.27	1.51	83	4110.27	1.27	112	3838.22	0.25
26	4866.18	1.09	55	4407.02	6.75	84	4078.02	2.70	113	3834.47	1.33
27	4855.17	0.20	56	4401.41	0.33	85	4074.65	0.54	114	3818.57	0.32
28	4849.28	0.22	57	4374.29	0.62	86	4062.63	1.17	115	3816.89	0.24
29	4837.34	2.80	58	4356.13	4.54	87	4058.43	0.70	116	3805.24	4.34

TABLE D.2

PHOTON ENERGIES AND INTENSITIES OBSERVED IN THE $^{162}Dy(n,\gamma)^{163}Dy$ REACTION

NO.	ENERGY keV	INTENSITY per 1000	NO.	ENERGY keV	INTENSITY per 1000	NO.	ENERGY keV	INTENSITY per 1000	NO.	ENERGY keV	INTENSITY per 1000
1	5919.93	0.69	29	4578.38	6.48	57	4001.57	9.06	85	3688.53	1.42
2	5881.17	12.53	30	4496.01	0.25	58	3980.94	0.84	86	3684.21	2.84
3	5849.12	12.30	31	4480.04	0.43	59	3933.53	0.81	87	3664.54	1.13
4	5533.18	3.14	32	4460.56	0.22	60	3931.80	1.57	88	3658.34	1.70
5	5504.75	2.23	33	4457.52	0.24	61	3923.72	1.44	89	3654.86	1.17
6	5477.33	0.48	34	4435.53	0.84	62	3909.50	5.34	90	3643.63	1.99
7	5450.08	26.57	35	4425.83	1.36	63	3890.03	2.16	91	3636.55	0.32
8	5411.56	1.27	36	4397.01	2.37	64	3885.63	0.21	92	3622.27	1.74
9	5386.60	2.02	37	4348.47	5.27	65	3878.01	3.72	93	3615.60	0.98
10	5354.45	0.16	38	4340.16	0.54	66	3851.73	0.35	94	3609.90	0.30
11	5335.66	2.79	39	4320.41	5.94	67	3839.17	2.38	95	3600.24	0.33
12	5221.73	11.21	40	4313.31	11.18	68	3819.40	0.26	96	3596.06	0.30
13	5214.98	7.36	41	4305.98	0.34	69	3810.49	3.59	97	3576.17	1.15
14	5212.42	3.59	42	4285.07	0.58	70	3798.99	1.63	98	3573.74	0.36
15	5205.07	0.21	43	4266.56	9.00	71	3794.92	2.00	99	3565.14	0.48
16	5186.33	1.74	44	4221.00	0.73	72	3779.89	0.57	100	3563.03	0.96
17	5123.48	2.99	45	4175.65	0.19	73	3764.03	0.38	101	3555.49	0.55
18	5110.45	2.75	46	4160.97	1.67	74	3762.40	0.79	102	3552.95	1.10
19	5074.95	6.68	47	4111.70	1.70	75	3756.12	0.60	103	3546.55	0.57
20	5017.74	0.40	48	4104.67	0.71	76	3748.55	0.87	104	3543.67	0.79
21	4840.77	0.34	49	4094.94	0.57	77	3746.31	0.30	105	3539.52	2.34
22	4831.90	1.48	50	4074.49	2.86	78	3739.20	0.57	106	3536.59	1.00
23	4781.86	7.37	51	4071.20	6.21	79	3735.97	1.18	107	3532.90	0.47
24	4755.26	0.32	52	4048.54	2.60	80	3719.16	1.05	108	3529.64	0.34
25	4741.75	1.80	53	4029.17	1.75	81	3713.91	2.47	109	3527.40	0.42
26	4685.71	0.58	54	4027.81	3.82	82	3710.23	0.75	110	3523.59	0.82
27	4655.90	2.06	55	4023.06	0.24	83	3701.65	0.72	111	3516.44	5.21
28	4621.29	0.23	56	4011.10	1.69	84	3691.80	3.02	112	3511.06	0.77

TABLE D.2 (cont'd.)

PHOTON ENERGIES AND INTENSITIES OBSERVED IN THE $^{162}Dy(n,\gamma)^{163}Dy$ REACTION

NO.	ENERGY keV	INTENSITY per 1000	NO.	ENERGY keV	INTENSITY per 1000	NO.	ENERGY keV	INTENSITY per 1000	NO.	ENERGY keV	INTENSITY per 1000
113	3507.16	2.76	140	3371.17	1.80	167	3218.98	1.50	194	3090.27	0.54
114	3505.07	1.24	141	3367.53	1.01	168	3214.33	0.37	195	3087.88	0.95
115	3499.51	0.48	142	3357.52	3.49	169	3212.54	0.87	196	3084.92	0.93
116	3497.17	1.93	143	3355.01	0.35	170	3203.50	4.25	197	3083.48	1.95
117	3492.89	0.80	144	3350.53	3.78	171	3188.45	0.99	198	3077.96	1.44
118	3485.45	0.47	145	3346.90	2.77	172	3185.00	0.77	199	3074.91	2.50
119	3481.45	0.69	146	3335.05	0.42	173	3182.19	0.40	200	3067.62	2.12
120	3475.10	0.73	147	3332.66	0.70	174	3179.61	0.50	201	3066.10	0.39
121	3464.65	1.02	148	3328.23	1.08	175	3172.18	0.87	202	3062.65	1.05
122	3461.92	0.59	149	3315.41	1.37	176	3167.63	3.13	203	3058.93	1.71
123	3457.45	0.87	150	3314.23	0.77	177	3164.10	1.44	204	3056.29	0.71
124	3451.14	1.49	151	3312.67	0.96	178	3154.99	0.94	205	3053.70	0.44
125	3440.36	1.05	152	3299.69	0.82	179	3152.46	1.77	206	3052.60	0.36
126	3436.82	3.38	153	3294.07	2.09	180	3151.40	0.43	207	3050.87	0.93
127	3434.52	2.17	154	3292.19	0.68	181	3149.87	0.63	208	3049.68	0.75
128	3431.59	0.63	155	3287.96	1.99	182	3146.56	0.42	209	3045.60	2.27
129	3424.18	0.40	156	3285.74	0.52	183	3140.94	0.65	210	3042.88	0.80
130	3418.39	0.52	157	3280.57	0.71	184	3133.18	2.31	211	3039.83	3.04
131	3415.44	1.42	158	3275.45	0.40	185	3124.78	0.85	212	3035.44	0.75
132	3407.92	2.86	159	3272.81	2.96	186	3122.81	1.07	213	3032.54	1.03
133	3404.41	2.22	160	3268.63	0.34	187	3116.87	1.67	214	3028.64	1.92
134	3401.52	1.63	161	3257.34	0.98	188	3105.17	0.51	215	3027.05	2.45
135	3399.51	0.75	162	3245.25	1.08	189	3103.70	0.94	216	3016.18	1.07
136	3393.42	0.31	163	3243.33	0.97	190	3098.62	2.31	217	3013.84	1.85
137	3390.94	2.67	164	3236.89	0.61	191	3094.40	0.49	218	3010.52	1.20
138	3383.83	0.36	165	3225.30	1.69	192	3092.87	2.67	219	3006.94	0.62
139	3377.11	1.17	166	3222.10	0.63	193	3091.72	0.65	220	3001.58	1.50

TABLE D.2 (cont'd.)

PHOTON ENERGIES AND INTENSITIES OBSERVED IN THE $^{162}Dy(n,\gamma)^{163}Dy$ REACTION

NO.	ENERGY keV	INTENSITY per 1000	NO.	ENERGY keV	INTENSITY per 1000	NO.	ENERGY keV	INTENSITY per 1000	NO.	ENERGY keV	INTENSITY per 1000
221	2997.87	0.88	248	2831.42	2.20	275	2675.67	1.47	302	2534.99	1.52
222	2993.89	0.47	249	2824.38	1.04	276	2670.61	0.54	303	2533.44	1.37
223	2987.25	2.01	250	2817.71	2.23	277	2662.98	0.93	304	2530.82	1.43
224	2984.38	1.81	251	2810.38	2.04	278	2660.66	0.76	305	2513.74	1.98
225	2982.22	1.12	252	2806.57	0.71	279	2657.83	1.93	306	2511.91	1.29
226	2979.20	1.12	253	2802.83	2.45	280	2654.88	0.60	307	2505.26	0.98
227	2975.46	0.86	254	2794.17	0.67	281	2635.25	1.50	308	2501.42	3.44
228	2973.10	0.81	255	2791.47	0.86	282	2627.63	2.24	309	2493.31	0.73
229	2953.37	0.96	256	2788.94	1.09	283	2619.03	1.76	310	2490.87	1.13
230	2951.88	0.94	257	2785.83	2.10	284	2615.77	1.86	311	2489.05	0.74
231	2944.38	2.80	258	2783.73	1.26	285	2607.89	0.99	312	2485.72	1.51
232	2937.51	4.05	259	2771.74	2.51	286	2605.38	1.28	313	2468.54	1.07
233	2932.97	1.32	260	2766.36	3.55	287	2599.29	1.60	314	2451.47	0.90
234	2927.25	1.92	261	2756.58	2.44	288	2594.17	1.13	315	2446.18	1.42
235	2920.93	2.71	262	2755.11	1.98	289	2587.62	1.12	316	2441.28	0.74
236	2914.43	0.96	263	2747.74	1.34	290	2585.96	1.79	317	2434.84	1.22
237	2904.71	0.97	264	2745.17	1.78	291	2579.71	0.60	318	2432.31	1.74
238	2897.16	2.58	265	2743.93	0.90	292	2576.53	2.84	319	2421.49	1.06
239	2891.57	0.52	266	2739.63	1.33	293	2568.91	1.27	320	2419.01	1.04
240	2872.29	1.80	267	2728.57	1.29	294	2566.61	0.70	321	2412.78	2.09
241	2867.17	1.62	268	2721.70	1.71	295	2563.97	0.98	322	2408.61	2.00
242	2858.13	2.44	269	2715.31	0.55	296	2561.45	1.33	323	2393.25	1.11
243	2854.11	1.64	270	2706.78	1.09	297	2556.94	2.49	324	2388.70	2.46
244	2851.17	1.31	271	2702.04	0.72	298	2553.84	1.24	325	2386.35	2.16
245	2847.23	1.88	272	2696.86	1.57	299	2551.74	0.96	326	2381.46	1.59
246	2843.54	1.11	273	2680.67	2.03	300	2548.98	2.12	327	2379.77	1.47
247	2834.70	0.48	274	2678.33	1.42	301	2538.69	1.05	328	2361.86	1.37

TABLE D.3

PHOTON ENERGIES AND INTENSITIES OBSERVED IN THE $^{164}Dy(n,\gamma)^{165}Dy$ REACTION

NO.	ENERGY keV	INTENSITY per 1000	NO.	ENERGY keV	INTENSITY per 1000	NO.	ENERGY keV	INTENSITY per 1000	NO.	ENERGY keV	INTENSITY per 1000
1	5607.75	37.80	33	3920.25	0.71	65	3477.34	3.74	97	3171.06	0.56
2	5557.27	30.44	34	3901.66	0.93	66	3445.65	4.69	98	3169.32	3.93
3	5177.25	6.27	35	3885.56	4.78	67	3443.59	10.21	99	3158.61	4.29
4	5145.51	9.07	36	3881.38	0.42	68	3431.51	1.42	100	3148.87	2.89
5	5142.39	7.81	37	3842.88	0.84	69	3424.88	0.78	101	3146.17	1.63
6	5110.80	6.60	38	3840.33	3.64	70	3417.81	8.26	102	3142.02	0.66
7	4804.01	0.14	39	3830.12	0.30	71	3409.29	2.02	103	3129.49	0.93
8	4699.98	0.28	40	3825.53	0.33	72	3408.02	2.05	104	3114.00	6.75
9	4635.87	1.26	41	3820.19	2.80	73	3405.31	0.74	105	3105.84	5.50
10	4612.92	6.10	42	3772.29	3.19	74	3394.34	0.60	106	3097.06	1.76
11	4607.86	1.64	43	3753.38	1.84	75	3375.17	0.52	107	3084.06	0.37
12	4557.52	0.25	44	3747.08	2.96	76	3365.32	0.48	108	3080.72	0.95
13	4549.12	1.01	45	3727.59	0.34	77	3349.36	3.62	109	3071.02	3.82
14	4497.55	0.64	46	3708.66	3.45	78	3336.96	1.12	110	3067.52	2.35
15	4459.47	1.57	47	3650.29	0.84	79	3321.08	1.98	111	3050.76	2.74
16	4339.60	0.94	48	3627.96	2.64	80	3317.23	0.59	112	3045.89	0.76
17	4335.18	0.33	49	3609.09	3.66	81	3313.73	2.70	113	3042.70	0.41
18	4315.84	1.18	50	3603.43	0.62	82	3305.46	0.62	114	3036.25	5.35
19	4275.30	0.89	51	3585.23	0.50	83	3302.04	0.36	115	3035.16	5.78
20	4259.62	0.17	52	3576.40	0.35	84	3284.24	0.31	116	3032.00	0.49
21	4251.16	0.97	53	3555.80	3.47	85	3276.12	6.80	117	3030.14	0.39
22	4160.52	0.18	54	3543.65	0.70	86	3268.93	3.28	118	3021.16	0.64
23	4155.85	2.10	55	3537.73	3.44	87	3260.71	2.36	119	3017.69	3.91
24	4124.15	12.41	56	3534.09	0.66	88	3251.51	0.57	120	3012.31	7.28
25	4092.73	0.57	57	3529.15	4.66	89	3243.23	2.12	121	3010.08	1.05
26	4083.85	3.11	58	3525.38	1.06	90	3238.10	4.17	122	3002.93	0.60
27	4081.59	0.70	59	3518.06	0.27	91	3230.46	0.31	123	2999.69	1.34
28	4067.68	2.53	60	3513.42	1.67	92	3225.45	0.63	124	2989.40	1.57
29	4044.81	0.37	61	3507.74	0.54	93	3217.17	0.76	125	2982.35	0.74
30	4022.36	0.28	62	3499.19	0.35	94	3198.44	1.37	126	2974.89	0.86
31	3961.08	4.08	63	3491.58	2.37	95	3177.77	0.71	127	2970.19	0.92
32	3945.32	2.41	64	3488.40	0.53	96	3174.55	0.63	128	2968.30	1.79

TABLE D.3 (cont'd)

PHOTON ENERGIES AND INTENSITIES OBSERVED IN THE ^{164}Dy (n,γ) ^{165}Dy REACTION

NO.	ENERGY keV	INTENSITY per 1000	NO.	ENERGY keV	INTENSITY per 1000	NO.	ENERGY keV	INTENSITY per 1000	NO.	ENERGY keV	INTENSITY per 1000
129	2967.23	2.14	161	2806.89	2.82	193	2659.98	3.85	225	2507.52	5.66
130	2950.75	2.71	162	2800.80	2.37	194	2658.06	1.02	226	2501.86	1.85
131	2947.71	13.10	163	2789.88	0.57	195	2654.09	0.57	227	2497.40	2.94
132	2939.35	0.53	164	2785.71	1.57	196	2651.66	1.09	228	2492.01	1.65
133	2932.10	2.31	165	2783.72	1.35	197	2638.65	0.62	229	2489.23	1.46
134	2929.48	1.16	166	2778.69	1.95	198	2636.11	1.49	230	2486.01	1.91
135	2921.22	1.14	167	2776.85	0.60	199	2631.13	0.85	231	2482.21	1.67
136	2916.99	0.64	168	2772.32	0.76	200	2629.47	0.54	232	2480.84	1.11
137	2907.23	0.45	169	2767.60	0.95	201	2625.58	1.18	233	2477.03	1.41
138	2902.50	0.43	170	2756.80	5.56	202	2623.15	2.03	234	2473.15	2.16
139	2900.67	3.45	171	2752.86	2.35	203	2613.69	3.87	235	2464.74	0.84
140	2892.42	0.63	172	2748.19	2.89	204	2611.71	1.66	236	2460.50	3.37
141	2888.80	0.73	173	2745.16	5.28	205	2607.08	3.47	237	2454.33	0.69
142	2881.21	1.30	174	2741.10	0.84	206	2604.03	0.88	238	2450.66	3.39
143	2878.92	1.15	175	2734.39	14.62	207	2598.13	0.76	239	2448.93	1.99
144	2872.40	5.19	176	2728.77	4.17	208	2595.03	2.58	240	2443.50	4.72
145	2869.34	0.53	177	2724.75	5.30	209	2590.87	3.03	241	2441.81	2.50
146	2865.40	1.46	178	2722.95	0.80	210	2587.74	1.84	242	2439.49	3.18
147	2864.04	4.76	179	2721.42	1.49	211	2584.87	0.62	243	2437.15	0.77
148	2859.79	0.74	180	2715.64	4.50	212	2580.69	1.29	244	2434.09	3.04
149	2853.87	4.46	181	2705.08	16.08	213	2564.73	1.06	245	2429.51	3.77
150	2843.45	7.28	182	2702.91	8.64	214	2561.26	1.70	246	2427.09	3.32
151	2839.85	4.05	183	2697.82	4.23	215	2559.15	1.76	247	2422.10	0.80
152	2835.45	0.71	184	2695.00	2.40	216	2552.75	5.27	248	2420.05	1.29
153	2831.98	1.85	185	2691.11	2.24	217	2549.38	1.38	249	2416.46	1.63
154	2829.81	3.74	186	2689.06	1.25	218	2545.38	1.23	250	2411.48	3.52
155	2827.60	1.20	187	2687.78	0.82	219	2538.88	1.91	251	2408.29	3.17
156	2823.37	1.98	188	2684.36	1.66	220	2535.49	1.65	252	2403.02	0.86
157	2820.07	0.70	189	2677.05	3.28	221	2526.64	0.73	253	2400.75	2.70
158	2816.28	0.66	190	2672.91	0.53	222	2523.80	2.93	254	2388.45	3.05
159	2812.62	1.06	191	2668.29	1.92	223	2522.22	1.29	255	2387.27	2.22
160	2810.25	1.93	192	2662.85	2.24	224	2518.48	0.82	256	2381.80	1.02

TABLE D.4

PHOTON ENERGIES AND INTENSITIES OBSERVED IN THE $^{165}Ho(n,\gamma)^{166}Ho$ REACTION

NO.	ENERGY keV	INTENSITY per 1000	NO.	ENERGY keV	INTENSITY per 1000	NO.	ENERGY keV	INTENSITY per 1000	NO.	ENERGY keV	INTENSITY per 1000
1	6189.53	0.08	30	5559.83	0.13	59	5225.38	0.05	88	4971.62	0.09
2	6072.52	0.55	31	5550.10	0.56	60	5213.05	3.41	89	4953.99	0.23
3	6063.08	0.10	32	5538.64	0.04	61	5188.82	0.05	90	4949.57	0.48
4	6052.72	3.16	33	5524.08	2.22	62	5181.59	3.65	91	4943.31	0.10
5	5982.88	1.27	34	5507.13	0.10	63	5155.36	0.77	92	4942.19	0.74
6	5914.03	0.09	35	5501.44	0.27	64	5145.80	0.57	93	4938.66	0.20
7	5895.52	0.10	36	5484.54	0.20	65	5128.55	2.23	94	4932.73	0.15
8	5871.54	3.14	37	5473.68	0.57	66	5121.62	0.29	95	4925.32	0.07
9	5827.45	0.22	38	5451.48	0.12	67	5111.77	0.07	96	4921.65	0.09
10	5813.53	7.82	39	5437.27	0.15	68	5108.08	0.54	97	4916.05	0.08
11	5779.37	0.16	40	5428.41	3.53	69	5105.60	0.47	98	4904.39	0.69
12	5772.75	1.22	41	5418.81	0.41	70	5102.45	0.11	99	4900.44	0.29
13	5768.07	0.99	42	5411.26	0.48	71	5096.20	0.06	100	4893.37	0.67
14	5761.74	1.91	43	5373.36	0.22	72	5088.48	0.59	101	4888.58	0.70
15	5721.53	0.36	44	5367.32	0.04	73	5081.92	2.80	102	4880.49	0.16
16	5699.92	0.22	45	5362.86	0.93	74	5068.33	0.04	103	4876.39	0.14
17	5695.79	0.36	46	5358.14	0.10	75	5053.20	0.94	104	4866.39	1.55
18	5684.88	1.73	47	5352.39	0.67	76	5041.39	0.36	105	4855.50	2.66
19	5680.68	0.15	48	5338.07	1.55	77	5034.79	0.22	106	4851.09	0.13
20	5650.99	0.89	49	5318.08	0.05	78	5027.46	0.40	107	4846.63	0.48
21	5645.32	0.65	50	5296.72	0.28	79	5022.34	0.16	108	4841.57	0.26
22	5638.22	0.07	51	5292.14	0.08	80	5013.08	1.21	109	4837.87	0.05
23	5615.37	0.06	52	5282.33	0.42	81	5008.37	0.07	110	4827.71	2.18
24	5605.56	0.45	53	5266.70	0.06	82	5002.24	0.77	111	4824.29	0.12
25	5588.18	0.07	54	5264.08	0.07	83	4998.87	0.62	112	4822.05	0.14
26	5586.98	0.07	55	5258.24	0.16	84	4995.14	0.30	113	4813.62	0.64
27	5585.50	0.23	56	5238.61	0.50	85	4990.73	0.15	114	4809.94	0.30
28	5581.64	0.34	57	5232.74	0.08	86	4987.06	0.20	115	4794.50	0.86
29	5575.44	0.40	58	5226.96	0.25	87	4979.53	0.7[illegible]	116	4783.51	0.13

TABLE D.4 (cont'd.)

PHOTON ENERGIES AND INTENSITIES OBSERVED IN THE $^{165}Ho(n,\gamma)^{166}Ho$ REACTION

NO.	ENERGY keV	INTENSITY per 1000	NO.	ENERGY keV	INTENSITY per 1000	NO.	ENERGY keV	INTENSITY per 1000	NO.	ENERGY keV	INTENSITY per 1000
117	4779.68	1.20	144	4588.00	0.08	171	4444.18	0.10	198	4292.66	1.21
118	4771.25	0.14	145	4585.95	0.18	172	4438.02	0.22	199	4286.51	0.28
119	4769.20	0.06	146	4582.10	0.13	173	4433.88	0.15	200	4283.17	0.64
120	4765.20	0.28	147	4577.41	0.45	174	4430.66	0.11	201	4273.51	0.17
121	4756.29	0.21	148	4571.82	0.54	175	4426.68	0.99	202	4269.24	0.13
122	4748.66	0.20	149	4566.69	0.23	176	4423.56	0.12	203	4265.69	0.47
123	4745.27	0.07	150	4562.36	0.09	177	4419.77	0.96	204	4257.52	0.27
124	4737.91	0.08	151	4560.04	0.13	178	4415.39	0.37	205	4247.83	0.29
125	4732.86	0.54	152	4556.20	0.05	179	4412.38	0.28	206	4244.32	0.15
126	4716.04	0.09	153	4548.49	0.62	180	4408.12	0.70	207	4239.03	1.10
127	4711.45	0.94	154	4539.18	0.47	181	4405.21	0.14	208	4237.82	0.26
128	4705.79	0.43	155	4532.72	0.17	182	4400.59	1.11	209	4236.67	0.06
129	4696.02	0.45	156	4530.24	0.30	183	4392.65	0.08	210	4233.10	0.33
130	4690.69	0.12	157	4526.82	0.19	184	4388.68	0.36	211	4228.60	0.48
131	4684.27	0.84	158	4519.77	0.05	185	4384.41	0.42	212	4227.12	0.19
132	4672.68	0.81	159	4512.37	0.32	186	4366.66	0.48	213	4219.02	0.44
133	4666.45	0.15	160	4501.29	0.26	187	4360.58	0.14	214	4217.44	0.40
134	4654.18	0.26	161	4491.11	0.10	188	4352.42	0.44	215	4213.73	0.24
135	4651.19	0.13	162	4486.59	0.08	189	4348.16	1.24	216	4211.78	0.67
136	4643.11	0.54	163	4483.77	0.13	190	4344.72	0.29	217	4206.08	0.52
137	4639.02	0.86	164	4482.68	0.08	191	4335.90	0.40	218	4203.50	0.17
138	4627.93	0.58	165	4480.89	0.09	192	4329.11	0.24	219	4191.43	0.15
139	4623.77	0.07	166	4479.62	0.59	193	4324.48	0.57	220	4188.60	0.47
140	4614.20	0.56	167	4474.07	0.17	194	4315.33	0.52	221	4185.97	0.76
141	4607.83	0.73	168	4466.76	1.31	195	4310.55	0.19	222	4183.20	0.10
142	4604.90	0.15	169	4458.02	0.08	196	4304.59	0.50	223	4178.58	0.86
143	4599.09	0.09	170	4449.21	0.22	197	4297.76	0.23	224	4170.72	0.60

TABLE D.4 (cont'd.)

PHOTON ENERGIES AND INTENSITIES OBSERVED IN THE $^{165}Ho(n,\gamma)^{166}Ho$ REACTION

NO.	ENERGY keV	INTENSITY per 1000	NO.	ENERGY keV	INTENSITY per 1000	NO.	ENERGY keV	INTENSITY per 1000	NO.	ENERGY keV	INTENSITY per 1000
225	4166.92	0.22	252	4022.94	0.83	279	3876.79	0.34	306	3740.09	0.63
226	4165.80	0.48	253	4018.34	0.92	280	3869.99	0.15	307	3737.71	0.11
227	4155.71	0.35	254	4013.16	0.89	281	3867.63	0.15	308	3733.37	0.12
228	4152.66	0.38	255	4009.89	0.65	282	3862.36	0.63	309	3726.20	0.66
229	4149.96	0.07	256	4002.85	0.15	283	3855.46	0.22	310	3723.70	0.28
230	4145.45	0.35	257	4000.33	0.90	284	3853.41	0.20	311	3718.41	0.12
231	4139.05	0.27	258	3998.02	0.25	285	3847.33	0.53	312	3715.62	0.40
232	4132.89	0.09	259	3993.79	0.53	286	3842.52	0.13	313	3706.80	0.33
233	4127.68	0.27	260	3982.11	0.18	287	3838.86	0.87	314	3703.21	0.38
234	4115.42	0.23	261	3970.78	0.12	288	3831.74	0.24	315	3699.26	0.60
235	4112.58	0.21	262	3965.10	0.26	289	3828.06	0.34	316	3693.57	0.30
236	4105.48	0.28	263	3956.31	0.47	290	3814.10	0.05	317	3690.16	0.13
237	4097.78	0.59	264	3952.74	0.61	291	3809.88	0.29	318	3689.09	0.28
238	4093.57	0.37	265	3949.56	0.14	292	3808.22	0.22	319	3682.51	0.64
239	4091.69	0.44	266	3942.54	0.30	293	3802.88	0.54	320	3676.64	0.71
240	4086.20	0.76	267	3936.61	0.57	294	3799.99	0.21	321	3669.84	0.14
241	4081.93	0.23	268	3934.24	0.24	295	3795.11	0.54	322	3663.44	0.08
242	4079.68	0.32	269	3930.26	0.52	296	3791.92	0.14	323	3659.86	0.33
243	4075.22	0.18	270	3925.69	0.58	297	3784.79	0.60	324	3658.11	0.32
244	4074.03	0.80	271	3919.63	0.20	298	3781.12	0.70	325	3654.62	0.10
245	4072.33	0.22	272	3909.65	0.14	299	3776.87	0.54	326	3642.63	0.36
246	4063.27	0.24	273	3907.48	0.54	300	3771.23	0.16	327	3637.98	0.56
247	4060.86	0.28	274	3902.29	0.64	301	3763.33	0.52	328	3633.30	0.27
248	4050.29	0.81	275	3897.92	0.16	302	3754.17	0.16	329	3629.98	0.48
249	4047.08	0.41	276	3895.60	0.66	303	3750.97	0.24	330	3628.15	0.20
250	4037.76	0.12	277	3891.89	0.33	304	3747.74	0.25	331	3621.54	0.16
251	4031.34	0.38	278	3887.31	0.30	305	3744.05	0.59	332	3618.12	0.34

TABLE D.4 (cont'd.)

PHOTON ENERGIES AND INTENSITIES OBSERVED IN THE $^{165}Ho(n,\gamma)^{166}Ho$ REACTION

NO.	ENERGY keV	INTENSITY per 1000
333	3611.25	0.51
334	3608.46	0.33
335	3604.66	0.19
336	3602.34	0.43
337	3599.57	0.14
338	3595.44	0.13
339	3586.11	0.37
340	3582.23	0.14
341	3579.24	0.21
342	3575.64	0.53
343	3572.18	0.53
344	3568.12	0.31
345	3564.90	0.15
346	3556.13	0.24
347	3552.46	0.09
348	3550.55	0.16
349	3540.55	0.47
350	3532.99	0.23
351	3528.96	0.29
352	3526.31	0.21
353	3525.24	0.09
354	3522.16	0.31
355	3515.71	0.31
356	3510.57	0.17
357	3506.56	0.66
358	3502.73	0.74
359	3492.36	0.18
360	3489.99	0.20
361	3486.42	0.07
362	3482.43	0.37
363	3479.70	0.13
364	3474.07	0.14
365	3464.89	0.40
366	3463.21	0.09
367	3461.46	0.34
368	3455.80	0.30
369	3451.19	0.46
370	3448.82	0.19
371	3447.14	0.21
372	3444.10	0.23
373	3441.25	0.45
374	3435.84	0.41
375	3432.66	0.22
376	3429.98	0.31
377	3424.21	0.19
378	3417.96	0.38
379	3416.14	0.30
380	3412.31	0.12
381	3396.15	0.40
382	3389.30	0.21
383	3383.05	0.60
384	3379.14	0.39
385	3373.50	0.21
386	3366.59	0.38
387	3362.94	0.30
388	3354.84	0.16
389	3352.91	0.46
390	3348.88	0.58
391	3346.70	0.30
392	3336.09	0.31
393	3332.99	0.18
394	3326.10	0.10
395	3321.91	0.11
396	3313.03	0.30
397	3310.65	0.71
398	3308.12	0.20
399	3306.95	0.38
400	3296.26	0.22
401	3293.03	0.40
402	3282.18	0.19
403	3279.37	0.34
404	3276.86	0.15
405	3271.78	0.37
406	3264.36	0.40
407	3258.06	0.77
408	3254.97	0.50
409	3250.28	0.17
410	3247.46	0.14
411	3242.36	0.29
412	3238.71	0.16
413	3236.44	0.12
414	3231.21	0.64
415	3225.94	0.17
416	3221.91	0.31
417	3214.71	0.23
418	3204.10	0.16
419	3202.63	0.33
420	3198.74	0.22
421	3196.01	0.40
422	3192.38	0.41
423	3189.87	0.11
424	3186.87	0.36
425	3184.60	0.38
426	3180.83	0.44
427	3175.10	0.34
428	3165.35	0.36
429	3162.51	0.16
430	3154.91	0.35
431	3153.55	0.11
432	3152.40	0.14
433	3150.91	0.40
434	3137.22	0.23
435	3131.34	0.26
436	3126.00	0.41
437	3121.02	0.37
438	3117.58	0.63
439	3113.43	0.36
440	3110.76	0.76

TABLE D.5

PHOTON ENERGIES AND INTENSITIES OBSERVED IN THE $^{173}Yb(n,\gamma)^{174}Yb$ REACTION

NO.	ENERGY keV	INTENSITY per 1000	NO.	ENERGY keV	INTENSITY per 1000	NO.	ENERGY keV	INTENSITY per 1000	NO.	ENERGY keV	INTENSITY per 1000
1	7388.02	14.13	26	5341.25	3.32	51	4864.73	3.73	76	4645.91	2.74
2	7211.48	9.73	27	5301.19	7.71	52	4862.41	0.62	77	4640.02	1.24
3	6146.09	0.50	28	5292.57	6.19 b	53	4845.12	0.35	78	4626.45	0.67
4	6082.70	0.38	29	5277.35	0.89	54	4841.00	2.25	79	4619.80	2.79
5	5996.32	0.31	30	5226.95	2.56	55	4822.05	1.42	80	4615.71	0.48
6	5903.59	11.44 a	31	5217.61	4.87	56	4816.73	0.15	81	4605.37	0.53
7	5858.37	5.47	32	5208.03	4.56	57	4807.92	0.59	82	4581.84	1.06
8	5840.29	0.54	33	5174.49	0.34 c	58	4806.37	1.20	83	4569.02	2.90
9	5830.62	15.29	34	5168.22	0.47	59	4801.29	1.92	84	4562.06	2.00
10	5790.07	0.91	35	5143.14	0.61	60	4794.98	0.39	85	4555.33	0.73
11	5763.02	0.57	36	5126.59	0.53	61	4784.17	4.04	86	4546.58	0.32
12	5754.88	3.57	37	5102.29	1.88	62	4764.16	0.95	87	4523.69	0.15
13	5749.35	2.08	38	5080.40	1.03	63	4759.32	3.60	88	4519.98	1.81
14	5731.12	0.69	39	5060.42	0.32	64	4751.95	8.86	89	4501.96	1.06
15	5678.16	0.56 a	40	5017.06	0.21	65	4739.42	0.47	90	4497.89	0.65
16	5659.54	2.24 a	41	4999.91	1.16	66	4732.07	4.65	91	4462.25	0.98
17	5613.19	1.04	42	4964.04	0.59	67	4715.60	1.09	92	4450.33	0.29
18	5605.81	4.29	43	4959.83	0.38	68	4714.39	0.65	93	4431.92	0.92
19	5506.24	0.65	44	4951.24	0.94	69	4697.43	0.47	94	4427.32	0.64
20	5448.40	3.74	45	4945.36	10.81 d	70	4690.84	0.38	95	4426.16	1.24
21	5427.02	0.29	46	4937.53	0.79	71	4680.52	0.54	96	4424.87	0.16
22	5411.80	0.04	47	4917.14	0.43	72	4671.61	2.27	97	4417.62	1.24
23	5396.50	0.32	48	4883.20	3.95	73	4665.79	0.54	98	4414.18	1.05
24	5363.23	6.37	49	4879.66	1.01	74	4655.82	0.33	99	4406.38	0.33
25	5353.16	0.29	50	4875.86	1.69	75	4651.80	0.20	100	4401.68	1.34

TABLE D.5 (cont'd.)

PHOTON ENERGIES AND INTENSITIES OBSERVED IN THE $^{173}Yb(n,\gamma)^{174}Yb$ REACTION

NO.	ENERGY keV	INTENSITY per 1000	NO.	ENERGY keV	INTENSITY per 1000	NO.	ENERGY keV	INTENSITY per 1000	NO.	ENERGY keV	INTENSITY per 1000
101	4391.98	0.54	110	4308.05	0.42	119	4227.88	2.76	128	4101.59	0.82
102	4389.25	0.32	111	4301.41	4.45	120	4170.52	1.79	129	4089.89	1.08
103	4378.10	0.71	112	4290.40	2.69	121	4164.44	0.87	130	4081.26	2.64
104	4370.09	0.85	113	4284.60	0.47	122	4154.43	0.70	131	4072.27	0.49
105	4368.71	0.80	114	4281.38	0.47	123	4151.14	0.47	132	4068.68	1.83
106	4352.32	0.63	115	4254.54	1.92	124	4148.95	1.23	133	4056.34	0.64
107	4343.05	0.66	116	4247.47	2.09	125	4115.68	1.41	134	4052.80	1.43
108	4327.77	0.41	117	4237.95	0.88	126	4111.05	1.15	135	4044.30	1.50
109	4312.26	0.82	118	4230.57	1.24	127	4108.52	0.57	136	4037.39	1.20

[a]Contaminated with Gd by 7%, 55% and 13% respectively.

[b]Contaminated with ^{173}Yb by 2%.

[c]Contaminated with ^{172}Yb by 5%.

[d]Contaminated with C by 80%.

TABLE D.6

Weak Transitions in ^{144}Nd and ^{165}Dy

Final Nucleus	No.	Energy (keV)	I_γ (photons/1000)
^{144}Nd	1	5602.4	0.04
	2	5496.6	0.12
	3	5432.3	0.08
	4	5373.4	0.01
	5	5324.7	0.06
	6	5301.2	0.04
	7	5259.8	0.03
	8	5189.4	0.06
	9	5174.9	0.08
	10	5137.0	0.08
	11	5103.3	0.09
	12	5092.2	0.03
	13	5071.2	0.06
	14	4966.0	0.06
	15	4891.0	0.08
	16	4805.0	0.10
	17	4680.5	0.05
	18	4656.3	0.16
	19	4605.5	0.05
	20	4482.9	0.25
	21	4447.4	0.02
	22	4384.5	0.20
	23	4364.0	0.03
	24	4333.7	0.04
	25	4285.6	0.13
	26	4197.3	0.05
	27	3880.8	0.12
^{165}Dy	1	4300.21	0.09
	2	4292.02	0.03
	3	4236.86	0.11
	4	4224.88	0.06
	5	4214.93	0.16
	6	4194.57	0.05
	7	4179.10	0.06

TABLE D.7

Low-Lying Levels in ^{165}Dy with Spin $\leq 3/2$

No.	This work		Previous work	
	Photon energy (keV)	Level[a] energy (keV)	Level energy (keV)	Spin
1	5607.75	108.13	108.160	$1/2^-$
2	5557.27	158.61	158.591	$3/2^-$
3	5177.25	538.64	538.61	$3/2^+$
4	5145.51	570.38	570.25	$1/2^-$
5	5142.39	573.50	573.56	$3/2^-$
6	5110.80	605.09	605.10	$3/2^-$
7	4804.01	911.95		
8	4699.98	1015.93		
9	4635.87	1080.04		
10	4612.92	1102.99	1103.3	$(3/2^-)$
11	4607.86	1108.05		
12	4557.52	1158.39		
13	4549.12	1166.79	1167	$(3/2^+)$
14	4497.55	1218.37		
15	4459.47	1256.45	1253	
16	4339.60	1376.32		
17	4335.18	1380.73		
18	4315.84	1400.08	1401	
19	4275.30	1440.62		
20	4259.62	1456.30		
21	4251.16	1464.76		
22	4214.93	1501.05		
23	4160.52	1555.41		
24	4155.85	1560.07	1563	$1/2,3/2^-$
25	4124.15	1591.77	1590.9	$(3/2)$
26	4092.73	1623.19		
27	4083.85	1632.08	1628	
28	4081.58	1634.34		
29	4067.68	1648.25	1646	$(1/2,3/2^-)$

[a] Average error is 0.18 keV.

[b] Ref. Bu74.

TABLE D.8 Comparison between observed[a] $\langle\Gamma_{\gamma i}/D\rangle$ and theoretical prediction for ^{208}Pb with $\langle D\rangle$= 8 KeV

No.	E (MeV)	$\Gamma_{\gamma i}$ (eV)	$\langle\Gamma_{\gamma i}/D\rangle_{exp}$ x10^7	$\langle\Gamma_{\gamma i}/D\rangle_{th}$ x10^7	exp/theo
1	7.371	0.013	16.2	28.22	0.58
2	7.378	0.039	48.7	28.40	1.72
3	7.384	0.032	40.0	28.55	1.40
4	7.401	0.005	6.2	28.98	0.22
5	7.416	0.035	43.7	29.37	1.49
6	7.431	0.012	15.0	29.76	0.50
7	7.436	0.031	38.7	29.89	1.30
8	7.436	0.036	45.0	29.89	1.51
9	7.451	0.025	31.2	30.29	1.03
10	7.456	0.021	26.2	30.42	0.86
11	7.522	0.037	46.2	32.26	1.43
12	7.609	0.037	46.2	34.86	1.33
13	7.617	0.090	112.5	35.11	3.20
14	7.638	0.036	45.0	35.78	1.26
15	7.737	0.180	225.0	39.10	5.75
16	7.747	0.100	125.0	39.46	3.17
17	7.750	0.120	150.0	39.56	3.79
18	7.820	0.220	275.0	42.15	6.52
19	7.905	0.210	262.5	45.53	5.77
20	7.907	0.210	262.5	45.62	5.75
21	7.917	0.200	250.0	46.03	5.43
22	8.011	0.560	700.0	50.17	13.95
23	8.055	0.360	450.0	52.25	8.61
24	8.075	0.150	187.5	53.22	3.52
25	8.113	0.180	225.0	55.13	4.08
26	8.148	0.510	637.5	56.95	11.19
27	8.171	0.300	375.0	58.18	6.45

AVERAGE EXP/THEO =5.1

[a]Ref. Ra78

TABLE D.9 Comparison between observed[a] $\langle\Gamma_{\gamma i}/D\rangle$ and theoretical prediction for ^{208}Pb with $\langle D\rangle$=14 KeV

No.	E (meV)	$\Gamma_{\gamma i}$ (eV)	$\langle\Gamma_{\gamma i}/D\rangle_{exp}$ x10^7	$\langle\Gamma_{\gamma i}/D\rangle_{th}$ x10^7	exp/theo
1	7.371	0.013	9.3	28.22	0.33
2	7.378	0.039	27.9	28.40	0.98
3	7.384	0.032	22.9	28.55	0.80
4	7.401	0.005	3.6	28.98	0.12
5	7.416	0.035	25.0	29.37	0.85
6	7.431	0.012	8.6	29.76	0.29
7	7.436	0.031	22.1	29.89	0.74
8	7.436	0.036	25.7	29.89	0.86
9	7.451	0.025	17.9	30.29	0.59
10	7.456	0.021	15.0	30.42	0.49
11	7.522	0.037	26.4	32.26	0.82
12	7.609	0.037	26.4	34.86	0.76
13	7.617	0.090	64.3	35.11	1.83
14	7.638	0.036	25.7	35.78	0.72
15	7.737	0.180	128.6	39.10	3.29
16	7.747	0.100	71.4	39.46	1.81
17	7.750	0.120	85.7	39.56	2.17
18	7.820	0.220	157.1	42.15	3.73
19	7.905	0.210	150.0	45.53	3.29
20	7.907	0.210	150.0	45.62	3.29
21	7.917	0.200	142.9	46.03	3.10
22	8.011	0.560	400.0	50.17	7.97
23	8.055	0.360	257.1	52.25	4.92
24	8.075	0.150	107.1	53.22	2.01
25	8.113	0.180	128.6	55.13	2.33
26	8.148	0.510	364.3	56.95	6.40
27	8.171	0.300	214.3	58.18	3.68

AVERAGE EXP/THEO =2.9

[a]Ref. Ra78

REFERENCES

Al 71 G. Alenius, S. E. Arnell, C. Schale and E. Wallander, Nucl. Phys. A161 (1971) 209.

Ax 62 P. Axel, Phys. Rev. 126 (1962) 671.

Ba 57 G. A. Bartholomew and P. J. Campion, Can. J. Phys. 35 (1957) 1347.

Ba 61 G. A. Bartholomew, Ann. Rev. Nucl. Sci. 11 (1961) 259.

Ba 67 A. Backlin et al., Phys. Rev. 160 (1967) 1011.

Ba 73 G. A. Bartholomew, E. D. Earle, A. J. Ferguson, J. W. Knowles and M. A. Lone, Ad. in Nucl. Phys., Vol. 7, Ed. M. Baranger and E. Vogt, Plenum Press, New York - London (1973) p. 229.

Ba 76 K. A. Baskova, A. B. Vovk, L. I. Govor, E. P. Grigorev, A. M. Demidov, M. M. Komkov and T. V. Chugai, Izv. Akad. Nauk SSR. 40 (1976) 794.

Be 54 C. A. Bennett and N. L. Franklin, Statistical Analysis in Chemistry and the Chemical Industry, John Wiley & Sons, Inc., New York (1954) p. 196.

Be 71 D. Bellman, Atomkernergie 17 (1971) 145.

Be 76 F. E. Bertrand, Ann. Rev. Nucl. Sci. 26 (1976) 457.

Bl 52 J. M. Blatt and W. V. Weisskopf, Theoretical Nuclear Physics, John Wiley & Sons, New York (1952), p. 644.

Bo 67 L. M. Bollinger and G. E. Thomas, Phys. Rev. Lett. 18 (1967) 223.

Bo 68 L. M. Bollinger and G. E. Thomas, Phys. Rev. Lett. 21 (1968) 233.

Bo 68a H. H. Boltin, Phys. Rev. 168 (1968) 1317.

Bo 69 A. G. Bohr and B. R. Mottleson, Nuclear Structure, Vol. 1, W. A. Benjan Inc., New York, Amsterdam (1969) p. 382.

Bo 70 L. M. Bollinger and G. E. Thomas, Phys. Rev. C2 (1970) 1951.

Bo 70a L. M. Bollinger in Experimental Neutron Resonance Spectroscopy, ed. J. A. Harvey, Academic Press, New York and London (1970) p. 235.

Bo 72 L. M. Bollinger and G. E. Thomas, Phys. Rev. 6 (1972) 1322.

Br 55 D. M. Brink, Doctoral Thesis, Oxford University 1955.

Br 71 D. Breitig, Z. Naturforsch. 26a (1971) 371.

Br 79 F. Braumandl, K. Schreckenback and T. von Egidy, Nucl. Instr. and Meth. 166 (1979) 243.

Bu 70 D. J. Buss and R. K. Smither, Phys. Rev. C2 (1970) 1513.

Bu 73 W. E. Burcham, Nuclear Physics, Second edition, Longman Group Ltd., London 1973.

Bu 74 D. L. Bushnell, D. J. Buss, R. K. Smither, Phys. Rev. C10 (1974) 2483.

Bu 75 T. W. Burrows, Nucl. Data Sheets, 14 (1975) 413.

Bu 75a A. Buyron, Nucl. Data Sheets 14 (1975) 471.

Bu76 T. W. Burrows, Nucl. Data Sheets 18 (1976) 553.

Bu 76a A. Buyron, Nucl. Data Sheets 11 (1976) 789.

Ca 80 R. F. Casten et al., Phys. Rev. C21 (1980) 65.

Ch 71 R. E. Chrien, K. Rimavi and J. B. Garg, Phys. Rev. C3 (1971) 2054.

Ch 73 R. E. Chrien, M. R. Bhat and O. A. Wasson, Phys. Rev. C8 (1973) 297.

Ch 74 R. E. Chrien, G. W. Cole, J. L. Holm and O. A. Wasson, Phys. Rev. C9 (1974) 1622.

Co 71 C. Coceva, F. Corvi, P. Giacobbe and Stefanon, Nucl. Phys. A170 (1971) 153.

Co 75 G. C. Cormick, M.Sc. Thesis, McMaster University, (1975).

En 66 H. A. Enge, Introduction to Nuclear Physics, Addison-Wesley, Reading, MA (1966) p. 194.

Er 58 T. Ericson, Nucl. Phys. 8 (1958) 265.

Ev 55 R. D. Evans, The Atomic Nucleus, McGraw-Hill, New York, 1955.

Fu 72 A. Fubini, P. R. Oliva and D. Prosperi, Lett. Nuvo Cimento 3 (1972) 401.

Gi 65 A. Gilbert and A. G. W. Cameron, Can. J. Phys. 43 (1965) 1446.

Gr 65 I. S. Gradsteyn and I. M. Ryzhik, Table of Integrals, Series and products, Translation from the Russian edited by A. Jeffery, Academic Press, New York and London, I965.

Gr 66 L. V. Groshev, A. M. Demidov, V. A. Ivanov, V. N. Lutsenko, V. I. Pelekhov and N. Shadiev, Bull. Acad. Sci. USSR 29 (1966) 775.

Gr 69 L. V. Groshev, V. N. Dvoretskii, A. M. Demidov and A. S. Rakhimov; Sov. J. Nucl. Phys. 8 (1969) 619.

Gr 72 L. V. Groshev, L. I. Govor and A. M. Demidov, Yad. Fiz. 15 (1972) 625. Sov. J. Nucl. Phys. 15 (1972) 347.

Gr 74 R. C. Greenwood and R. G. Helmer, Nucl. Instr. and Meth., 121 (1974) 385.

Gr. 74a L. R. Greenwood, Nucl. Data Sheets, 11 (1974) 385.

Gr 74b L. R. Greenwood, Nucl. Data Sheets, 13 (1974) 549.

Gr 75 R. C. Greenwood, C. W. Reich and S. H. Vegors, Jr. Nucl. Phys. A252 (1975) 260.

Gr 78 R. E. Greenwood et al., Nucl. Phys. A304 (1978) 327.

Gr 79 R. C. Greenwood and R. E. Chrien, Neutron Capture Gamma-Ray Spectroscopy, ed. R. E. Chrien, W. R. Kane, Plenum Press, New York, 1979.

Gr 80 R. C. Greenwood and R. E. Chrien, Phys. Rev. C21 (1980) 498.

Gr 80a R. C. Greenwood and R. E. Chrien, Nucl. Instr. and Meth. 175 (1980) 515.

Gr 81 R. C. Greenwood and C. W. Reich, Phys. Rev. C23 (1981) 153.

Ha 55 C. Hastings, Jr., Approximations for digital computers, Princeton University Press, Princeton, N.J., 1955.

Ha 64 E. Hayword, Photonuclear Reactions, Nuclear Structure and Electromagnetic Interactions, Oliver and Boyd, 1964, p. 141.

Ho 78 D. J. Horen, J. A. Harvey and N. W. Hill, Phys. Rev. C18 (1978) 722.

Ha 75 T. J. Haste and B. W. Thomas, J. Phys. G1 (1975) 981.

Is 79 M. A. Islam, M.Sc. Thesis, McMaster University, 1979.

Is 80 M. A. Islam, T. J. Kennett, S. A. Kerr and W. V. Prestwich, Can. J. Phys. 58 (1980) 168.

Is 81 M. A. Islam, W. V. Prestwich and T. J. Kennett, Nucl. Instr. and Meth. 188 (1981) 243.

Is 82 M. A. Islam, T. J. Kennett and W. V. Prestwich, Phys. Rev. C25 (1982) 3184.

Ju 63 E. T. Jurney and M. T. Motz, ANL-6797 (1963) p. 236.

Ju 69 E. T. Jurney, in Proceedings of the International Symposium on Neutron Capture Gamma-Ray Spectroscopy, Studsvik (IAEA, 1969) p. 431.

Ke 61 M. G. Kendal, A. Stuart, The Advanced Theory of Statistics, Vol. 2, Hafner Publishing Co., New York, 1969.

Ke 67 T. J. Kennett, W. P. Archer and L. B. Hughes, Nucl. Phys. A96 (1967) 658.

Ke 78 T. J. Kennett, W. V. Prestwich and A. Robertson, Nucl. Instr. and Meth. 151 (1978) 285.

Ke 78a T. J. Kennett, W. V. Prestwich and A. Robertson, Nucl. Instr. and Meth. 151 (1978) 293.

Ke 78b T. J. Kennett, P. Brewster, A. Robertson and W. V. Prestwich, Nucl. Instr. and Meth. 153 (1978) 125.

Ke 80 T. J. Kennett, W. V. Prestwich, M. A. Islam and S. A. Kerr, Nucl. Instr. and Meth. 174 (1980) 539.

Ke 81 T. J. Kennett, M. A. Islam and W. V. Prestwich, Can. J. Phys. 59 (1981) 93.

Ke 81a T. J. Kennett, W. V. Prestwich and M. A. Islam, Can. J. Phys. 59 (1981) 1212.

Ke 81b T. J. Kennett, W. V. Prestwich and M. A. Islam, Z. Phys. A299 (1981) 323.

Ke 81c T. J. Kennett, W. V. Prestwich and R. J. Tervo, Nucl. Instr. and Meth. 190 (1981) 313.

Ke 82 T. J. Kennett, private communication.

Kh 57 Iu. K. Khoklov, Sov. Phys. JETP 5 (1957) 88.

Kl 29 O. Klein and Y. Nishina, Z. Phys. 52 (1929) 853.

Ko 81 J. Kopecky, ECN-99, 1981.

Le 78 C. M. Lederer and V. S. Shirley (editors). Table of Isotopes. 7th ed. John Wiley & Sons, New New York, 1978.

Lo 73 A. M. Lopez, Doctoral Thesis, McMaster University, 1973.

Lo 79 M. A. Lone, Neutron Capture Gamma-Ray Spectroscopy, ed. R. E. Chrien and W. R. Kane, Plenum Press, New York (1979) p. 161.

Lo 81 M. A. Lone, R. A. Leavitt and D. A. Harrison, Atomic Data Nucl. Data Tables 26 (1981) 511.

Ly 68 J. E. Lynn, The Theory of Neutron Resonance Reactions, Clarendon Press, Oxford 1968.

Ma 67 G. Markus, W. Michaelis, H. Schmidt and C. Weilkamp, Z. Phys. 206 (1967) 84.

Ma 72 M. A. J. Mariscotti, W. Gelletly and W. R. Kane, Phys. Rev. C5 (1972) 178.

Mi 70 W. Michaelis, H. Ottmar and F. Weller, Nucl. Phys. A150 (1970) 161.

Mi 73 M. M. Minor, Nucl. Data Sheets 10 (1973) 515.

Mi 76 M. M. Minor, Nucl. Data Sheets 18 (1976) 323.

Mo 67 H. T. Motz et al., Phys. Rev. 155 (1967) 1265.

Mo 71 H. T. Motz, E. T. Jurney, E. B. Shera and R. K. Sheline, Phys. Rev. Lett. 26 (1971) 854.

Mu 73 Neutron Cross Sections, compiled by S. F. Mughabghab and W. I. Garber, Brookhaven National Report No. BLN 325 (U.S. Government Printing Office) Washington D.C. (1973) 3rd ed.

Mu 81 S. F. Mughabghab, M. Divadeenam, N.E. Holden, Neutron Cross Sections vol. 1, Academic Press, New York (1981).

Na 66 A. Namenson, H. E. Jackson and R. K. Smither, Phys. Rev. 146 (1966) 844.

Na 67 A. Namenson and H. H. Bolotin, Phys. Rev. 158 (1967) 1206.

Ni 70 L. Nicol, A. M. Lopez, A. Robertson, W. V. Prestwich and T. J. Kennett, Nucl. Instr. and Meth. 81 (1970) 263.

Or 70 V. J. Orphan, N. C. Rasmussen and T. L. Harper, Gulph General Atomic Report No. GA-10248 (1970), unpublished.

Po 56 C. E. Porter and R. G. Thomas, Phys. Rev. 104 (1956) 483.

Pr 68 D. L. Price, R. E. Price, R. E. Chrien, O. A. Wasson, M. R. Bhat, M. Beer, M. A. Lone and R. Graves, Nucl. Phys. A121 (1968) 630.

Pr 75 M. A. Preston and R. K. Bhaduri, Structure of the Nucleus, Addison-Wesley, Reading, MA (1975) p. 672.

Pr 81 W. V. Prestwich, M. A. Islam and T. J. Kennett, Nucl. Sci. Eng. 78 (1981) 182.

Qu 72 P. Quittner, Gamma Ray Spectroscopy, Adam Hilgerm, London, 1972.

Ra 67 S. Raman, Nucl. Data Sheets, B2-1-47 (1967).

Ra 69 N. C. Rasmussen, Y. Inouye and V. J. Orphan, MITNE-85 (1969).

Ra 73 S. Raman and N. B. Gove, Phys. Rev. C7 (1973) 1995.

Ra 74 S. Raman et al., II Internat. Symp. on Neutron Capture Gamma-Ray Spectroscopy and Related Topics, Petten, Netherlands (1974) p. 77.

Ra 76 D. Rabenstein, Ya. Ya. Berzin, A. E. Kruminya and P. T. Prokof'ev, Bull. Acad. Sci. USSR 40 (1976) 55.

Ra 78 S. Raman, M. Mizomoto, G. G. Slaughter and R. L. Macklin, Phys. Rev. Lett. 40 (1978) 1306.

Ra 79 S. Raman, Neutron Capture Gamma-Ray Spectroscopy, ed. R. E. Chrien and W. R. Kane, Plenum Press, New York (1979) p. 193.

Ra 81 S. Raman, Invited paper presented at the Fourth International Symposium on Neutron Capture Gamma-Ray Spectroscopy, Grenoble, France, 1981.

Ri 70 K. Rimavi, J. B. Grag, R. E. Chrien and R. G. Graves, Phys. Rev. C2 (1970) 1793.

Ri 72 W. H. Richardson, J. Opt. Soc. Am 62 (1972) 55.

Ro 72 A. Robertson, W. V. Prestwich and T. J. Kennett, Nucl. Instr. and Meth. 100 (1972) 317.

Ro 75 A. Robertson, G. C. Cormick, T. J. Kennett and W. V. Prestwich, Nucl. Instr. and Meth. 127 (1975) 373.

Sa 74 G. R. Satchler, Physics Reports, 14 (1974) 97.

Sa 78 F. Saporetti and R. Guidotti, Neutron Capture Gamma-Ray Spectroscopy, ed. R. E. Chrien and W. A. Kane, Plenum Press, New York (1978) p.

Sc 64 O. W. B. Schult, U. Gruber, B. P. Maier, F. W. Stauck, Z. Physik 180 (1964) 298.

Sc 67 O. W. B. Schult et al., Phys. Rev. 154 (1967) 1146.

Se 69 E. Selin and R. Hardell, Nucl. Phys. A139 (1969) 375.

So 60 D. de Soete, R. Gijbels, J. Hoste, Neutron Activation Analysis, John Wiley & Sons, New York, 1972, p. 178.

St. 78 M. L. Steits and R. E. Chrien, Nuclear Instr. and Meth. 155 (1978) 253.

Th 67 G. E. Thomas, D. E. Batchley and L. M. Bollinger, Nucl. Instr. and Meth. 56 (1976) 325.

Tu 78 J. K. Tuli, Nucl. Data Sheets 25 (1978) 603.

Wa 69 E. K. Warburton and J. Weneser in Isospin in Nuclear Physics, ed. D. H. Wilkinson, North-Holland, Amsterdam, 1969, p. 173.

Ti 82 T. A. A. Tielens et al., Nucl. Phys. A376 (1982) 421.

Ts 82 J-S. Tsai, T. J. Kennett and W. V. Prestwich (1982) Submitted to Phys. Rev. C.

Wa 73 O. A. Wasson and G. G. Slaughter, Phys. Rev. C8 (1973) 297.

Wa 77 A. H. Wapstra and K. Bos, Atomic Data Nucl. Data Tables 19 (1977) 179.

We 66 C. Weilkamp, W. Michaelis, H. Schmidt and U. Fanger, Z. Physik 192 (1966) 423.

We 72 H. Weigmann, G. Rohr and M. Heske, Nucl. Phys. A185 (1972) 229.